U.S. Department of
Transportation

**Federal Railroad
Administration**

Estimation of Residual Stresses in Railroad Commuter Car Wheels Following Manufacture

Office of Research
and Development
Washington, DC 20590

Jeff Gordon
A. Benjamin Perlman

Research and Special Programs Administration
John A. Volpe National Transportation Systems Center
Cambridge, MA 02142-1093

DOT/FRA/ORD-03/24

Final Report
June 2003

REPORT DOCUMENTATION PAGE

Form Approved
OMB No. 0704-0188

1. AGENCY USE ONLY (Leave blank)	2. REPORT DATE	3. REPORT TYPE AND DATES COVERED
	June 2003	Final Report October 2001

4. TITLE AND SUBTITLE
Estimation of Residual Stresses in Railroad Commuter Cars Wheels Following Manufacture

5. FUNDING NUMBERS
R2050/RR228

6. AUTHOR(S)
Jeff Gordon and A. Benjamin Perlman

7. PERFORMING ORGANIZATION NAME(S) AND ADDRESS(ES)
U.S. Department of Transportation
Research and Special Programs Administration
Volpe National Transportation Systems Center
Cambridge, MA 02142-1093

8. PERFORMING ORGANIZATION REPORT NUMBER
DOT-VNTSC-FRA-02-02

9. SPONSORING/MONITORING AGENCY NAME(S) AND ADDRESS(ES)
U.S. Department of Transportation
Federal Railroad Administration
Office of Research and Development
1120 Vermont Avenue, NW: Mail Stop 20
Washington, DC 20590

10. SPONSORING/MONITORING AGENCY REPORT NUMBER
DOT/FRA/ORD-03/24

11. SUPPLEMENTARY NOTES

12a. DISTRIBUTION/AVAILABILITY STATEMENT
This document is available to the public through the National Technical Information Service, Springfield, Virginia 22161. This document is also available on the FRA web site at www.fra.dot.gov.

12b. DISTRIBUTION CODE

13. ABSTRACT (Maximum 200 words)

A computer simulation of the manufacturing process of railroad car wheels is described to determine the residual stresses in the wheel following fabrication. Knowledge of, and the ability to predict, these stresses is useful in assessing the ability of wheels to perform safely under expected service conditions.

A finite element analysis is performed which simulates portions of the processing sequence. A heat transfer analysis determines the transient thermal distribution during quenching. The mechanical (stress) analysis employs an elastic-plastic material model with kinematic hardening and includes viscoelastic creep behavior. A baseline scenario is developed to represent the best available estimate of processing parameters and material properties for the analysis.

predictions indicate development of residual circumferential (hoop) compression on the order of 200 MPa (29 ksi) in the wheel rim of approximately 3.75 cm (1.48 inches). Modifications to the baseline scenario were studied in order to understand which stics of the analysis resulted in the most significant changes in the results.

14. SUBJECT TERMS
Residual stress, railroad wheels, quenching, finite element analysis, viscoelastic creep

15. NUMBER OF PAGES
104

16. PRICE CODE

17. SECURITY CLASSIFICATION OF REPORT	18. SECURITY CLASSIFICATION OF THIS PAGE	19. SECURITY CLASSIFICATION OF ABSTRACT	20. LIMITATION OF ABSTRACT
Unclassified	Unclassified	Unclassified	Unlimited

EXECUTIVE SUMMARY

This report is tenth in a series of engineering studies on railroad vehicle wheel performance. The work was performed by the Volpe National Transportation Systems Center (Volpe Center), in support of the Office of Research and Development of the Federal Railroad Administration (FRA). The reports in the series are listed on page 91.

In the fall of 1991, FRA safety inspectors became aware of frequent wheel cracking observed in several fleets of commuter railcars in the New York City metropolitan area. The defects appeared as small parallel cracks oriented axially on the wheel. Several of the defects were metallurgically sectioned to expose the crack faces. Characteristic beachmarks (small ridges) confirm fatigue as the crack growth driving mechanism. Each of the ridges corresponds to incremental crack growth as a consequence of an extreme braking event.

This report describes a simulation of the manufacturing process of railroad car wheels. Specifically, the goal is to determine the residual stresses, those stresses which remain in the wheel following fabrication. Knowledge of, and the ability to predict, these stresses is useful in assessing the ability of wheels to perform safely under expected service conditions and is required for application of the shakedown residual stress estimation technique which was documented in the seventh report.

A finite element analysis is performed which simulates the processing sequence. Following initial forming, the wheels are quenched, then placed in an annealing furnace for several hours, and finally air-cooled to room temperature. A heat transfer analysis determines the transient thermal distribution during quenching of these wheels from high temperature. It is followed by a decoupled stress analysis designed to predict the resultant stress distribution which evolves during cooling.

The mechanical (stress) analysis employs an elastic-plastic material model with kinematic hardening and includes viscoelastic creep behavior to simulate the effects of stress relaxation during the annealing portion of the manufacturing process. A baseline scenario is developed to represent the best available estimate of processing parameters and material properties for the analysis.

Baseline predictions indicate development of residual circumferential (hoop) compression in the wheel rim, the target of the manufacturing process, to a depth of approximately 3.75 cm (1.48 inches). The value of the compressive stress at the wheel tread is on the order of 200 MPa (29 ksi). Several modifications to the baseline scenario were studied in order to understand which characteristics of the analysis resulted in the most significant changes in the results. Of the variations examined, the inclusion of viscoelastic creep behavior has been identified as an important requirement in these simulations.

METRIC/ENGLISH CONVERSION FACTORS

ENGLISH TO METRIC

LENGTH (APPROXIMATE)

1 inch (in)	=	2.5 centimeters (cm)
1 foot (ft)	=	30 centimeters (cm)
1 yard (yd)	=	0.9 meter (m)
1 mile (mi)	=	1.6 kilometers (km)

AREA (APPROXIMATE)

1 square inch (sq in, in^2)	=	6.5 square centimeters (cm^2)
1 square foot (sq ft, ft^2)	=	0.09 square meter (m^2)
1 square yard (sq yd, yd^2)	=	0.8 square meter (m^2)
1 square mile (sq mi, mi^2)	=	2.6 square kilometers (km^2)
1 acre = 0.4 hectare (he)	=	4,000 square meters (m^2)

MASS - WEIGHT (APPROXIMATE)

1 ounce (oz)	=	28 grams (gm)
1 pound (lb)	=	0.45 kilogram (kg)
1 short ton = 2,000 pounds (lb)	=	0.9 tonne (t)

VOLUME (APPROXIMATE)

1 teaspoon (tsp)	=	5 milliliters (ml)
1 tablespoon (tbsp)	=	15 milliliters (ml)
1 fluid ounce (fl oz)	=	30 milliliters (ml)
1 cup (c)	=	0.24 liter (l)
1 pint (pt)	=	0.47 liter (l)
1 quart (qt)	=	0.96 liter (l)
1 gallon (gal)	=	3.8 liters (l)
1 cubic foot (cu ft, ft^3)	=	0.03 cubic meter (m^3)
1 cubic yard (cu yd, yd^3)	=	0.76 cubic meter (m^3)

TEMPERATURE (EXACT)

[(x-32)(5/9)] °F = y °C

METRIC TO ENGLISH

LENGTH (APPROXIMATE)

1 millimeter (mm)	=	0.04 inch (in)
1 centimeter (cm)	=	0.4 inch (in)
1 meter (m)	=	3.3 feet (ft)
1 meter (m)	=	1.1 yards (yd)
1 kilometer (km)	=	0.6 mile (mi)

AREA (APPROXIMATE)

1 square centimeter (cm^2)	=	0.16 square inch (sq in, in^2)
1 square meter (m^2)	=	1.2 square yards (sq yd, yd^2)
1 square kilometer (km^2)	=	0.4 square mile (sq mi, mi^2)
10,000 square meters (m^2)	=	1 hectare (ha) = 2.5 acres

MASS - WEIGHT (APPROXIMATE)

1 gram (gm)	=	0.036 ounce (oz)
1 kilogram (kg)	=	2.2 pounds (lb)
1 tonne (t)	=	1,000 kilograms (kg)
	=	1.1 short tons

VOLUME (APPROXIMATE)

1 milliliter (ml)	=	0.03 fluid ounce (fl oz)
1 liter (l)	=	2.1 pints (pt)
1 liter (l)	=	1.06 quarts (qt)
1 liter (l)	=	0.26 gallon (gal)
1 cubic meter (m^3)	=	36 cubic feet (cu ft, ft^3)
1 cubic meter (m^3)	=	1.3 cubic yards (cu yd, yd^3)

TEMPERATURE (EXACT)

[(9/5) y + 32] °C = x °F

QUICK INCH - CENTIMETER LENGTH CONVERSION

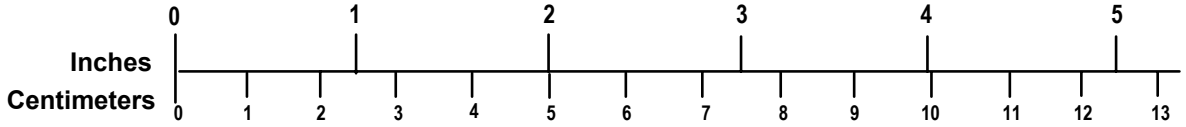

QUICK FAHRENHEIT - CELSIUS TEMPERATURE CONVERSION

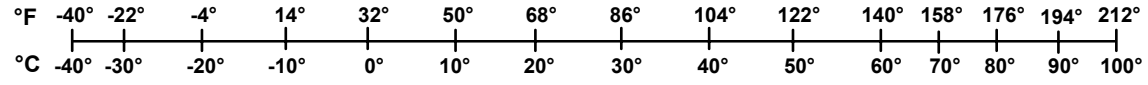

For more exact and or other conversion factors, see NIST Miscellaneous Publication 286, Units of Weights and Measures. Price $2.50 SD Catalog No. C13 10286

Updated 6/17/98

TABLE OF CONTENTS

Section **Page**

EXECUTIVE SUMMARY iii

LIST OF FIGURES vii

LIST OF TABLES x

1. INTRODUCTION 1

    1.1 Background 1
    1.2 Wheel Performance Assessment Strategy 3
    1.3 Purpose and Scope 5
    1.4 Estimation of Residual Stresses in Wheels 6
        1.4.1 Freight Wheel Studies 6
        1.4.2 Passenger Wheel Studies 7

2. MANUFACTURING PROCESS MODEL 9

    2.1 Wheel Manufacturing Process 9
    2.2 Metallurgical Considerations 11
    2.3 Transient Heat Transfer Model 13
    2.4 Mechanical Model 16

3. IMPLEMENTATION 21

    3.1 Finite Element Code Selection 21
    3.2 Finite Element Mesh Development 22
    3.3 Heat Transfer Analysis 25
        3.3.1 Thermal Material Properties 26
        3.3.2 Convection Boundary Conditions 26
        3.3.3 Radiation Boundary Conditions 28
        3.3.4 Execution 29
    3.4 Stress Analysis 30
        3.4.1 Mechanical Properties 30
        3.4.2 Time-Dependent Deformation 32
        3.4.3 Execution 33

4. MANUFACTURING RESIDUAL STRESS ESTIMATION STRATEGY - RESULTS 35

    4.1 Baseline Conditions 35
        4.1.1 Results of Baseline Thermal Analysis 36
        4.1.2 Results of Baseline Stress Analysis 39

TABLE OF CONTENTS (cont.)

Section **Page**

4.2 Modifications to Baseline Conditions....45
4.2.1 Effect of Inclusion of Creep Effects....46
4.2.2 Effect of Variation of Quench Duration....48
4.2.3 Effect of Variation of Annealing Temperature....52
4.2.4 Effect of Variation of Thermal Expansion Coefficient....54
4.3 Assessment of Baseline Variations....58

5. CONCLUSIONS....59

APPENDIX A: Material Properties Used in Analyses....63
A.1 Thermal Properties....63
A.2 Mechanical Properties....64
A.3 Conversion of Tangent CTE to Secant CTE....66
A.4 Determination of Plastic Material Constants....67

APPENDIX B: Sample ABAQUS Data Files....71
B.1 Input file for Thermal Analysis....71
B.2 Input File for Stress Analysis....80

LIST OF FIGURES

Figure **Page**

1. Thermal cracks on 81.28 cm (32") diameter commuter wheels 2
2. Exposed crack faces on two wheels 2
3. Schematic representation of three different railroad car wheel designs 3
4. Master plan for investigating the effects of service variables on wheel residual stresses 4
5. Simplified schematic of wheel forging operation 9
6. Isothermal transformation diagram for 1050 wheel steel (adapted from van der Voort [18] 12
7. Austenite (fcc) and ferrite (bcc) crystal structures (from Krauss [39]) 12
8. Effect of residual hoop compression in cracked wheel 13
9. Schematic of quenching process 14
10. Wheel quench schematic illustrating support concept 15
11. Translation of cartesian (a) to cylindrical (b) coordinate systems 17
12. Elastic-plastic material models 17
13. Finite element representation of S-plate wheel 23
14. Wheel rim detail for three meshes used in present study 24
15. Passenger wheel quench schedule 25
16. Tread region of Mesh 2 exposed to water spray quench, approximately 8.25 cm (3.25 in) 27
17. Heat transfer coefficient of water spray quench (from Liš…i‰ et al [49]) 27
18. Relative heat loss due to convection and radiation 28
19. Hardening model used in ABAQUS 31
20. Temperature-dependent stress-strain data used in quench simulation 31
21. Creep strain rates for different assumed values of σ_{eff} and temperature 33
22. Timing for thermal and stress analyses using ABAQUS v. 5.5 34
23. Line through wheel rim along which data is plotted 36
24. Temperature distribution along line through rim for three meshes used in current study at end of quench (time=125 seconds) 37
25. Temperature distribution (in °C) in wheel rim at end of quench (time=125 seconds, MESH 2) 38
26. Baseline temperature-time history of two nodes superposed on isothermal transformation diagram of representative steel alloy 38
27. Circumferential (hoop) stress distribution (in MPa) in wheel rim at end of quench (time=125 seconds) 40
28. Circumferential (hoop) stress distribution (in MPa) in wheel rim at end of annealing (time=5 hours) 41
29. Circumferential (hoop) stress distribution (in Mpa) in wheel rim at end of process (time=10 hours) 41

LIST OF FIGURES (cont.)

Figure **Page**

30. Circumferential (hoop) stress distribution (in MPa) in wheel rim at end of quench (time=125 seconds, MESH 2) 42
31. Circumferential (hoop) stress distribution (in MPa) in wheel rim at end of annealing (time=5 hours, MESH 2) 43
32. Circumferential (hoop) stress distribution (in MPa) in wheel rim at end of process (time=10 hours, MESH 2) 43
33. Elements selected for hoop stress time histories 44
34. Time history of hoop stress evolution (in MPa) in two elements in wheel rim during first 500 seconds of quenching process 44
35. Time history of hoop stress evolution (in MPa) in two elements in wheel rim during entire quenching process 45
36. Time history of hoop stress (in MPa) in two elements in wheel rim during first 500 seconds of quenching process with and without creep effects 46
37. Time history of hoop stress (in MPa) in two elements in wheel rim during entire process with and without creep effects 47
38. Circumferential (hoop) stress distribution (in MPa) in wheel rim at end of process (time=10 hours) with and without inclusion of creep effects 48
39. Time history of hoop stress (in MPa) in wheel tread surface during first 500 seconds of process for different quench durations 49
40. Time history of hoop stress (in MPa) in base of rim during first 500 seconds of process for different quench durations 50
41. Time history of hoop stress (in MPa) in two elements in wheel rim during entire process for different quench durations 50
42. Circumferential (hoop) stress distribution (in MPa) in wheel rim at end of process (time=10 hours) for different quench durations 51
43. Time history of hoop stress (in MPa) in wheel tread surface during first 500 seconds of process for different annealing temperatures 53
44. Time history of hoop stress (in MPa) in base of rim during first 500 seconds of process for different annealing temperatures 53
45. Time history of hoop stress (in MPa) in two elements in wheel rim during entire process for different annealing temperatures 54
46. Circumferential (hoop) stress distribution (in MPa) in wheel rim at end of process (time=10 hours) for different annealing temperatures 55
47. Variation in coefficient of thermal expansion data for steel 55
48. Time history of hoop stress (in MPa) in two elements in wheel rim during first 500 seconds of process for different assumed expansion coefficients 57

LIST OF FIGURES (cont.)

Figure **Page**

49. Time history of hoop stress (in MPa) in two elements in wheel rim during entire process for different assumed expansion coefficients 57
50. Circumferential (hoop) stress distribution (in MPa) in wheel rim at end of process (time=10 hours) for different assumed expansion coefficients 58
51. Results of simulations of manufacturing process modifications 60

A1. Specific heat versus temperature (°C) 63
A2. Thermal conductivity versus temperature (°C) 63
A3. Young's modulus versus temperature (°C) 64
A4. Poisson's ratio versus temperature (°C) 64
A5. Yield strength versus temperature (°C) 64
A6. Secant coefficient of thermal expansion for quench simulation versus temperature (°C) 65
A7. Hardening modulus versus temperature (°C) 65

LIST OF TABLES

Table **Page**

1. Chemical composition of wheel steel 10
2. AAR wheel classes 10
3. Time step information for ABAQUS heat transfer analysis (MESH 2) 29
4. Time step information for ABAQUS stress analysis (MESH 2) 34
5. Baseline conditions for quench simulation 35
6. Effect of creep behavior on hoop stress prediction (MPa) 47
7. Effect of quench duration on hoop stress prediction (MPa) 49
8. Effect of annealing temperature on hoop stress prediction (MPa) 52
9. Modifications to thermal expansion coefficient 56
10. Effect of thermal expansion coefficient on hoop stress prediction (MPa) 56
11. Summary of results of estimates of manufacturing stresses 60

A1. Specific heat 63
A2. Thermal conductivity 63
A3. Young's modulus 64
A4. Poisson's ratio 64
A5. Yield strength 64
A6. Secant coefficient of thermal expansion for quench simulation 65
A7. Hardening modulus 65

1. INTRODUCTION

This report is tenth in a series of studies conducted at the John A. Volpe National Transportation Systems Center (Volpe Center), which began in the fall of 1991.[1]

Under Project Plan Agreement RR-28 sponsored by the Federal Railroad Administration (FRA) Office of Research and Development Equipment and Operating Practices Research Division, the Volpe Center is conducting studies to determine mechanisms causing wheel failures in service, developing predictive techniques, and assessing options for improving safety performance.

Recent research indicates that the magnitude and distribution of residual stresses in railroad car wheels may be a good indicator of their likelihood to experience fatigue cracking under service conditions. Investigation of the effects of service conditions on wheel residual stresses requires knowledge of the as-manufactured condition of the wheel.

1.1 BACKGROUND

In the fall of 1991, FRA safety inspectors became aware of frequent wheel cracking observed in several fleets of commuter railcars in the New York City metropolitan area. The defects appeared as small parallel cracks oriented axially on the wheel as shown in Figure 1. Several of the defects were metallurgically sectioned to expose the crack faces, an example of which is shown in Figure 2. Characteristic beachmarks (small ridges) confirm fatigue as the crack growth driving mechanism. Each of the ridges corresponds to incremental crack growth as a consequence of an extreme braking event.

These cars are owned and operated by the Metro North Commuter Railroad (MNCRR), the Long Island Rail Road (LIRR), and New Jersey Transit (NJT). The FRA requested the Volpe Center's assistance in determining the cause of the cracking and developing a plan of action which could permit continued transit operation while remedial actions to deal with the cracking were sought and implemented, since current FRA regulations prohibit operation of a train with cracked wheels. Suspension of operation of these fleets in compliance with the regulations would have caused severe problems for the thousands of commuters who rely on this service daily.

[1] The reports in the series are listed at the end of this document.

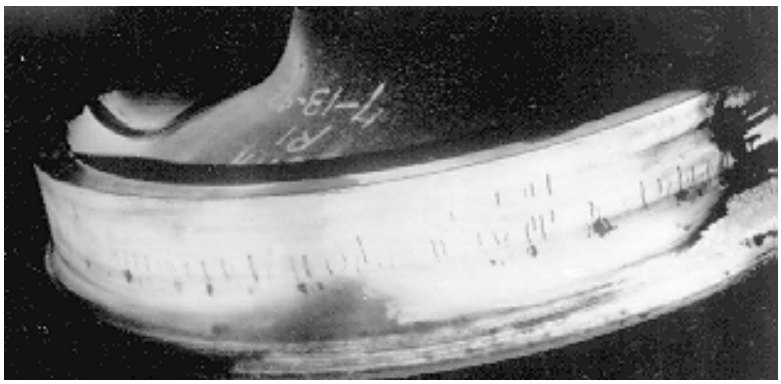

Figure 1. Thermal cracks on 81.28 cm (32") diameter commuter wheels.

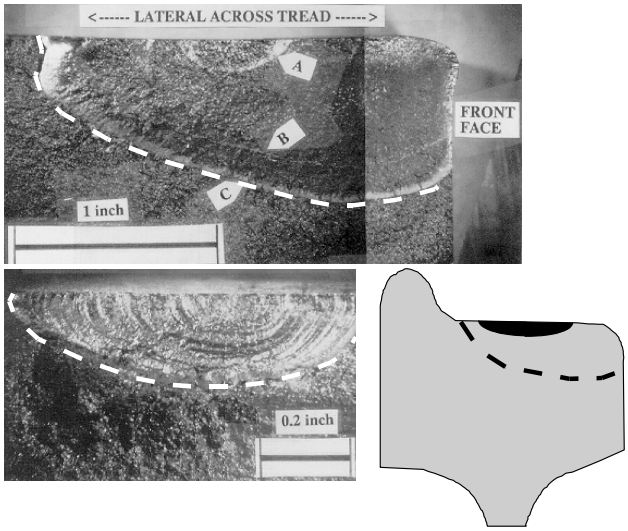

Figure 2. Exposed crack faces on two wheels.

All commuter railroads use the same basic wheel design under their vehicles. Railcar wheels serve several functions, which include supporting the car weight and steering the vehicle through curves, as well as serving as heat sinks during on-tread braking. An 81 cm (32 inch) diameter S-plate wheel is employed for these electric multiple unit operations. These passenger vehicle wheels are manufactured in the United States by three major manufacturers: Griffin Wheel (Chicago, Illinois), Standard Steel (Cranberry Township, Pennsylvania) and Edgewater Steel Company (Oakmont, Pennsylvania).

The plate acts like a spring to permit radial breathing of the wheel when the rim is heated during braking and the plate and hub remain cooler and stiffer. This results in lower thermally induced wheel stresses as the flexible plate allows the hot rim to expand without creating significant radial stresses in the plate.

Figure 3 contains a schematic of three different wheel designs. These are the straight and S-plate 81 cm (32 inch) diameter passenger wheels and a 91 cm (36 inch) diameter wheel used

for freight service, and illustrate the differences between the wheels used for various applications.

The passenger wheels shown are multiple-wear wheels which means that they have thicker rims (on the order of 6.35 cm or 2.5 inches). These wheels may be trued (reprofiled) several times during their life until the rim thickness is reduced to the condemning limit. The freight wheel shown is a one-wear wheel, which means that its reprofiling and condemning limits are approximately equal. The actual geometric differences in the radial direction are somewhat diminished in the figure as only one-half of the cross-section is shown and the region occupied by the axle has been removed. Figure 3 also includes reference to the regions in the wheel cross-section which will be used hereafter to identify those portions of the profile.

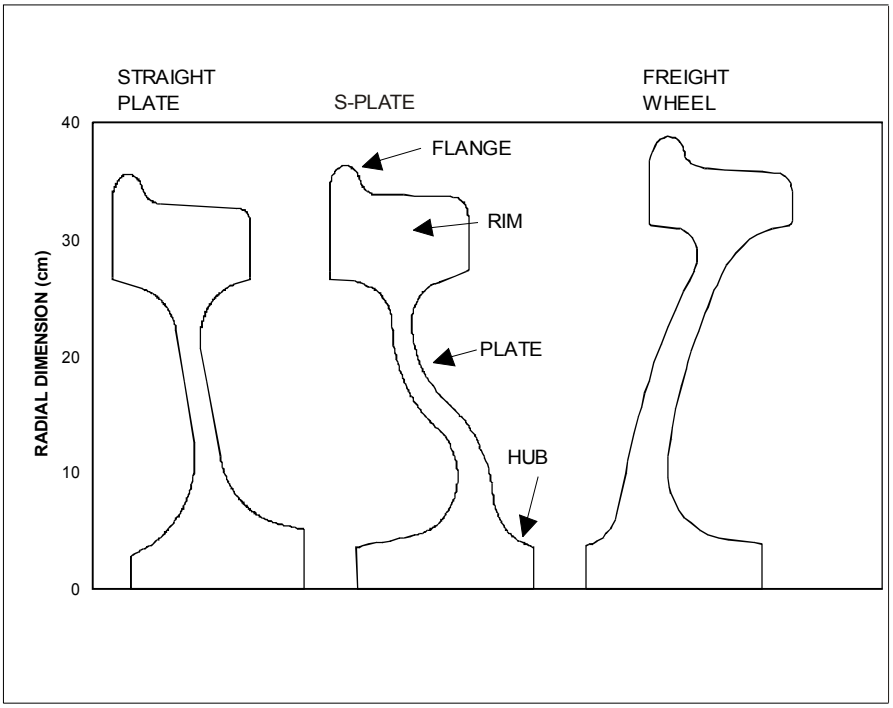

Figure 3. Schematic representation of three different railroad car wheel designs.

1.2 WHEEL PERFORMANCE ASSESSMENT STRATEGY

During the course of this investigation, the Volpe Center supported the FRA by providing engineering analyses and simulations to study the effects of operational loads on temperatures and stresses in these wheels [1-4]. The results of this body of research concluded that knowledge of the residual stress distribution in wheels may be an accurate indicator of their likelihood to experience cracking under operational conditions. A "master plan" (shown in Figure 4) was developed which lays out the strategy for investigating the distribution and magnitude of manufacturing and service-induced residual stresses.

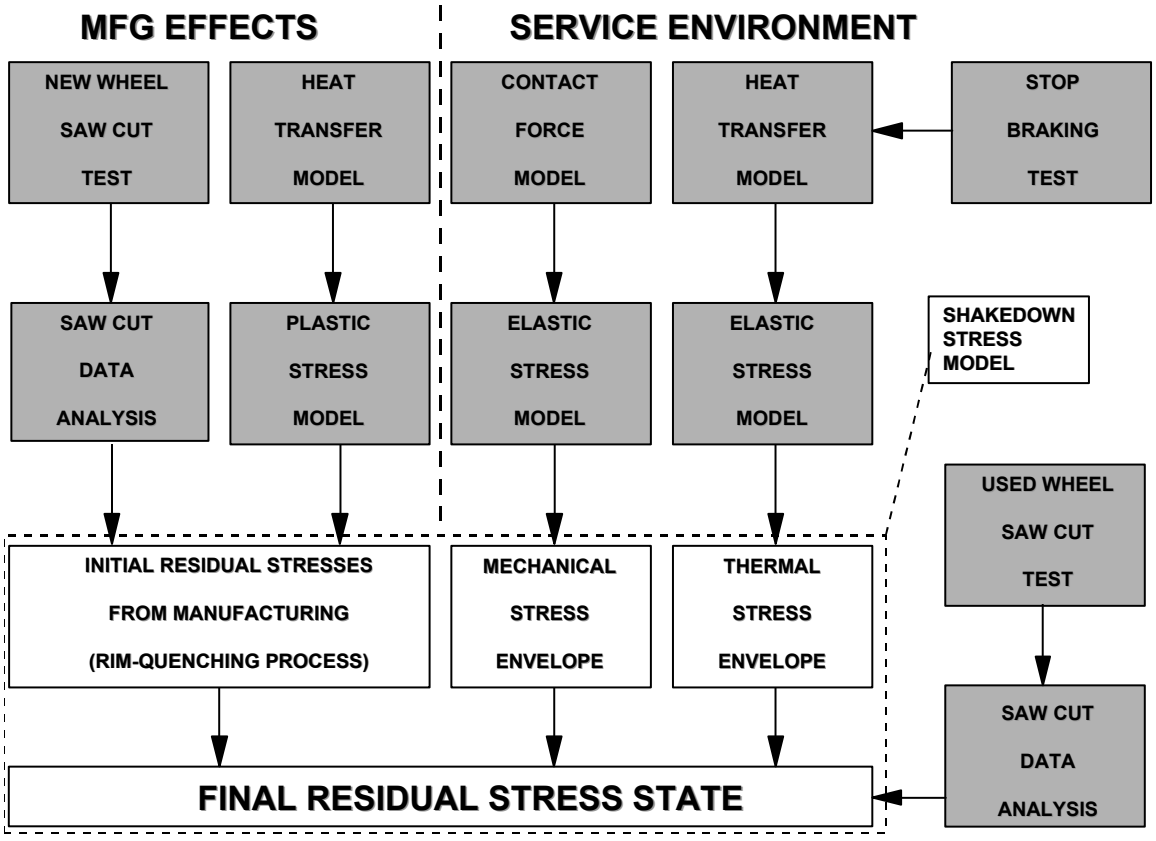

Figure 4. Master plan for investigating the effects of service variables on wheel residual stresses.

Residual stresses, those stresses which remain in a body after all applied loads are removed, exist in many engineering structures. These stresses can be induced intentionally during manufacture of a component, typically to improve its performance. When the part is eventually put to use, however, these initial stresses can be modified by service loading, sometimes to such an extent that the benefits of the manufacturing stresses are completely negated.

Residual stresses induced by manufacture, or modifications to these stress distributions after exposure to service conditions, are not apparent visually. The presence of these stresses can, however, have significant impact on the ability of the structure to resist failure under expected loads. The goal of many manufacturing processes is to establish a layer of compressive residual stress at the surface of parts to inhibit the formation and growth of cracks. The benefits of such processes may be jeopardized by service conditions which impose stresses, which, if sufficiently large, overcome the residual surface compression and may leave the structure in a state of surface tension. In this case, the structure becomes prone to the formation and growth of fatigue cracks.

This research plan calls for the development and exploitation of various numerical models to estimate the final residual stress state. This state is due to the combined effects on the initial residual stresses in wheels of contact loads from wheel and rail interaction, and thermal stresses from on-tread braking as shown in the dashed box in Figure 4. At each step, the modeling effort

is validated by laboratory and field tests designed to collect sufficient information to corroborate the model predictions (as shown in the shaded boxes in Figure 4).

Figure 4 shows how an estimate of the final residual stress state in railroad wheels can be made, based on the combined effects of manufacturing and service conditions. The left-hand portion of the figure illustrates the requirement that the initial residual stresses in the wheels following manufacture must be known. Requirements for computational procedures which take into account the transient heat transfer and stress analysis of a simulated manufacturing process are identified. Saw-cut testing is a destructive procedure by which relieved stresses in wheels are inferred from the opening or closing of a cut made in the wheel rim. This information can be used to validate the computer predictions of residual stress.

The right-hand side of Figure 4 lays out a strategy for making an estimate of the contribution of service loads to the final residual stress state. Similar to the manufacturing portion, analysis of the contact forces between the wheel and the rail defines the envelope of expected mechanical stresses in service. This analysis in ongoing and will be the subject of a future report.

1.3 PURPOSE AND SCOPE

This report focuses on an approach for estimating the residual stresses in a railroad commuter car wheel due to its manufacturing process. The strategy involves a finite element simulation of the process which takes into account the complex combination of boundary conditions and non-linear temperature-dependent material properties. Knowledge of the as-manufactured state is a key element in estimating residual stresses in wheels in service.

The scope is limited to engineering design analysis, computational mechanics (formulation and numerical analysis using computers), and related activities. The report does not include laboratory or field testing, instrumentation, or formal preparation of any detailed test plans or requirements.

The remainder of this section consists of background on the problem and related work on establishment of methodologies for making such estimates. The physical aspects of the manufacturing process and the associated metallurgical considerations which require attention during model development will be presented in Section 2. Section 3 describes the implementation strategy for executing the simulation and how the boundary conditions and material property dependencies are incorporated. The results of numerical simulations of the processing sequence will be presented in Section 4. The results emphasize the magnitude and depth of penetration of the circumferential (hoop) residual stress in the wheel rim since this has been identified as a reasonable means of assessing the likelihood of fatigue cracks to initiate and grow.

Section 5 consists of a summary of the work presented including comparisons with other published results, where possible, and recommendations for future extensions to this study.

1.4 ESTIMATION OF RESIDUAL STRESSES IN WHEELS

Most of the analytical work described in the literature which involves estimation of residual stresses in wheels has been performed under the assumption that the wheel is initially stress free. These studies seek instead to perform simulations of the effects of wheel-on-rail contact forces and thermal stresses due to braking for the purposes of evaluating their *relative* contributions to wheel stresses.

This type of analysis is appropriate for examining the residual stresses resulting from contact between the wheel and rail when considering, for example, increasing the load-carrying capacity of freight cars from 1175 kN (264,000 lb) to 1388 kN (312,000 lb). Thermal stresses will have different magnitudes (and possible different distributions) if the vehicle is stopping from 160 kph (100 mph) or from 128 kph (80 mph). These studies are useful, therefore, from the point of view of assessing the implications of change to current practice. In addition, most of the published work has involved study of these effects on freight car wheel performance. Some of the pertinent work is discussed below.

1.4.1 Freight Wheel Studies

Mikrut [5] provides a detailed study of the development of residual stresses in a 102 cm (40 inch) locomotive wheel. A rather coarse finite element mesh is employed in the analysis. Temperature-dependent thermal and mechanical properties were used with the exception of the coefficient of thermal expansion, which was assumed to be constant. This work does not examine service (contact and braking) effects but provides some experimental results on the time-dependent deformation (creep) phenomenon. Viscoelastic creep, or stress relaxation, occurs when a stressed body is held at elevated temperature for an extended period of time. Mikrut conducted a series of laboratory experiments to determine the required constants for use in the creep equation in his ANSYS[2] model. Creep permits relaxation of residual stresses and will be shown later to be an important consideration.

Perfect [6] describes an investigation of rim quenching of 102 cm (40 inch) Class C wheels which are instrumented with thermocouples during the process. The data collected from this experiment are used to conduct a finite element simulation of the quenching process for 84 cm (33 inch) wheels. Residual stresses were measured in an actual wheel using the hole drilling technique. Other wheels were induction heated to simulate drag braking and similarly tested to obtain estimates of residual stress. The conclusions of this work, however, indicate that quenched wheels (Class C) exhibit lower residual stresses than unquenched wheels (Class U) when subjected to simulated drag braking.

The work of Kuhlman et al. [7] represents a complete description of the application of the finite element technique to the prediction of residual stresses in railroad wheels due to the post-forming heat treatment. In this study, the Perfect analysis is extended to include the effects of creep and some of the characteristics of the phase transformation which occurs as the material

[2] ANSYS is a commercial finite element software package.

cools. The quench schedule is identical to that used in the work of Perfect. The most significant contribution of this work is the application of a power law creep equation (developed in [8]) which yields the strain rate due to the combined effects of stress and temperature. Kuhlman et al. show that the inclusion of creep effects is an important consideration in analytical estimates of residual stress in quenched wheels.

1.4.2 Passenger Wheel Studies

Rusin et al. [9] conducted an analysis to estimate residual stresses in passenger car (transit) wheels. In this approach, a finite element model is constructed which employs the same decoupled thermo-mechanical analysis scheme to determine the residual stresses in these wheels. The 81 cm (32 inch) S-plate passenger wheel is modeled; however, this wheel represents an improved design which has been optimized to minimize rim hoop stress reversal when the new wheel is exposed to service braking conditions. Initial manufacturing residual stresses are calculated using the procedure outlined by Kuhlman, et al. [7]. The quenching program and material parameters used were obtained from the same study. According to Coughlin [10], this specification is not appropriate for the passenger wheel application, and some modifications to the process variables have been suggested which will be incorporated in this study. No details of the results of this calculation are provided. This initial, as-manufactured state is then modified by the braking simulation.

Elements of some of the various schemes developed by others have been modified and extended to analyze the subject passenger wheels. In particular, several of the parameters in the quenching procedure outlined by Kuhlman et al. [7] have been adjusted in this study.

2. MANUFACTURING PROCESS MODEL

A two-step approach is proposed for estimating the residual stresses which remain in the wheel following quenching. As described earlier, the physical process to be modeled involves a heat transfer analysis which estimates the transient temperature distribution during the quenching operation followed by a stress analysis which uses these thermal distributions to estimate the evolution of the residual stresses over time.

The thermal analysis represents the conditions imposed during the manufacturing process, and focuses on the development and application of the appropriate boundary conditions and temperature-dependent material properties. The residual stress predictions are essentially by-products of the heat transfer analysis. These stresses arise from metallurgical considerations and the transient temperature distributions in the wheel which alter the mechanical properties.

The remainder of this section addresses the manufacturing process, wheel metallurgy, and the issues which require consideration in the development of the heat transfer and mechanical models of the quenching process.

2.1 WHEEL MANUFACTURING PROCESS

The subject 81 cm (32 inch) passenger wheel is manufactured using a multi-step forging process to initially press and form the wheel. The process of forming the wheel from the rough billet is illustrated in Figure 5 adapted from Kalpakjian [11].

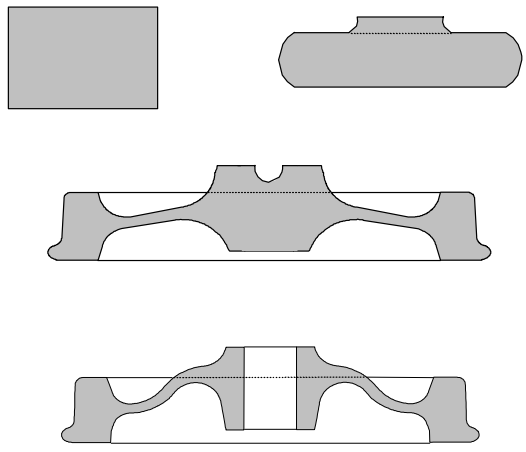

Figure 5. Simplified schematic of wheel forging operation.

The wheel blank is heated for approximately 5 hours to a temperature of 1175 °C (2150 °F). The wheel is formed through a series of pressing operations which transforms the original cylindrical block into the desired shape. The axle bore is produced by a punching operation, while the plate is formed by rolling as the wheel rotates. After the rolling process, the wheel diameter is increased. The conicity is introduced by pressing. The entire production occurs at high temperature to take advantage of the ductile properties of the material and to lessen the pressing forces required.

The wheel is then transported into an equalizing furnace which is maintained at 535 °C (1000 °F). The wheel is next moved into a tunnel-like gas-fired furnace in which it is uniformly reheated to 871 °C (1600 °F). The wheels are removed from this furnace in groups and are placed on rollers which support them during the spray quench [12]. The duration of the quench is dependent on the wheel rim thickness and on the diameter of the wheel. During spray quenching, only the tread portion of the wheel is quenched. This heat treatment establishes residual compressive stresses in the rim and is a common means of either creating or controlling the magnitude of residual stresses in a given part [13, 14, 15, 16].

The wheels are composed of AISI 1050 steel which has the alloy content, expressed in terms of weight percent (w/o), shown in Table 1. Wheels for railroad service are classified into several categories (or "classes") by the Association of American Railroads (AAR) as shown in Table 2 which lists some of the pertinent parameters of the wheels in each of these groups [17]. The wheels which are the subject of this study are Class L.

Table 1. Chemical composition of wheel steel.[3]

C	Mn	S	P	Si
≤ 0.47	0.60 to 0.85	< 0.05	< 0.05	> 0.15

Table 2. AAR wheel classes.

AAR WHEEL CLASS	CARBON CONTENT (weight %)	HARDNESS (BHN[4]) MIN-MAX	YIELD STRENGTH[5] MPa (ksi)	CONDITIONS FOR USE (TYPICAL)
U[6]	0.65-0.77		380 (55) RP	General service
L	≤0.47	197 - 277	430 (63) R 310 (45)P	High speed service Severe braking conditions Light wheel loads
A	0.47-0.57	255 - 321	450 (65) R 310 (45) P	High speed service Severe braking conditions Moderate wheel loads
B	0.57-0.67	277 - 341	550 (80) R 380 (55) P	High speed service Severe braking conditions Heavier wheel loads
C	0.67-0.77	321 - 363	620 (90) R 380 (55) P	(1) Light braking conditions, high wheel loads (2) Heavier braking conditions, off-tread braking systems employed

[3] Source: Association of American Railroads [17].

[4] Brinell Hardness Number.

[5] The wheel rim and plate have different properties (due to the heat treatment). R denotes the rim and P denotes the plate.

[6] Class U wheels are untreated. That is, there is no heat treatment applied to induce residual stresses in these wheels.

2.2 METALLURGICAL CONSIDERATIONS

Figure 6 is the isothermal transformation diagram for the AISI 1050 material, adapted from van der Voort [18]. The figure is used to approximate the microstructure of a material which is cooled from elevated temperature. The horizontal axis represents time (on a log scale) while the vertical axis denotes the temperature in Centigrade. The "A," "F," "C," and "M" designations on the figure denote the austenite, ferrite, cementite, and martensite microstructures, respectively. The horizontal lines in Figure 6 establish boundaries above or below which desired microstructures are formed in the material. The major difference in the possible microstructures is the introduction of carbon atoms.

The austenite start and finish lines (As and Af) indicate the temperatures at which a cool material will begin and complete its transformation into austenite when heated, along the path labeled 1 in Figure 6. Austenite has a face-centered cubic (fcc) crystalline structure, as shown in Figure 7, corresponding to the closest possible atomic spacing and is the parent phase of all other possible microstructures. For this material, the As temperature is 721 °C (1330 °F) and the Af temperature is 766 °C (1410 °F). Carbon atoms diffuse into the interstitial sites between the iron atoms shown in the figure. Iron atom spacing is denoted in the figure in angstroms (Å; 1 Å = 10^{-10} m). As such, austenite is a solid solution of iron and carbon.

The martensite start line (Ms) indicates the temperature at which hot material will transform into martensite, during rapid cooling as shown by path 2 in Figure 6. Martensite is a hard brittle structure which is unsuitable for application as a wheel material. It has a body-centered microstructure similar to ferrite, since the carbon atoms, not having sufficient time to diffuse, are trapped in the body-centered structure.

If austenite is cooled at a slower rate than would be necessary to form martensite (such as along paths 3 or 4 in Figure 6) two different phases, ferrite and cementite are formed. Such a transformation, in which a single phase transforms into two different phases, is called a eutectoid transformation. Ferrite is a body-centered cubic structure (bcc), as shown in Figure 7. Ferrite has much smaller interstitial sites, which means that the solubility of carbon in ferrite is much lower than in austentite. Cementite is formed when the solubility limit of carbon in ferrite is exceeded, and is a compound composed of one atom of carbon and three iron atoms (Fe_3C) [19].

The formation of ferrite and cementite in alternating lamellae (layers) is called pearlite. Rapid, controlled cooling (as along path 3 in Figure 6) results in fine-grained pearlite, as the grains are formed quickly and have insufficient time to grow. Pearlite is the desired microstructure for railroad wheel rims. Coarser-grained pearlite will be formed following cooling path 4 in Figure 6.

Transformation from austenite to ferrite and cementite involves a release of heat and a slight volume expansion (due to the fcc to bcc transformation). This heat release is called the latent heat of phase change. This process can be thought of as an internal heat source of short duration. This heat generation alters the cooling path while it is occurring. The implications of this phenomenon will be discussed later.

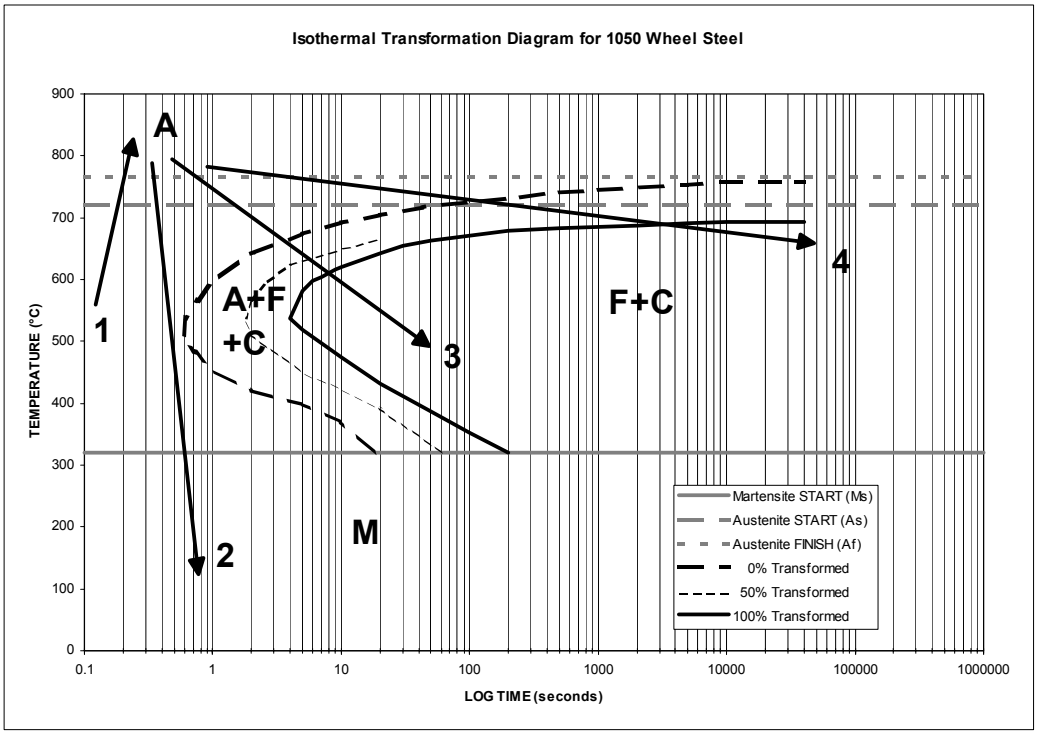

Figure 6. Isothermal transformation diagram for 1050 wheel steel (adapted from van der Voort [18]).

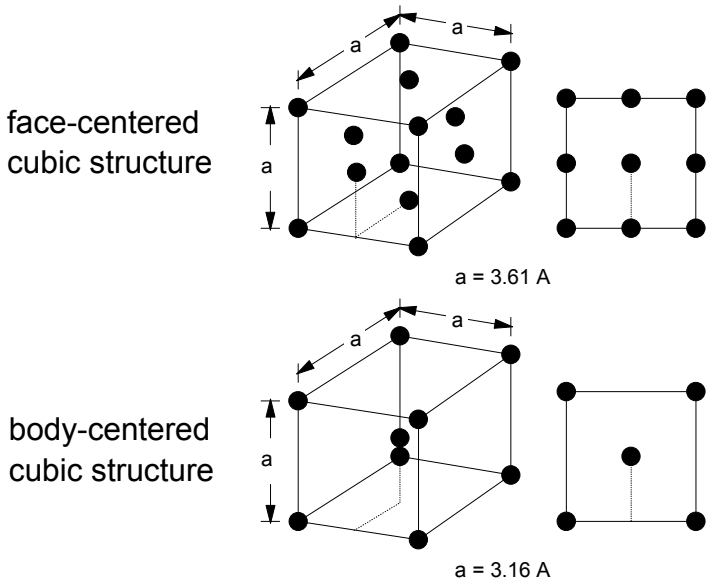

Figure 7. Austenite (fcc) and ferrite (bcc) crystal structures (adapted from Krauss [19]).

The post-forging heat treatment involves reheating the wheel to a temperature above its austenitizing temperature of 766 °C (1410 °F). At this temperature, any residual stresses which may have been induced during the forming process are relieved. Once reheated, the wheel rim is

exposed to a water spray quench of the tread area for several minutes. This is a super-critical quench, as the material is initially above the Af temperature. The non-quenched wheel surfaces are exposed to ambient conditions. The quenched area experiences accelerated cooling, and the material in the vicinity of the tread follows path 3 in Figure 6. This results in the formation of fine-grained pearlite in the rim. The remainder of the wheel cools at a much slower rate (path 4 in Figure 6) and coarser-grained pearlite is the resulting microstructure.

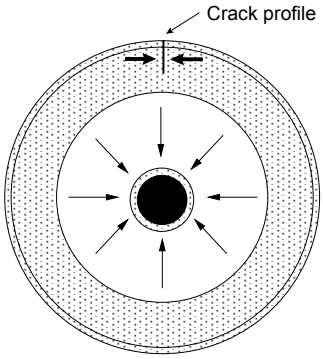

Figure 8. Effect of residual hoop compression in cracked wheel.

The variation in the microstructure (ranging from fine-grained pearlite in the rim to coarse-grained pearlite in the plate and hub) accounts for the differences in the room-temperature mechanical properties of the wheel as shown in Table 2. During the quench, the rim cools and stiffens quickly, while the plate and hub are still hot and somewhat softer. As the plate and hub of the wheel cool and contract radially, residual circumferential (hoop) compression is developed in the rim. This is a desired outcome, as hoop compression in the wheel rim helps to prevent the formation of fatigue cracks and retard their growth when they do occur, as illustrated in the schematic in Figure 8.

Following the quench, the wheel is annealed in a furnace at 496 °C (925 °F) for several hours. Steels are annealed to reduce brittleness (by transforming any martensite present into spheroidite) and to increase toughness (ability to resist cracking or fracture). Annealing is a suitable heat treatment for railroad wheels as it permits partial relief of residual stresses which remain after quenching. This process can be performed at any temperature (up to the As) and its selection is determined from the balance struck between the hardness (or strength) and toughness dictated by service demands. After the desired period at temperature is completed, the wheels are allowed to cool to room temperature, which requires about six hours.

2.3 TRANSIENT HEAT TRANSFER MODEL

The quenching process consists of several steps, each of which imposes different boundary conditions on the model. A schematic of the process is shown in Figure 9, which represents the ambient environment imposed on the tread. The wheel is assumed to be initially at a uniform temperature, QT, which is usually some temperature above its austenitizing temperature, Af, in Figure 6. As the forging operation induces large residual stresses due to the plastic deformation which occurs during pressing, the wheel is re-austenitized and held at elevated temperature (QT) for a sufficient time to remove these undesired stresses. For the purposes of this study, it is assumed that this period has elapsed, and the stress-free condition shall represent the initial state of the wheel.

Conduction in the wheel itself occurs during the cooling process. The unsteady heat conduction is governed by equation (1), [40]

$$\nabla^2 T = \frac{\rho c_p}{k}\frac{\partial T}{\partial t} - \dot{q}_v \qquad (1)$$

in which

ρ = the material density
c_p = the specific heat
k = thermal conductivity

all of which can vary with temperature. The $\dot{q}_v$ term in equation (1) represents the heat generated during the phase transformation from austenite. The latent heat release will be discussed later.

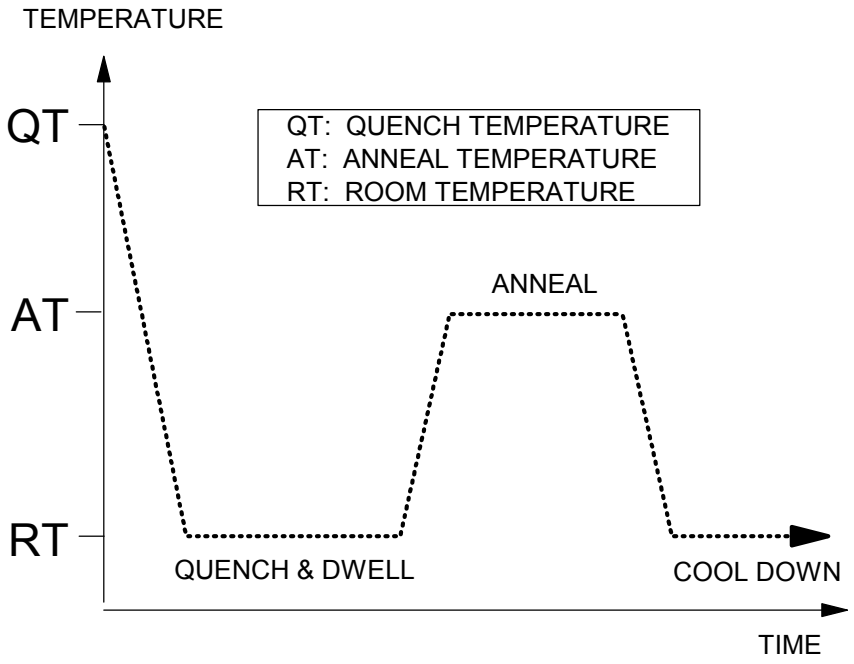

Figure 9. Schematic of quenching process.

At time t = 0, the wheel is assumed to be exposed to room temperature and the quenchant is applied. It is now necessary to characterize the heat transfer from the surfaces of the wheel to the environment. Convective losses and, due to the initially high temperature, radiative losses must be considered.

Due to the presence of the quenchant on the wheel tread surface, convective losses here differ from those elsewhere on the wheel surface. The rate of heat loss due to convection $\dot{q}_c''$ can be estimated according to equation (2):

$$\dot{q}_c'' = h_c (T - T_\infty)^a (T - T_\infty) \qquad (2)$$

where

$$h_c = h_{wa} \text{ or } h_c = h_{ww}$$

in which h_{wa} or h_{ww} denotes the heat transfer coefficient from the wheel to air or from the wheel to the water quenchant, which is assumed to be at room temperature. T represents the surface temperature and T_∞ denotes the ambient temperature. The exponent, a, has a value of zero for forced convection (in this case) and (usually) a value of 0.25 for free convection. Convection occurs from all surfaces of the wheel. The wheel surfaces in contact with the support, on which the wheel is assumed to lie, are treated somewhat differently. As it is assumed that the support is a runout table presumably made of steel, a heat transfer coefficient has been developed to simulate this condition. Assume that the portion of the wheel surface in contact with the support (referring to Figure 10) is of length L and the thickness of the table is also assumed to be L. The area of the interface, A, can be determined as

$$A = \pi (r_o^2 - r_i^2) \tag{3}$$

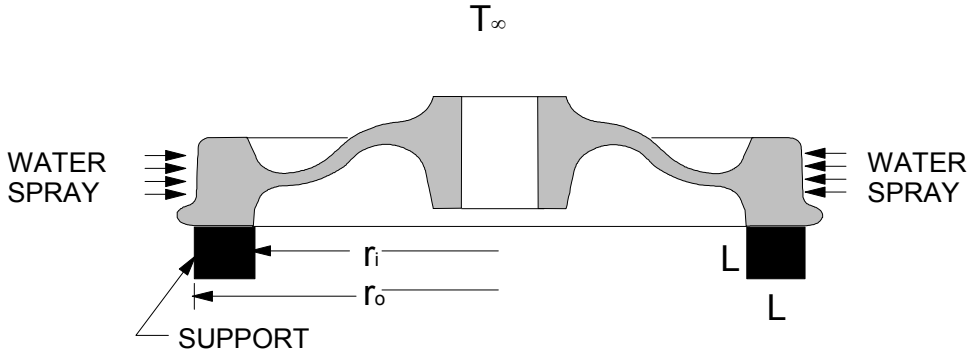

Figure 10. Wheel quench schematic illustrating support concept.

where r_o and r_i represent the outer and inner radii of the support. The simulated heat transfer coefficient is obtained by multiplying the thermal conductivity of the steel support (assumed to have the same value as the wheel material) by the ratio L/A, which is approximately equal to 0.5. This procedure accounts for the increased rate of heat loss across the steel on steel interface and assumes perfect (complete) contact. At room temperature, the thermal conductivity of steel is 60 W/m °C. The artificial heat transfer coefficient corresponding to this value is approximately 30 W/m^2 °C.

The latent heat of phase change, as described earlier, represents the evolution of heat during the austentite to pearlite transformation. Recalling Figure 6, the transformation begins in the material at the time when its temperature reaches the 0 percent transformed curve and is complete when the time-temperature trajectory crosses the 100 percent transformed curve. This process, therefore occurs over time, and does not occur simultaneously everywhere in the cooling body.

The latent heat of phase change for steel is 40310 J/kg K (9.63 BTU/lb$_m$ °F). This evolution of heat per unit mass causes a local rise in temperature during the transformation. Since the temperature gradients in the quenched wheel are responsible for development of the residual stresses, this effect is included in the analysis.

Radiation losses are also assumed to occur from all wheel surfaces. These losses can be characterized by the following equation [20]:

$$\dot{q}_r'' = \sigma \varepsilon (T^4 - T_\infty{}^4) \tag{4}$$

in which

σ = the Stefan-Boltzmann constant ($5.67 \bullet 10^{-08}$ W/m^2 K^4)

ε = the dimensionless surface emissivity ($0 \le \varepsilon \le 1$)

2.4 MECHANICAL MODEL

To conduct the stress analysis from the transient temperature distribution developed above, some simplifying assumptions are required. All residual stresses which had been introduced during the forging process have been removed following re-austenization for a sufficient period of time. An elastic-plastic analysis is required to account for material yielding as the wheel is cooled from high temperature (when its mechanical properties are severely diminished).

Yielding is predicted based on the Mises-Hencky yield criterion in which the octahedral shearing stress (the "effective stress," σ_{eff}) is determined from the following equation in cylindrical coordinates [21]:

$$\sigma_{eff} = \sqrt{\frac{1}{2}\left[\left(\sigma_{rr} - \sigma_{zz}\right)^2 + \left(\sigma_{zz} - \sigma_{\theta\theta}\right)^2 + \left(\sigma_{\theta\theta} - \sigma_{rr}\right)^2 + 6\left(\sigma^2{}_{rz} + \sigma^2{}_{z\theta} + \sigma^2{}_{\theta r}\right)\right]} \tag{5}$$

in which the subscripts denote the directions of the stress components. For an axisymmetric analysis, as proposed here, the origin is located at the center of the axle bore at the same height as the back face of the wheel ($z = 0$), assuming the orientation shown in Figure 11. If the value of σ_{eff} is greater than the yield strength, Y, yielding occurs; otherwise the material behaves in purely elastic manner.

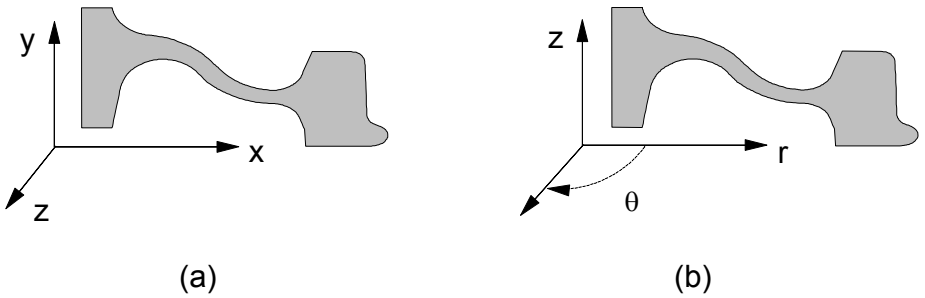

Figure 11. Translation of cartesian (a) to cylindrical (b) coordinate systems.

Figure 12 illustrates the possibilities for characterizing the stress-strain behavior. Figure 12(a) depicts a Ramberg-Osgood type stress-strain curve, which closely follows the typical curve for a metal. This type of curve is usually obtained from a uniaxial stress-strain test of a sample of the material. The material follows Hooke's Law in the elastic portion (stress is directly proportional to strain, and the slope of the curve is equal to Young's modulus) and, upon yielding, exhibits the characteristics shown in the figure. The dashed curves show the permanent strain in the material which is exhibited upon unloading. Figure 12(b) is a schematic of the stress-strain curve for an elastic perfectly plastic material. Using a model of this type, the material behaves like the previous one, however, upon yielding, the strain will increase with no increase in stress.

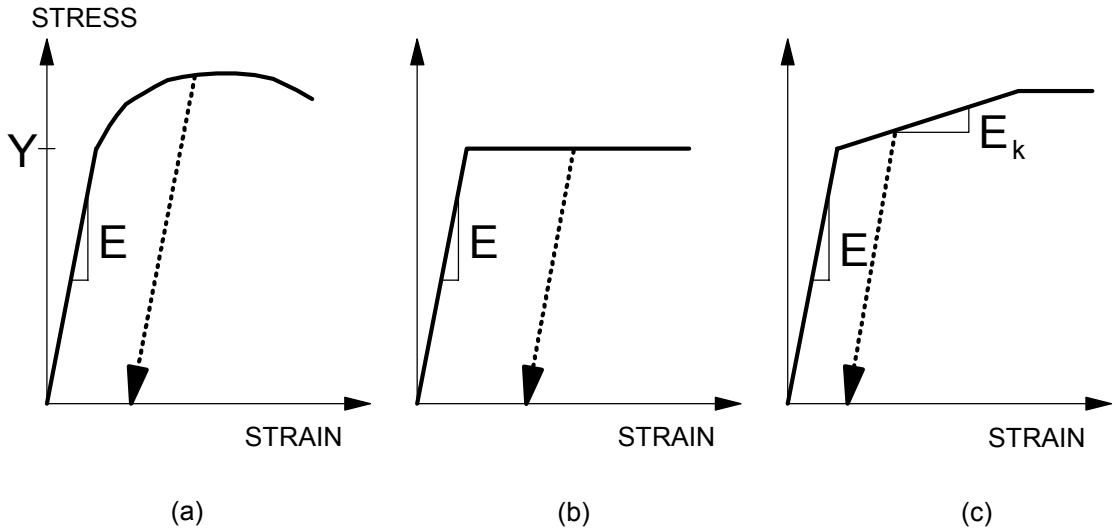

Figure 12. Elastic-plastic material models.

Figure 12(c) contains the bi-linear approximation which is considered for the current analysis. This material is an elastic plastic with kinematic hardening. It behaves as the others until yield occurs. Following the initial yielding, the material strain hardens and follows a new trajectory with a new slope, E_k. E_k is referred to as the hardening modulus and is on the order of $0.1E$ for many metals. Upon reaching the hardening limit, the material exhibits perfectly plastic behavior.

Further complicating this aspect of the analysis is the fact that the parameters which characterize the stress-strain behavior (Y, E, and E_k) all vary with temperature. This temperature dependency must be taken into account in order to properly estimate the manufacturing stresses in wheels.

Viscoelastic creep is considered in the mechanical analysis as well. The strains can be characterized by the following equation according to Sehitoglu and Morrow [8]:

$$\varepsilon_{total} = \varepsilon_e + \varepsilon_p + \varepsilon_c + \varepsilon_{th} \tag{6}$$

in which ε_e are the elastic strains, ε_p are the plastic strains, ε_c are the creep strains, and ε_{th} are the elastic thermal strains. Each of these individual strains can be defined to have the following form:

$$\varepsilon_e = \text{sgn}(\sigma)\,\frac{|\sigma|}{E} \tag{7}$$

$$\varepsilon_p = \text{sgn}(\sigma)\left(\frac{|\sigma|}{K'}\right)^{\frac{1}{n'}} \tag{8}$$

$$\varepsilon_c = \text{sgn}(\sigma)\int_0^t A\left(\frac{|\sigma|}{E}\right)^{\frac{1}{m}} e^{\frac{-\Delta H}{RT}}\,dt \tag{9}$$

$$\varepsilon_{th} = \int_{T_a}^{T_\infty} \alpha(T)\;dT \tag{10}$$

The *sgn(σ)* term serves to identify whether the individual strain component represents extension (positive) or contraction (negative). Equation (7) is the basic interpretation of Hooke's law. Equation (8) is a Ramberg-Osgood type power law equation which relates cyclic stress to cyclic plastic strain. This equation (and its parameters *K'* and *n'*) is used in fatigue studies and is therefore not of interest here. Equation (9) defines the steady-state creep strain. The sum of equations (7), (8), and (9) represent the mechanical strain and equation (10) defines the thermal strain.

Focusing on equation (9) the creep strain is shown to be related to the time integral of the product of some local area (A, say, of an element), the elastic strain raised to a power ($1/m$) and a decaying exponential. The exponent contains the variables ΔH and R which represent the activation energy (a material property expressed in cal/mol) and the universal gas constant (2 cal/mol °K) respectively. The temperature T is expressed in Kelvin.[7] From equation (11) it can be seen that the creep strain is primarily related to *time*, *stress,* and *temperature*.

[7] °K (Kelvin) = °C + 273.15.

The unknown in equation (9) is the value for m, which is determined from highly controlled laboratory experiments. These are basically cyclic tensile tests conducted at elevated temperatures. Experimental data has been developed by Sehitoglu and Morrow [8] which has enabled estimation of the creep strain rate by the power law in equation (11):

$$\dot{\varepsilon} = 4.64 \cdot 10^{-08} \left(\sigma_{eff}{}^{12.5} \right) e^{\frac{-53712}{T+460}} \tag{11}$$

in which $1/m = 12.5$, $\sigma = \sigma_{eff}$ (the Mises equivalent stress) and T is expressed in Fahrenheit. The rate obtained from equation (11) is valid over some increment of time during which the local value of σ_{eff} and T are defined.

3. IMPLEMENTATION

The finite element technique is used to estimate residual stresses in wheels following the post-forming heat treatment. A decoupled thermo-mechanical analysis is performed in which the temperature history of the wheel is developed first. The temperature data is then used to execute the stress analysis which yields the desired residual stress distribution.

In order to apply these techniques, several steps must be performed:

- select an appropriate code to implement the study,
- design and construct a finite element mesh suitable for the goals of the analysis,
- establish appropriate boundary conditions to impart sufficient realism to the model in order that results can be interpreted properly, and
- establish realistic external loading prescriptions so that the model response represents reality to the extent possible.

These steps will be discussed in the following sections.

3.1 FINITE ELEMENT CODE SELECTION

Recalling the requirements for the analysis specified in Section 2, the ABAQUS finite element code was selected for use in this study. ABAQUS [22] is a general purpose finite element code with the capability for uncoupled heat transfer analysis to model solid body heat conduction with general, temperature-dependent conductivity, internal energy and convection and radiation boundary conditions. All of these factors need to be included in the quenching model.

ABAQUS is well-suited to this application for several reasons. First, ABAQUS is an extremely versatile code and is extremely popular within the engineering community for solving problems in which simulation of complex material behavior is required. Also, ABAQUS possesses a special feature which allows the user to prescribe material properties and analysis parameters which can vary with time (and/or temperature) through the use of user subroutines. This represents a significant enhancement over other codes which permit variation of analysis conditions with time *or* temperature (but usually not both).

These user subroutines are written in the FORTRAN programming language. The user's routine is compiled at runtime and linked with the ABAQUS executable. This feature has been applied in the current analysis to control the selection of the appropriate heat transfer coefficient during the quenching process as well as to implement the viscoelastic creep model selected for use during the mechanical analysis. Preliminary models for the quenching process were developed using other computer codes such as TOPAZ2D [23] for the transient thermal analysis and NIKE2D [24] for the stress analysis. These programs perform essentially the same functions as

ABAQUS; however, NIKE2D lacks the appropriate material model necessary to include the combined effects of temperature and creep during the process.

3.2 FINITE ELEMENT MESH DEVELOPMENT

This project was initiated with several longer-term goals in mind. The target is to develop a means of estimating residual stresses in wheels due to all contributors (initial manufacturing, wheel on rail contact and thermal loads from braking) as illustrated in Figure 4. The strategy was to initially develop an estimate of the residual stresses due to manufacture and to subsequently apply the equivalent of contact stresses and thermal stresses from on-tread braking in order to estimate wheel rim stresses corresponding to service conditions. This goal has significant influence on the design of the mesh used in the quenching analysis. As the effects of contact and thermal loads are confined to a rather shallow region immediately below the tread surface, it is desirable to increase the mesh density in that location.

Since the manufacturing process and the eventual loading (contact and braking[8]) can be assumed to act uniformly along the wheel circumference, an axisymmetric (two-dimensional) representation of the wheel cross-section is deemed satisfactory for the purposes of this study. The wheel could, of course, be discretized in three dimensions by rotating the cross-section to generate an enormous number of brick elements. This will significantly impact solution time with no real gains in solution accuracy.

An initial finite element mesh was designed using the public domain code MAZE [25] as shown in Figure 13. A manufacturer's drawing [26] was digitized to generate the profile of the wheel, which was then manipulated into the mesh shown in Figures 13 and 14(a). This grid was subsequently modified in order that mesh density could be more easily increased in the tread region to accommodate calculation of contact and thermal stresses. The densification strategy is apparent in Figure 14 which illustrates the rim area of the models and identifies the numbers of nodes and elements in each. The portion of the mesh which is not illustrated is the same as that shown in Figure 13. The geometry of each of these meshes (nodal coordinates and element connectivity) was used to create an input file for ABAQUS to conduct the heat transfer analysis.

[8] Contact and thermal loads during braking are not axisymmetric loading conditions. Application of Fourier series techniques [8] permits an axisymmetric approximation of contact, and since a wheel in service is rotating rapidly, the thermal load can be assumed to act uniformly around the circumference.

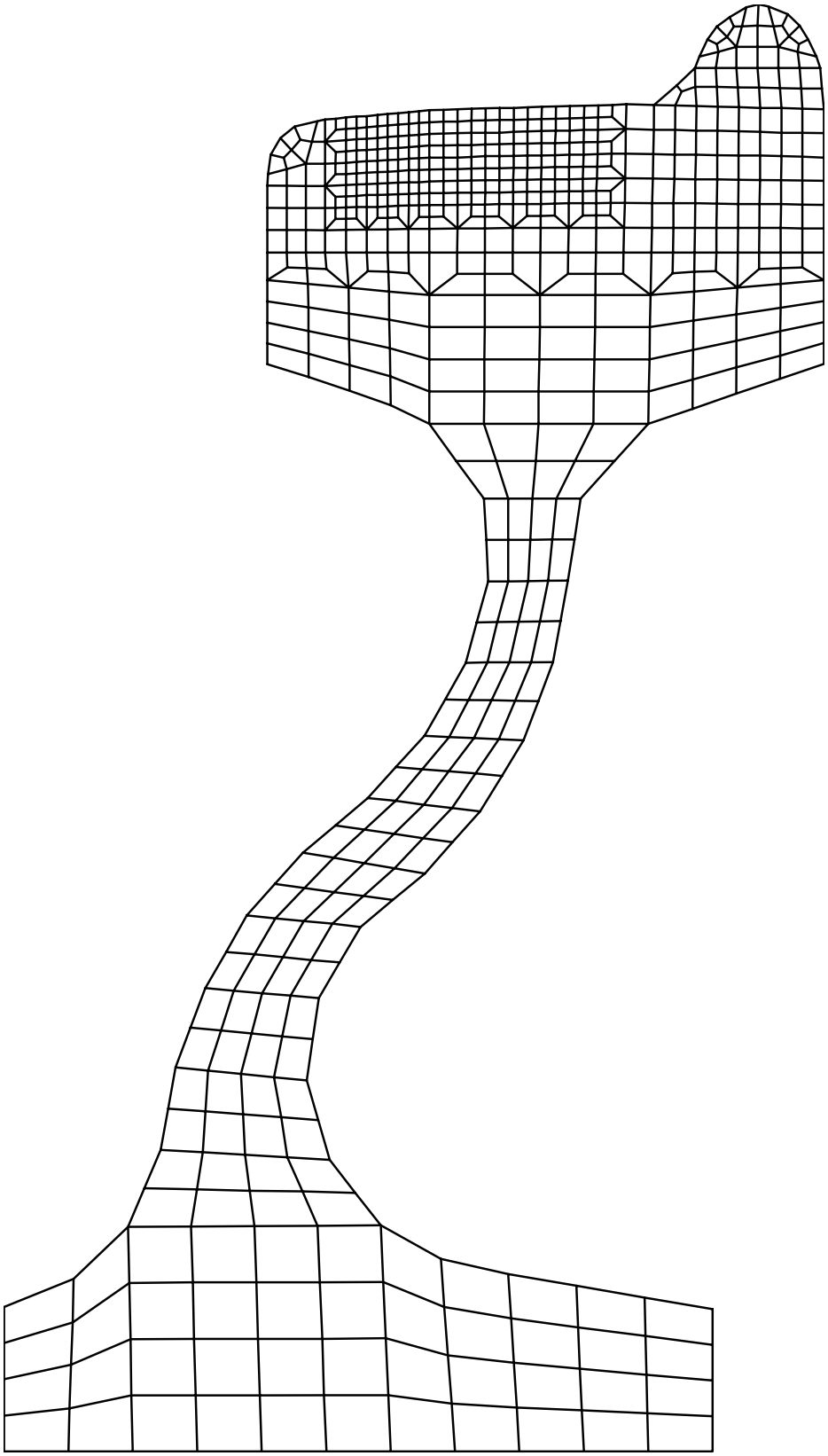

Figure 13. Finite element representation of S-plate wheel.

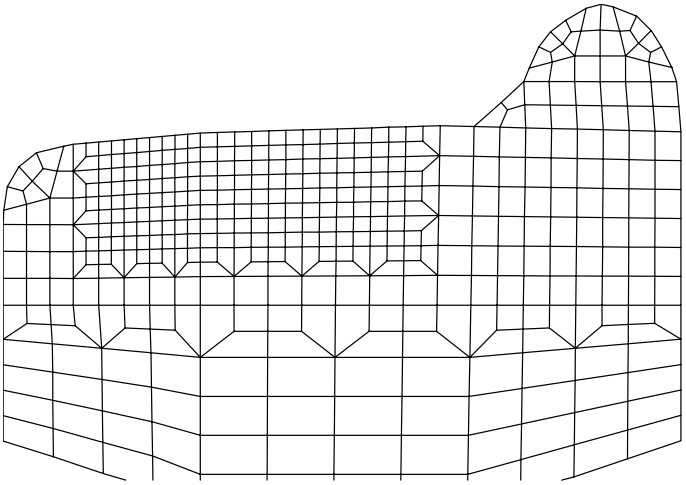

(a)

Mesh 1

632 nodes
559 elements

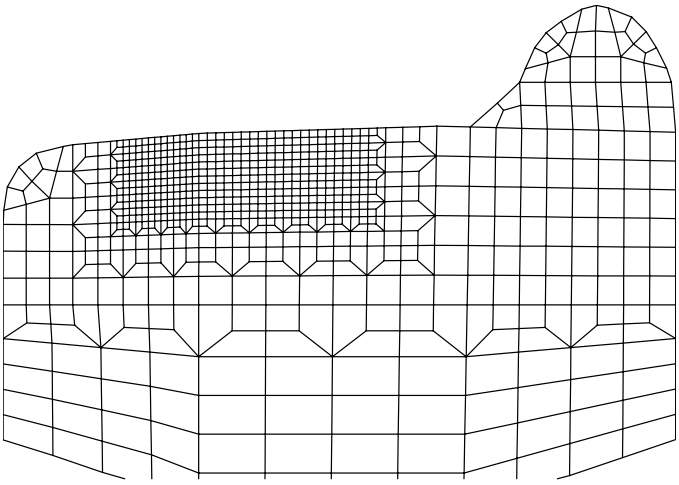

(b)

Mesh 2

989 nodes
907 elements

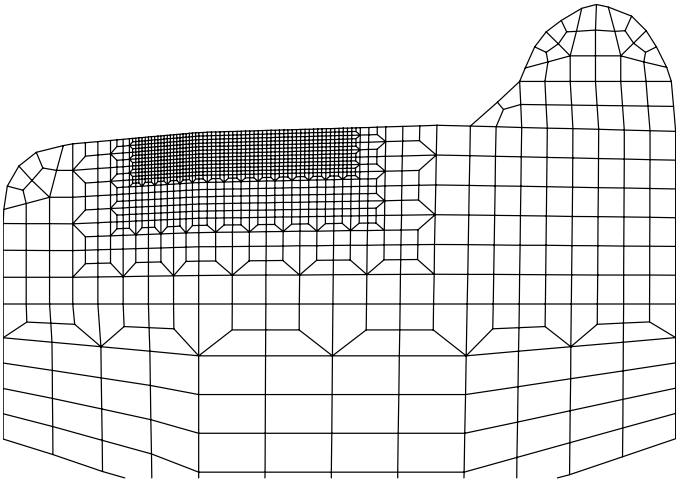

(c)

Mesh 3

1592 nodes
1495 elements

Figure 14. Wheel rim detail for three meshes used in present study.

3.3 HEAT TRANSFER ANALYSIS

To successfully model the quenching of the wheel, appropriate boundary conditions, which represent reality to the extent possible, must be prescribed. During the heat transfer portion of the analysis, nodal temperatures throughout the model are obtained for later use in the mechanical (stress) analysis. The thermal model consists of four phases: the initial quench from high temperature (2 minutes); the dwell at room temperature (4 minutes); the elevated temperature draw (5 hours); and finally, the period during which the wheel cools to room temperature (6 hours). The process is illustrated in Figure 15 with a log scale on the horizontal axis to improve clarity. This information is conveyed to the model through definition of a curve describing the time and the ambient temperature. This information (T_∞) is required for the convection and radiation boundary conditions.

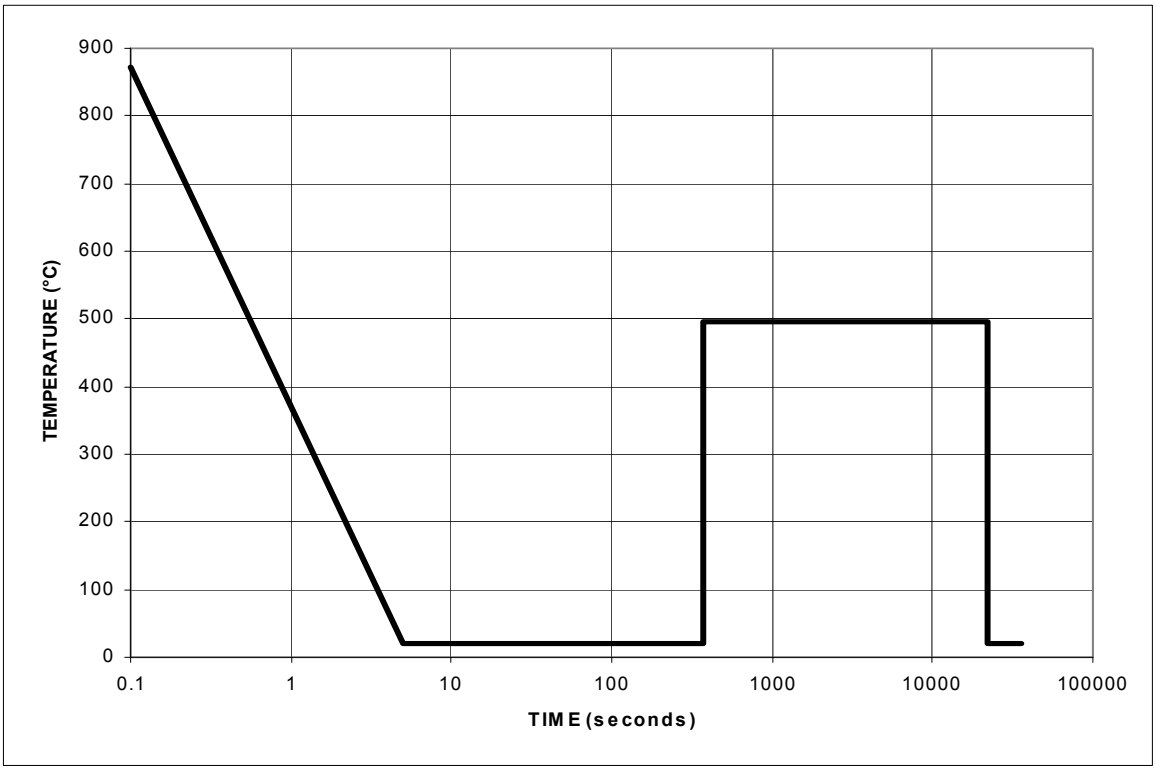

Figure 15. Passenger wheel quench schedule.

The ramp shown in Figure 15 corresponds to five-second "transition" periods over which the changes in the boundary conditions are assumed to occur. The transition zones were originally designed into the model to preclude numerical instabilities in the processing of the material properties (which are assumed to vary with temperature) through a step-like discontinuity. Experience has shown that these zones are not necessary for the current analysis; however their presence has no effect on the results.

3.3.1 Thermal Material Properties

The parameters required by ABAQUS for the heat transfer analysis include the thermal conductivity and specific heat. Thermal conductivity (k) describes the ability of the material to conduct thermal energy and is a material transport property, and is commonly expressed in units of W/m °C.[9] Temperature-dependent values for thermal conductivity have been collected and appear in Appendix A [4].

The specific heat represents the ability of a material to store energy. Since the current heat transfer analysis involves free expansion of the material, the constant pressure value (c_p) is used. Specific heat is commonly expressed in units of J/kg °C. The heat capacity is defined as the product of c_p and the material density (ρ) resulting in units of J/m^3 °C. In the current work ρ is assumed constant (7861 kg/m^3). The temperature dependence of the heat capacity is taken into account by allowing c_p to vary with temperature, as shown in Appendix A [4].

3.3.2 Convection Boundary Conditions

Convection occurs from all surfaces of the wheel during the quenching process. The heat transfer coefficient, h, takes on different values depending upon whether the surface is quenched or not. Heat loss from the surfaces of the wheel to the environment is characterized by a single heat transfer coefficient, h_{wa} (whether the subscript wa indicates "wheel to air"). The value for h_{wa} is 28 W/m^2 °C corresponding to that used in Kuhlman et al. [7]. The value of the ambient temperature, used to calculate the heat loss, is obtained from the ambient temperature description described above.

For the portion of the tread which is exposed to the water spray during the quench, shown as the region between the arrowheads in Figure 16, the heat transfer coefficient, h_{ww}, ("wheel to water") corresponds to 3066 W/m^2 °C. This value was also used in the Kuhlman et al. study [7] and is assumed constant with temperature. The h_{ww} coefficient ignores the complexities associated with water droplet size, spray impingement dynamics or film boiling. The possibility of the water spray striking other wheel surfaces exists, but has not been included in this analysis. A review of the literature yielded additional data published by Liš…i‰, et al. [27] for the heat transfer coefficient for a water spray which is plotted below in Figure 17. Visual inspection of the data confirms that the use of a constant value passes through the average of the data (more or less) and is not an unreasonable assumption for this analysis. ABAQUS is capable (through the use of the user subroutine option) of applying a temperature-dependent value of h_{ww} so that any of the curves shown in Figure 17 could be applied in this study, however, the use of a constant value permits comparison of these results with other published work.

[9] The thermal conductivity is usually expressed in units of W/m K. ABAQUS, however allows specification of a parameter which permits execution of a heat transfer analysis involving conduction, radiation, and convection in Centigrade without requiring use of the Kelvin temperature scale. This parameter is specified as: *PHYSICAL CONSTANTS,ABSOLUTE ZERO=-273.15 and has been used in this study.

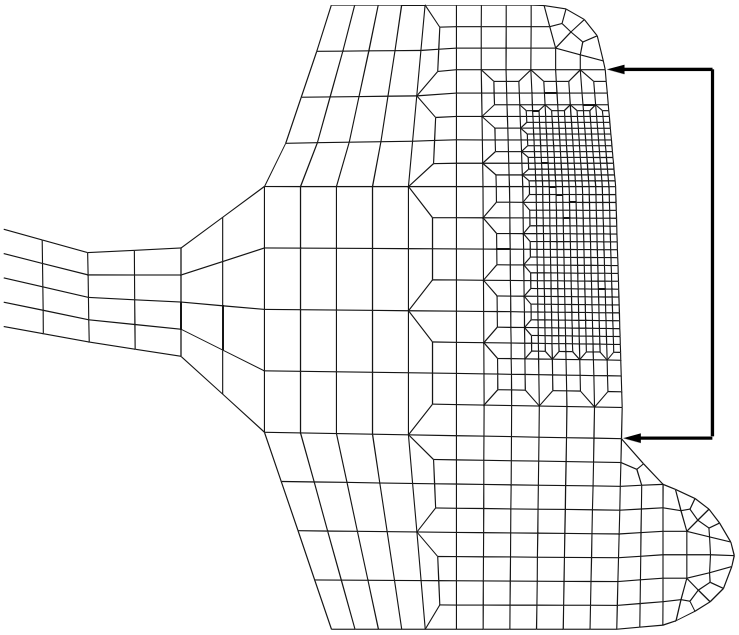

Figure 16. Tread region of Mesh 2 exposed to water spray quench, approximately 8.25 cm (3.25 in).

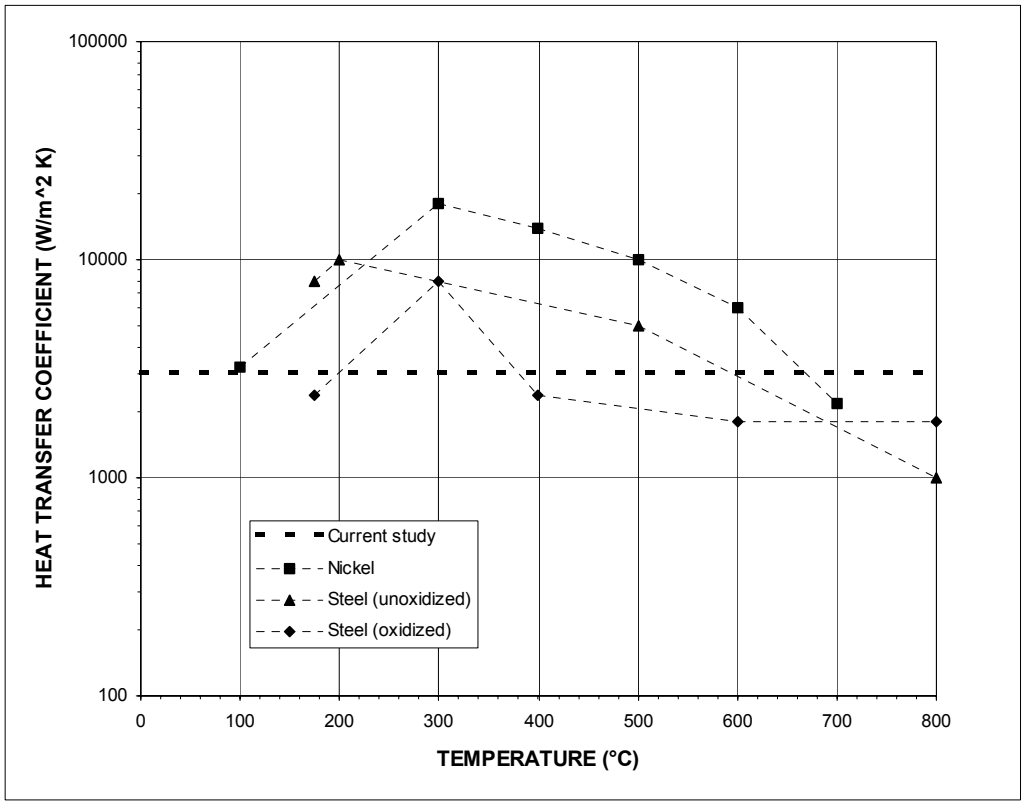

Figure 17. Heat transfer coefficient of water spray quench (from Liš…i‰ et al. [49]).

3.3.3 Radiation Boundary Conditions

Radiation from all surfaces of the wheel is permitted during the heat transfer portion of the quenching analysis. As described in equation (5), two parameters are used to characterize the radiative heat transfer. The Stefan-Boltzmann constant, σ has a value of $5.67 \bullet 10^{-08}$ W/m^2 °C^4. The surface emissivity, ε, is assumed to be 0.95 and constant. This value for ε assumes a relatively shiny surface which radiates well. The effects of surface oxidation (which would diminish ε and reduce the radiated energy) has not been taken into account. The value of the temperature of the surroundings, used to calculate the heat loss in equation (4), is obtained from the ambient temperature description described above.

Radiation is included in the analysis because of the elevated temperature at the beginning of the process. Consider the heat loss equations from convection and radiation as shown in Equations (2) and (4) applied to a body initially at 871 °C which is suddenly exposed to a 21 °C environment as shown in Figure 18.

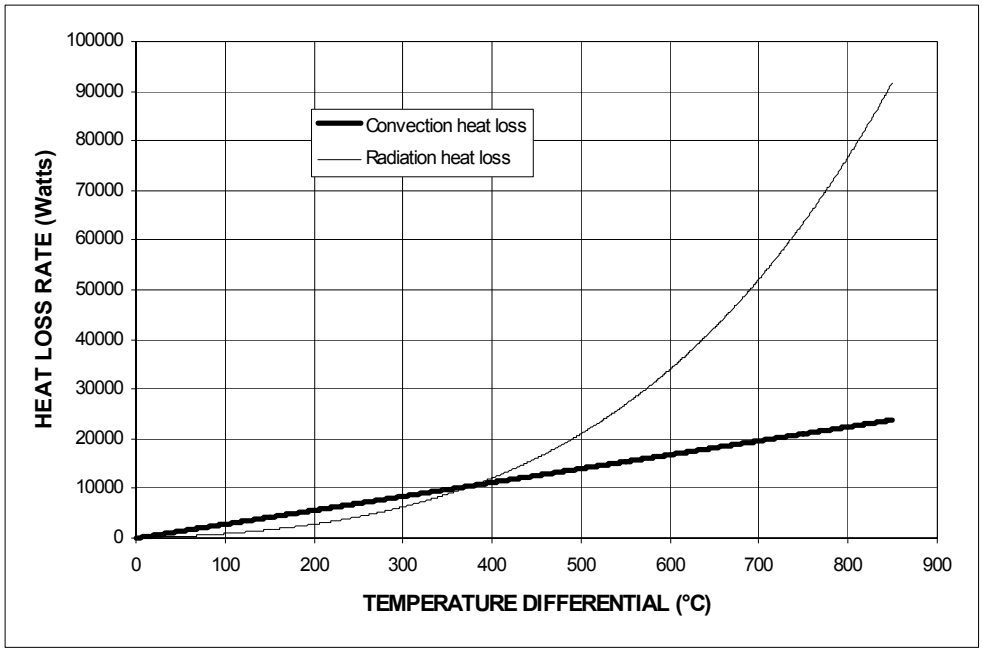

Figure 18. Relative heat loss due to convection and radiation.

The buoyancy of air and its effects on the rate of heat transfer from surfaces which are inverted or inclined to the horizontal have been neglected. Also, the diminished efficiency of radiation inside the axle bore (due to the cylindrical shape of this surface and the resulting enclosure effect) has also been ignored.

3.3.4 Execution

The DCAX4 (ABAQUS designation) element, used in the heat transfer segment of the analysis, is the four-node continuum-diffusive ("DC") axisymmetric element available in the ABAQUS library. The heat transfer analysis begins with the entire model above the austenitizing temperature of 871 °C (1600 °F). It is presumed that the wheel has been at this temperature for a sufficient time to permit complete transformation to austenite.

The analysis begins (time = 0) at this point. Through the initial transition zone, the ambient temperature is linearly reduced from 871 °C to 21 °C (1600 °F to 70 °F) during the first 5 seconds. The heat transfer coefficient on the tread surface of the quenched elements is linearly increased from the h_{wa} value of 28 W/m^2 °C to the h_{ww} value of 3066 W/m^2 °C. The unquenched surfaces of the wheel retain the h_{wa} value for the duration of the analysis.

The heat transfer portion of the simulation is executed in three "steps" consisting of several "increments." In terms of an ABAQUS execution, a step might be interpreted as a segment of manufacturing process. Steps are selected by the user, and in this study represent convenient breakpoints in the analysis (for the purposes of writing and saving results data). Increments refer to calculation intervals (like time steps in most other finite element codes). The duration of the increment can be prescribed absolutely by the user, or in this example, can be determined by the program within a range (minimum and maximum).

The timing parameters used are listed in Table 3. The complete ABAQUS input file for the heat transfer analysis appears in Appendix B, including additional information regarding the frequency and content of data output.

Table 3. Time step information for ABAQUS heat transfer analysis (MESH 2).

STEP	PROCESS	DUR-ATION (seconds)	STARTING TIME STEP (seconds)	INCRE-MENTS IN STEP	MAXIMUM ΔT/INC. (degrees)	MINIMUM STEP (seconds)	MAXIMUM STEP (seconds)
1	QUENCH AND DWELL	370	1	375	50	0.0001	1
2	ANNEAL	21610	1	2167	50	1.E-08 [10]	10
3	COOL DOWN	14195	10	148	50	0.1	100
	TOTAL	36175		2690			

[10] Such a small value for this parameter is not required for any analytical reasons. During the initial development of the input file for ABAQUS, the analysis terminated prematurely since, in the middle of the annealing portion, the temperature everywhere in the model had the same value. In order to force the analysis to continue regardless of the nodal temperatures, a small time step was chosen. In actuality, the use of the END=PERIOD option with the *HEAT TRANSFER command accomplishes the same thing.

3.4 STRESS ANALYSIS

The simulation is continued to estimate the residual stresses resulting from the quench and annealing processes. This is accomplished in a manner similar to that described for the heat transfer portion. The same finite element mesh is used for the stress analysis and several additional material properties must be specified.

3.4.1 Mechanical Properties

Temperature-dependent mechanical properties are determined for the wheel steel. Required for the stress analysis are data describing the variation of Young's modulus (E), Poisson ratio (ν), the coefficient of thermal expansion (α) and the appropriate stress-strain relations for the material over the expected temperature range. All the material properties used in the current study are listed in Appendix A.

The data for E, ν, and α have been obtained from the Association of American Railroad's Transportation Technology Center in Pueblo, Colorado. The coefficient of thermal expansion (α) requires special care in its specification for use by ABAQUS. Unlike other material properties, which are typically defined as a value *at* a temperature (a tangent to the curve), α is specified as the secant to the curve, or as a value *to* a specified temperature. The secant coefficient of thermal expansion, $\overline{\alpha}$, is obtained by integrating the tangent data from a reference temperature T_{ref} (in this case the initial temperature, 871 °C) to the target temperature, T, using the following equation:

$$\overline{\alpha}(T) = \frac{1}{T - T_{ref}} \int \alpha(T)\, dT \qquad (12)$$

The procedure for converting the tangent α into $\overline{\alpha}$ is illustrated in Appendix A as a MathCad 7 file following the tabulated material properties.

Specification of the stress-strain properties of the material over the anticipated temperature range is implemented somewhat differently in ABAQUS than in other finite element codes. As the chosen material model incorporates linear kinematic strain hardening behavior, the hardening modulus must be prescribed. ABAQUS requires specification of the yield strength as a function of plastic strain as shown in Figure 19. Curves similar to that shown in Figure 19 are generated for various temperatures. The procedure used to calculate the required quantities is given in Appendix A as a MathCad 7 file.

The temperature-dependent stress-strain curves are depicted graphically in Figure 20. These data have been scaled (by approximately 106 percent) so that the room temperature yield strength, 423 MPa (61.3 ksi[11]) corresponds to the AAR recommended value of 448 MPa (65 ksi) for Class L

[11] 1 ksi = 6.895 MPa.

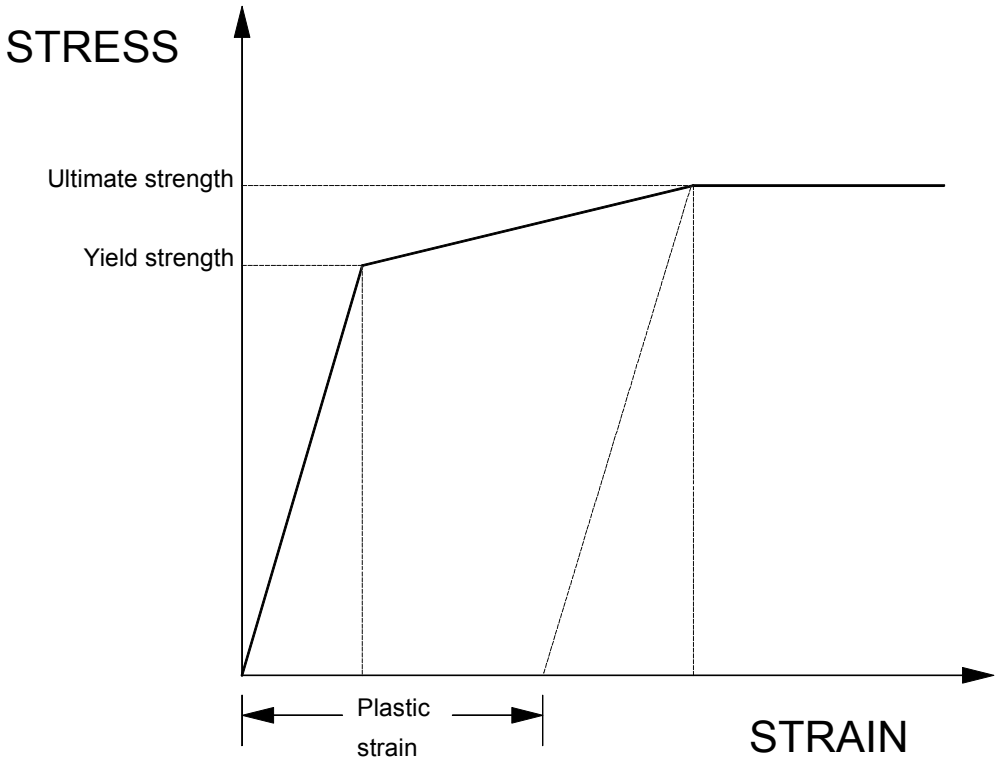

Figure 19. Hardening model used in ABAQUS.

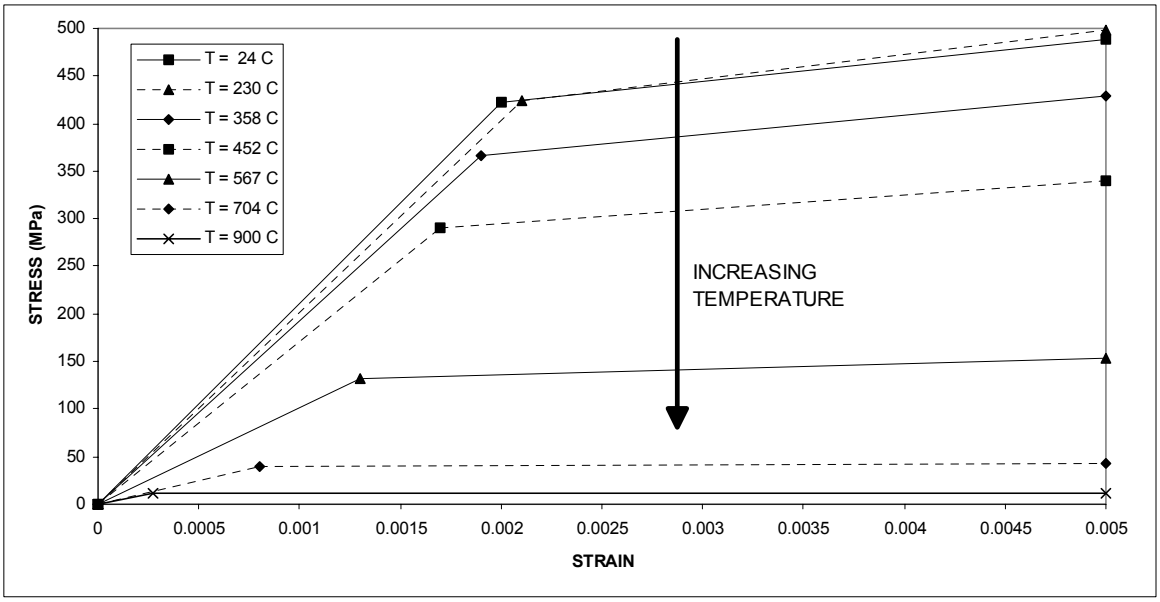

Figure 20. Temperature-dependent stress-strain data used in quench simulation.

and A wheels.[12] The adjusted values are used in the input file for ABAQUS. The material behaves as a perfectly plastic material when strained beyond 0.5 percent. Figure 20 highlights the degree to which these properties are degraded at elevated temperature.

3.4.2 Time-Dependent Deformation

As noted in Section 2, time-dependent deformation, or creep, behavior was included in other similar studies of railroad wheel quenching by Kuhlman et al. [7]. This feature is available in ABAQUS and is implemented via a user subroutine. Previous work employed a viscoelastic creep model which is reported to be based on experimental data collected using samples of actual wheel material. For modeling purposes, the creep strain rate, $\dot{\varepsilon}$, is given by the following equation:

$$\dot{\varepsilon} = 4.64 \cdot 10^{-08} \left(\sigma_{eff}{}^{12.5} \right) e^{\frac{-53712}{T+460}} \qquad (13)$$

where σ_{eff} is the current value of the Mises effective stress in the element in ksi, and T is the current temperature in Fahrenheit. The ABAQUS user subroutine is provided with sufficient information to accommodate calculation of the creep strain rate according to this formula. Due to the presence of the empirical constants, the subroutine converts the appropriate quantities (σ_{eff} and T) into English units, applies the rate equation, and returns the value of $\dot{\varepsilon}$ to the main program.

Figure 21 illustrates the behavior of Equation (13) for selected values of σ_{eff} and temperature (note the vertical log scale). The effect of the inclusion of creep behavior in the mechanical model is to provide for relaxation of the thermal stresses when the material is held at elevated temperature for extended periods of time. Figure 21 shows how the strain rate increases with temperature and stress. These curves represent constant values of stress over the temperature range.

In reality, however, the strain rates do not follow such curves. The local value of the stress in an element evolves over time as the temperature changes due to the "$E \alpha \Delta T$" thermal stresses and the temperature-dependent material properties. So, for each combination of local temperature and stress, the creep strain rate is determined for the current time interval. The heavy curve shown in Figure 21 represents the predicted creep rate for the case when σ_{eff} is on the order of the yield strength of the material at the initial temperature of 871 °C, or 150 MPa (20 ksi). The single data point identifies the creep strain rate predicted for this set of values (about 0.004/sec). This corresponds to the rate which would be exhibited in elements located near the quenched surface which are stressed to the yield limit at the beginning of the process when their strength is low.

[12] The AAR recommended room-temperature rim yield strengths for Class L and A wheels are 434.4 and 448.2 MPa (63 and 65 ksi) respectively (that is, they are more or less equal).

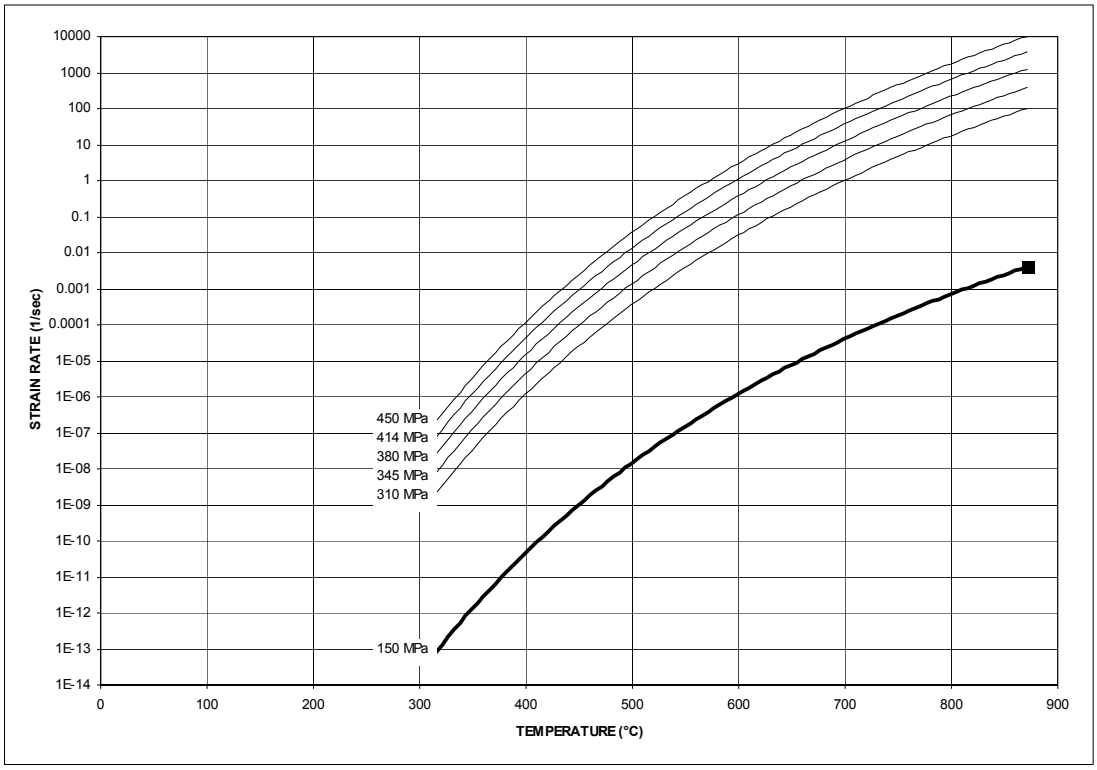

Figure 21. Creep strain rates for different assumed values of σ_{eff} and temperature.

3.4.3 Execution

The CAX4 four-node bilinear axisymmetric finite element was chosen from the ABAQUS library for the stress analysis. The initial "C" in the element name indicates that it is a continuum element. The mechanical analysis begins with a stress-free wheel. The transient temperatures at the model nodes are obtained from the ABAQUS results file created during the heat transfer analysis.

As described above, the stress analysis is carried out in several increments, each of which is made up of several steps. The pertinent parameters are listed in Table 4. Again, as in the heat transfer portion, the user subroutine (in this case, the creep model) is read by the program, compiled and linked to create a custom version of the ABAQUS executable for this analysis.

Table 4. Time step information for ABAQUS stress analysis (MESH 2).

STEP	PROCESS	DUR-ATION (seconds)	STARTING TIME STEP (seconds)	INCRE-MENTS IN STEP	CETOL[13]	MINIMUM STEP (seconds)	MAXIMUM STEP (seconds)
1	QUENCH AND DWELL	370	1	70	2.5 E-04	0.0001	1
2	ANNEAL	21610	1	227	2.5E-04	1.E-08 [14]	10
3	COOL DOWN	14195	10	149	2.5E-04	0.1	100
	TOTAL	36175		446			

The time required to execute the simulation varies depending on the computational load on the computer. Figure 22 shows the elapsed time in minutes for a typical execution of the decoupled heat transfer and stress analysis for the three meshes considered in this study. For the densest mesh, Mesh 3, total execution time is on the order of 3.5 hours on an average day.

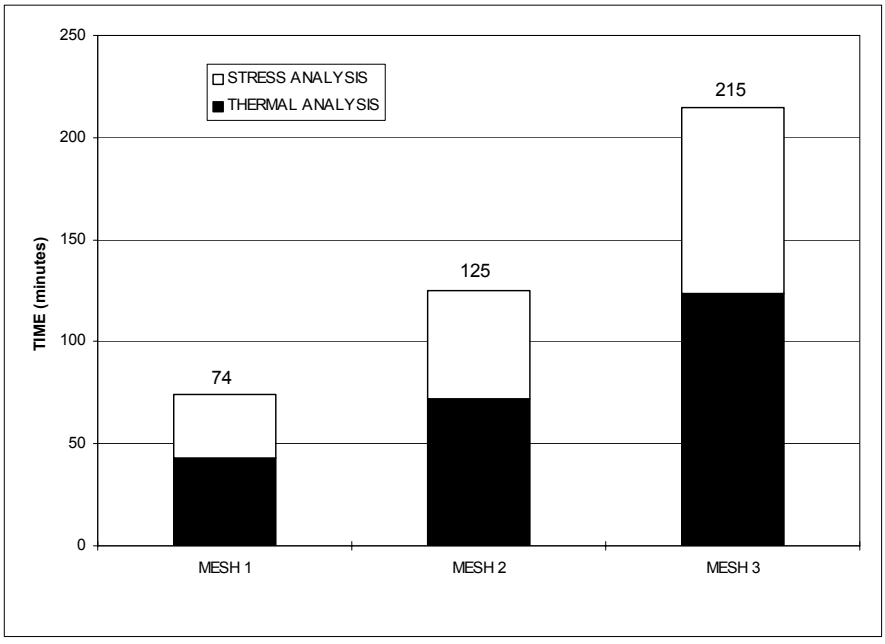

Figure 22. Timing for thermal and stress analyses using ABAQUS v. 5.5.

[13] CETOL represents the maximum change in the creep strain rate at the beginning and end of the calculation interval. This parameter is used to control the accuracy of the creep strain rate calculation. The value of 2.5E-04 is the default.

[14] See footnote 12.

4. MANUFACTURING RESIDUAL STRESS ESTIMATION STRATEGY - RESULTS

Results of the finite element simulations of the quenching process are presented in this section. The baseline scenario, described previously, represents the best estimate of the parameters characterizing the manufacturing process. Since this study includes no means for experimental validation of the results, and very little experimental evidence exists to corroborate these estimates, variations on the baseline conditions will be examined to establish reasonable limits on the predicted residual stresses. Several factors have been identified which warrant investigation.

The first portion of this section investigates the effects of mesh density on the quality of the results for the baseline analysis. As the thermal and stress analyses have been conducted separately, the results of each will be examined in the same fashion. Discussion of the modifications to the baseline conditions, and the rationale behind these modifications, appears next. These results are intended to ascertain the significance of the use of various analysis options and material properties on the quality of the results.

4.1 BASELINE CONDITIONS

Table 5. Baseline conditions for quench simulation.

EVENT	DURATION	START TIME (seconds)	END TIME (seconds)	SIGNIFICANT MODEL CHARACTERISTICS
RAMP 1	5 seconds	0	5	Ramp from elevated temperature to ambient. Ramp from passive cooling to elevated heat transfer coefficient.
RIM QUENCH	2 minutes	5	125	Apply water spray heat transfer coefficient to rim.
RAMP 2	5 seconds	125	130	Ramp from elevated heat transfer coefficient to passive cooling.
DWELL	4 minutes	130	370	All wheel surfaces experience passive cooling.
RAMP 3	5 seconds	370	375	Ramp from ambient temperature to annealing temperature.
ANNEAL	6 hours	375	21975	All wheel surfaces exposed to annealing temperature.
RAMP 4	5 seconds	21975	21980	Ramp from annealing temperature to ambient temperature.
COOL DOWN	4 hours	21980	36175	All wheel surfaces exposed to ambient temperature.
TOTAL	**10 HOURS**			

As discussed in Section 3, the baseline conditions represent the best estimate of the pertinent parameters of the manufacturing process. The variables (temperatures, durations, etc.) are specified for the passenger wheel quenching simulation, and differ somewhat from the schedule used for freight wheels, as reported in Kuhlman, et al. [7]. The data used in the present analysis are summarized in Table 5.

4.1.1 Results of Baseline Thermal Analysis

The heat transfer analysis was conducted using all three finite element meshes depicted in Figure 14. This examination determined the degree of mesh refinement required for a satisfactory solution.

As the problem in question evolves over time, contour plots of the output become difficult to interpret. Instead, many of the findings of this study are presented as *x*-*y* plots of selected data on a line passing through the rim as shown in Figure 23. Figure 23 depicts the finite element grid for mesh 2, from Figure 14(b), and the heavy line denotes the nodes which are selected for presentation.

The results of the heat transfer portion of the quenching simulation are plotted in Figure 24. This figure represents the temperature distribution through the rim at the end of the quench (at time, t = 125 seconds). As the three curves in Figure 24 are virtually indistinguishable, mesh density is not an important issue for the heat transfer analysis. The results for meshes 1 and 2 are nearly identical and the maximum temperature difference between these data and those for mesh 3 is 4 °C (7 °F). Therefore, the mesh density appears to be of no consequence in the thermal analysis, as long as the grid is at least as dense at that in Mesh 1.

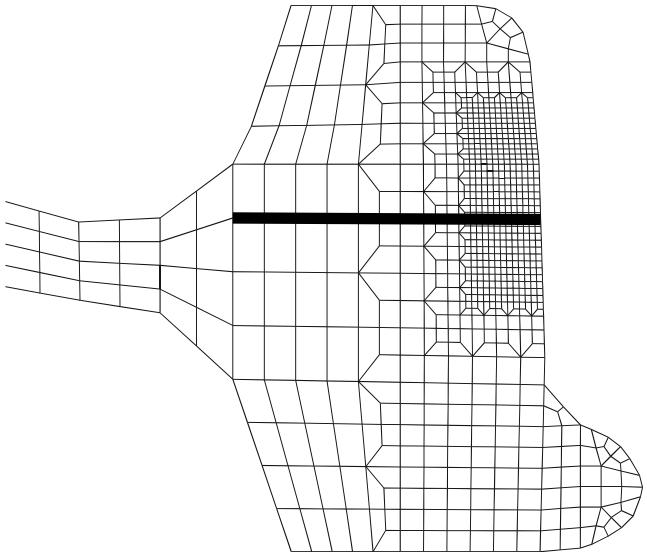

Figure 23. Line through wheel rim along which data is plotted.

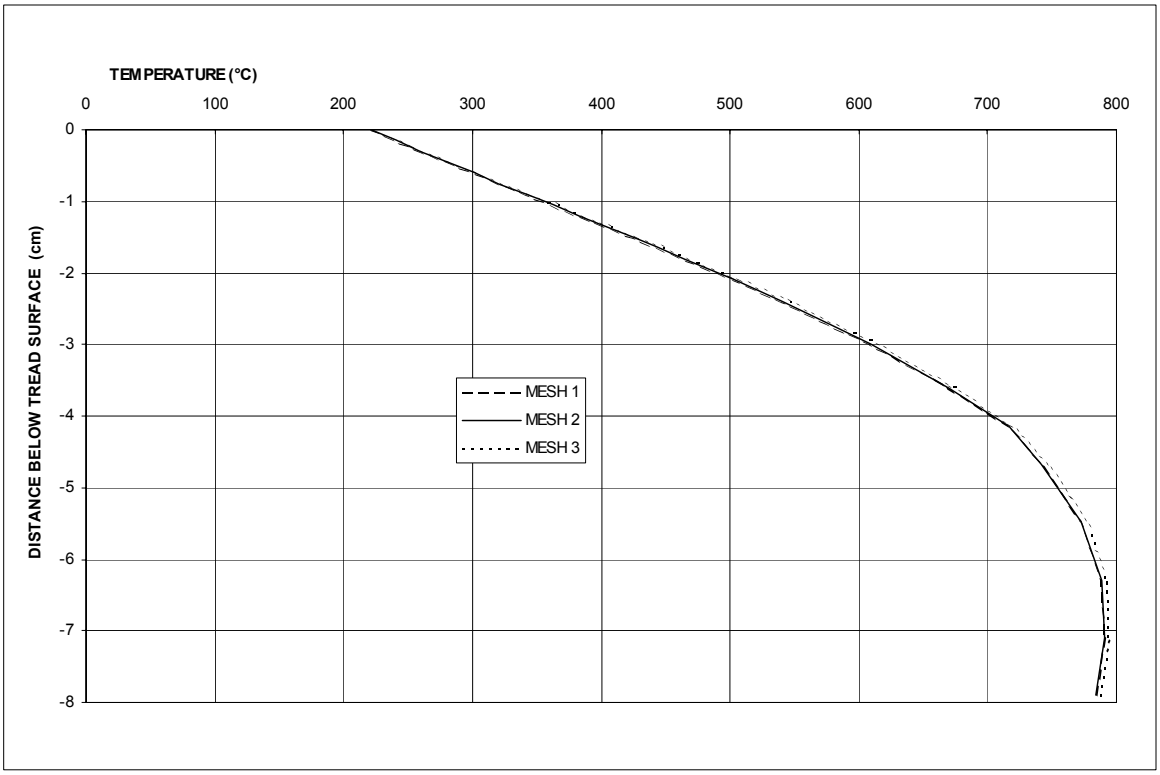

Figure 24. Temperature distribution along line through rim for three meshes used in current study at end of quench (time=125 seconds).

Figure 25 is a contour plot of the temperature distribution in the wheel rim (Mesh 2) at t = 125 seconds. The contours are plotted at 50 °C (122 °F) increments. At the end of the quench, the minimum temperature in the wheel rim is 220 °C (428 °F) and the maximum is 824 °C (1515 °F), reduced little from the initial temperature of 871 °C (1600 °F).

Figure 26 is a representation of the entire process. The temperature-time histories of two nodes in the model (one on the surface and the other at the base of the rim, corresponding to the endpoints of the heavy line in Figure 23) are overlaid on the isothermal transformation diagram of the AISI 1050 wheel steel (repeated from Figure 24). In this way, the microstructure in the rim can be inferred, since all intermediate nodes must follow temperature trajectories between those shown in Figure 26.

Figure 26 shows the time histories of the two points, beginning at the initial temperature (871 °C), through the quench, dwell and annealing, and finally to room temperature at the end of the cool down. The significant events in the process are noted in Figure 26. The figure also confirms the fact that the wheel rim should exhibit a pearlitic microstructure (a combination of ferrite and cementite as discussed in Section 1). This is an encouraging finding, as it implies that the manufacturing process parameters must resemble realistic conditions.

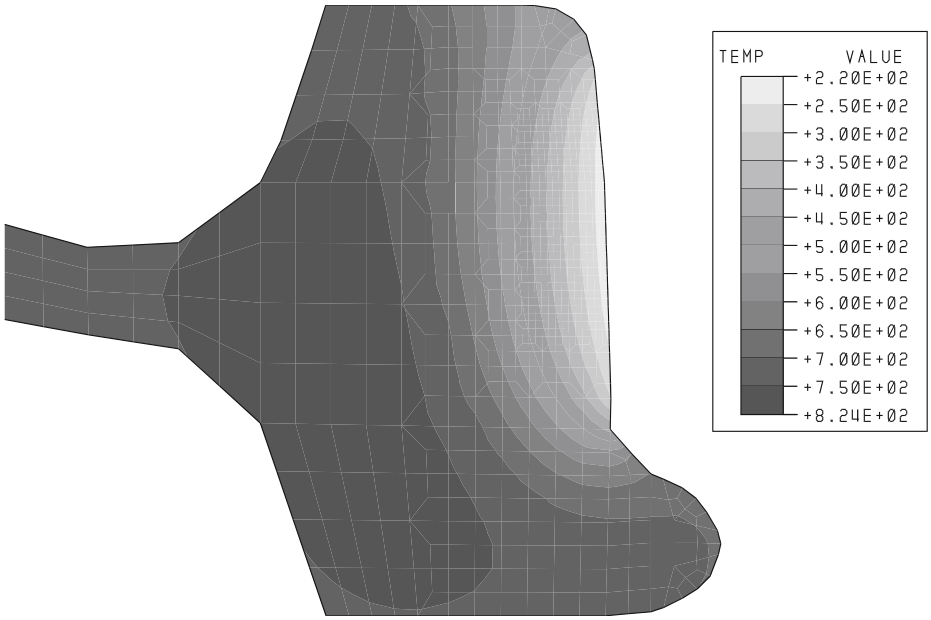

Figure 25. Temperature distribution (in °C) in wheel rim at end of quench (time=125 seconds, MESH 20).

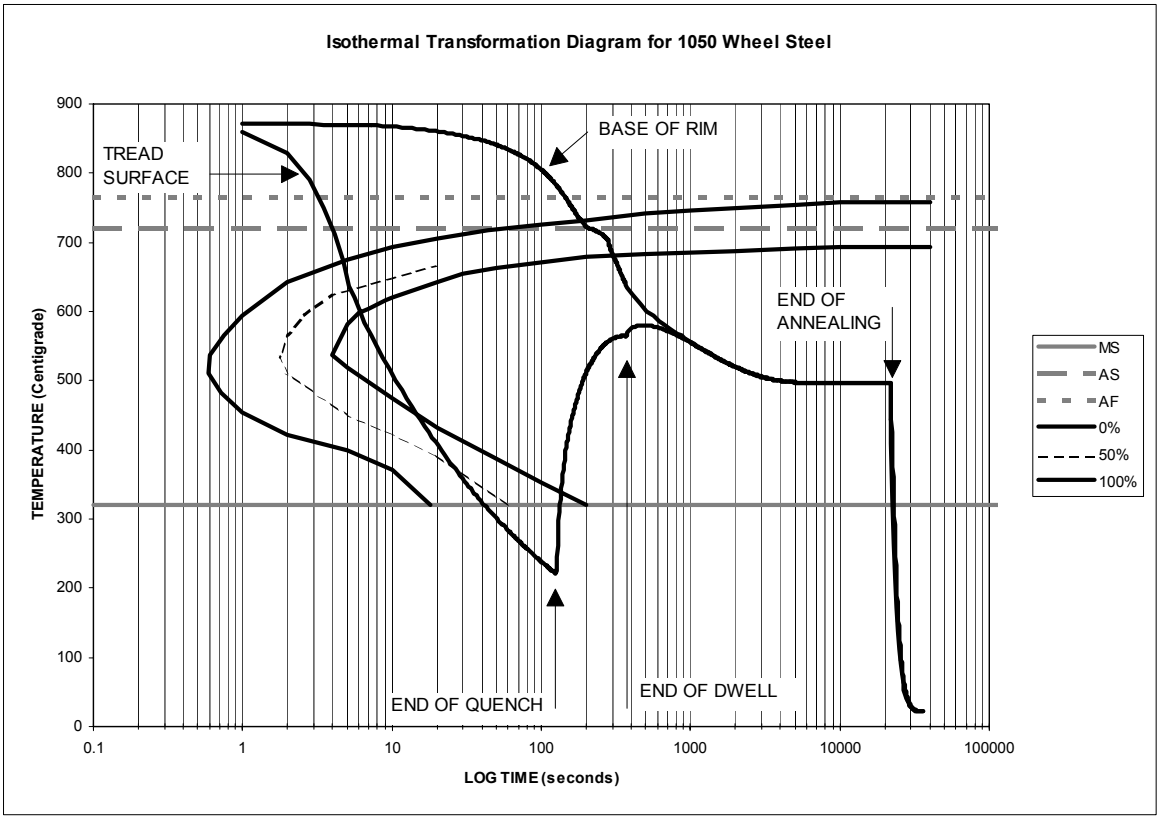

Figure 26. Baseline temperature-time history of two nodes superposed on isothermal transformation diagram of representative steel alloy.

Figure 26 also illustrates the effect of release of latent heat. Recalling the previous discussion, latent heat is released during the transformation from austenite to pearlite. The latent heat release corresponds to local heat generation during the transformation. The ABAQUS implementation of the phenomenon requires specification of a temperature range during which the transformation takes place. For this example, the range is from 720 °C to 703 °C, during cooling.

The amount of heat released is expressed in terms of the volume of transformed material ($3.2 \bullet 10^{08}$ kJ/m^3) and influences the temperature profiles in this range.[15] The change in slope of the cooling curve between 720 °C and 703 °C is evidence of the latent heat release. The effect is more apparent at the base of the rim, since the cooling rate is lower, however, the release occurs throughout the model as the material cools through this temperature range.

In reality, the latent heat release begins when the temperature-time trajectory at a point crosses the 0 percent transformed curve in Figure 26. The release continues until the transformation is complete (when the temperature-time trajectory crosses the 100 percent transformed curve). So, at the surface, the transformation (and the heat release) actually begins at a temperature somewhat lower than 720 °C.

In another study [28], the time and temperature at all points in a quenched plate were tracked in order to ensure that the latent heat release was triggered at the appropriate moment (when the temperature-time trajectory at any location in the model crossed the zero percent transformed curve). The latent heat was then released in proportion to the degree of completion of the transformation. This detailed accounting did little to effect the results. Since the effect of the release of latent heat is rather small and influences the temperature-time trajectories very little, the added complexity of tracking the amount of material transformed and allocating the heat evolution proportionately is not included here.

4.1.2 Results of Baseline Stress Analysis

Following the procedure outlined in Section 3, the temperature histories are used as input to the stress analysis. The temperatures throughout the model represent the thermal loads which cause the development of the residual stresses due to the manufacturing process.

The results of the baseline analysis are presented in Figures 27, 28, and 29 for the three meshes used in this investigation along the line through the rim identified in Figure 23 at three separate instances during the analysis. The three meshes predict hoop stress distributions with the same general character in each figure. The major differences appear in Figure 27 which depicts the stress profile at the end of the quench. The discrepancies in the three models, however, disappear after annealing (Figure 28) and the three finite element grids predict essentially the same distribution at the end of the process (Figure 29).

[15] The amount of heat released (40310 kJ/kg) is based on experiments with slow cooling rates in which the phase transformation occurs between 720 °C and 703 °C.

Figure 24 (temperatures) and Figure 29 (hoop stress) indicate that mesh density is not a significant variable in the current analysis. The thermal results for the three meshes are indistinguishable and the differences observed in the stress analysis disappear by the time the process is completed. Therefore, the remainder of the analysis will be accomplished using Mesh 2 only.

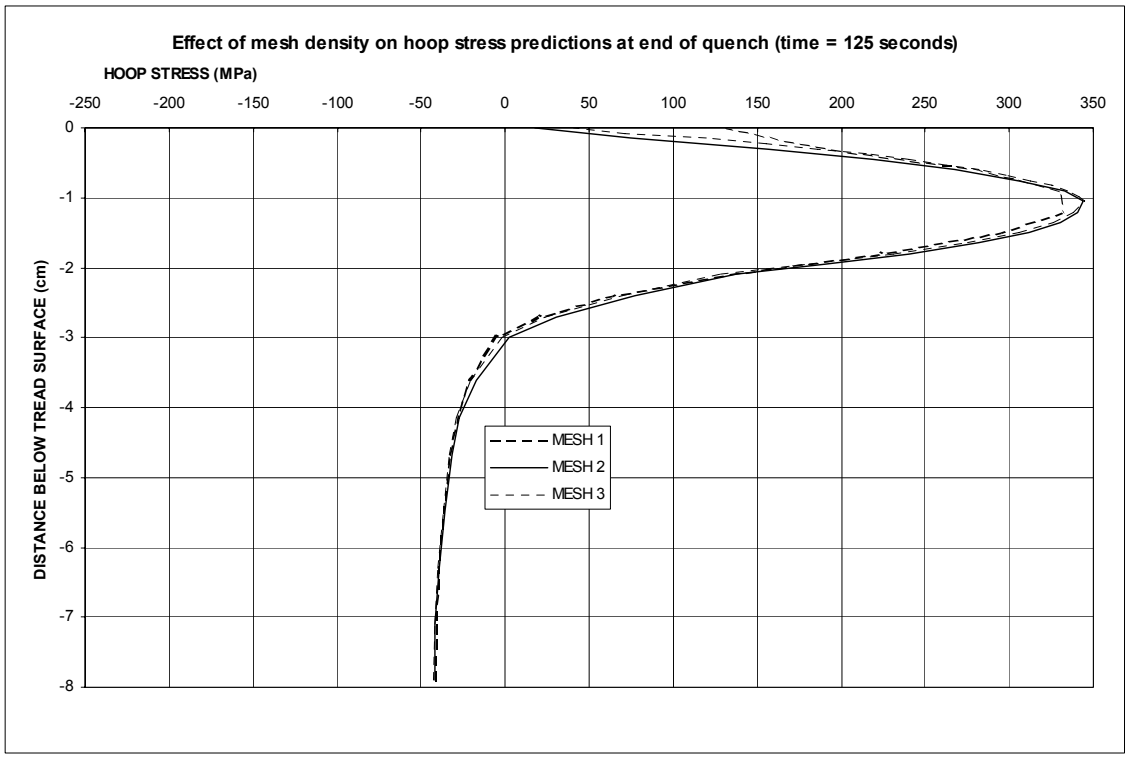

Figure 27. Circumferential (hoop) stress distribution (in MPa) in wheel rim at end of quench (time = 125 seconds).

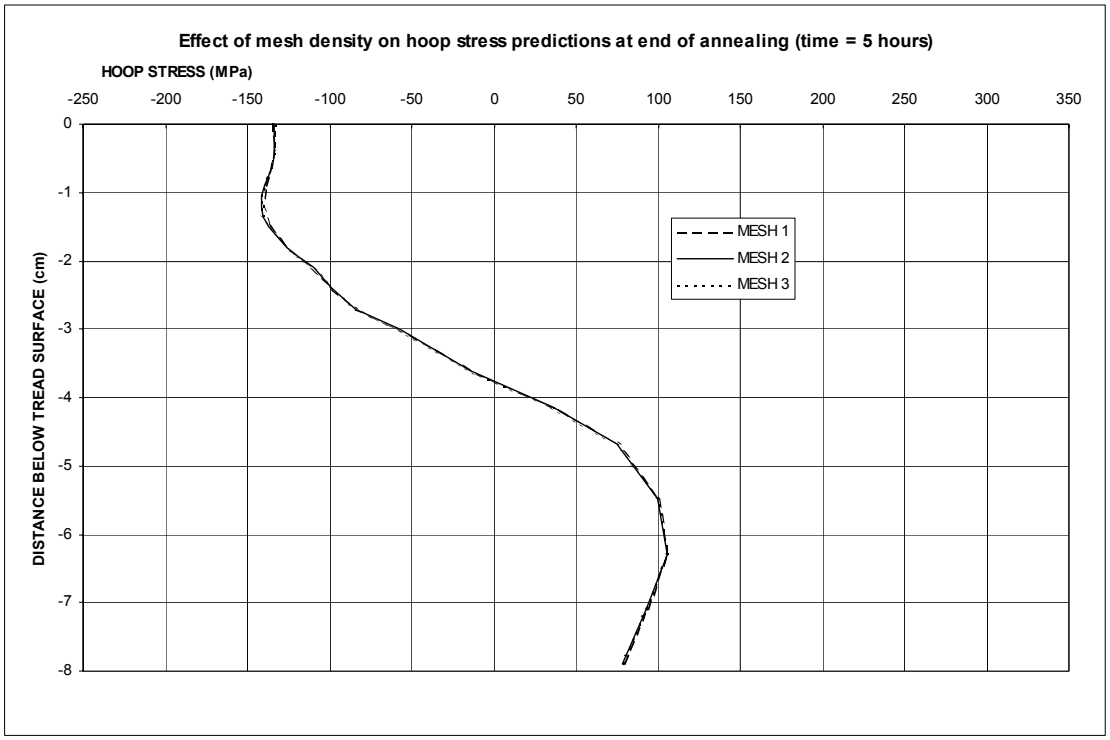

Figure 28. Circumferential (hoop) stress distribution (in MPa) in wheel rim at end of annealing (time = 5 hours).

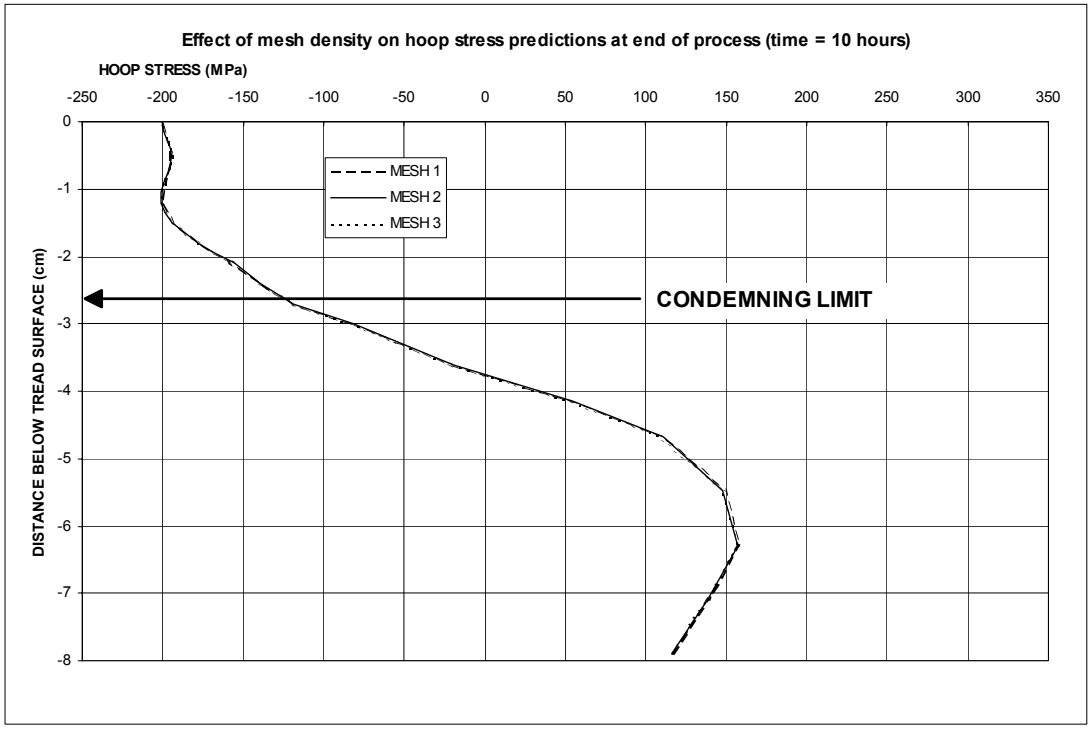

Figure 29. Circumferential (hoop) stress distribution (in MPa) in wheel rim at end of process (time = 10 hours).

Figures 30, 31, and 32 are contour plots of the hoop stresses at three points in time during the manufacturing sequence for the intermediate element density, Mesh 2. These figures, corresponding to the distribution plots in Figures 27, 28, and 29 illustrate the development of the residual compressive layer at the tread surface, which is shown in Figure 32 at the end of the process. The compressive layer is approximately 3.75 cm (1.5 inches) deep and agrees well with other simulations of the process [6, 7].

The predicted depth of penetration of the compressive layer also relates well to current wheel maintenance practices. The rim thickness for new wheels is 6.4 cm (2.5 inches). Wheels in EMU passenger applications are permitted to continue in service, in the absence of cracks, until the rim has worn (or been reprofiled) to a thickness of about 3.81 cm (1.5 inches), the condemning limit shown in Figure 29. Assuming the residual stress distribution present following manufacturing remains unchanged during the life of the wheel, residual hoop compression (although lower in magnitude) will remain in the rim at the point when the wheel must be scrapped.

Figure 33 identifies two elements in the wheel rim for which time histories of hoop stress will be examined. Figures 34 and 35 are plots of this data for the two elements during the simulated manufacturing process. Figure 34 represents the first 500 seconds of the process to illustrate the details at the beginning of the simulation. Figure 35 shows the result for the entire 10-hour process. The major milestones: the end of the quench, the end of the dwell, the end of the annealing, and the end of the process are identified on the figures.

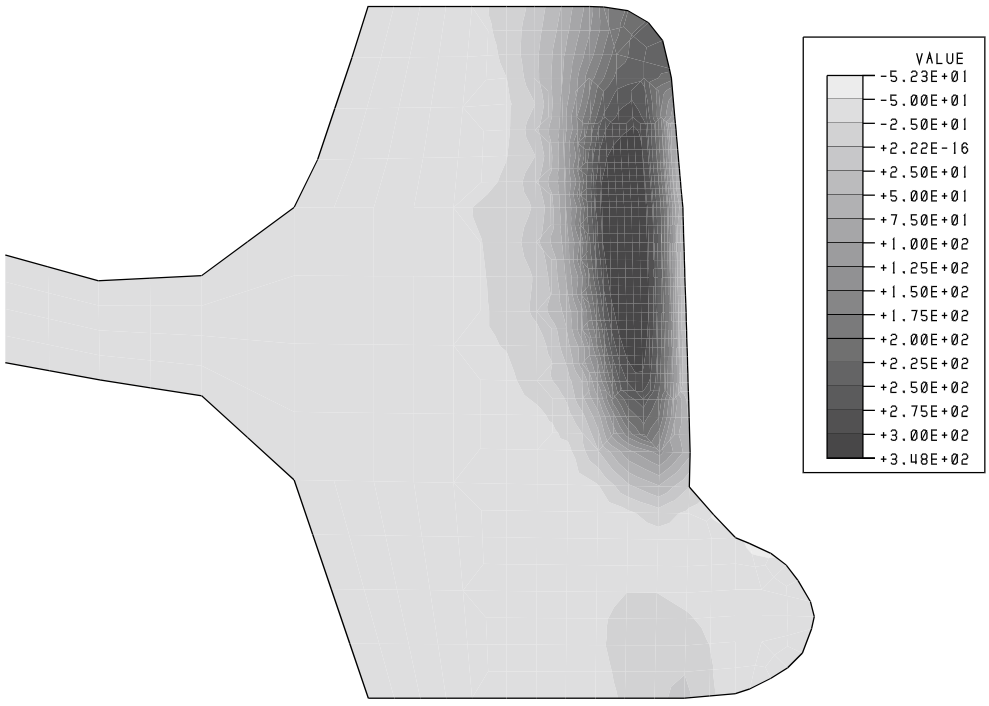

Figure 30. Circumferential (hoop) stress distribution (in MPa) in wheel rim at end of quench (time=125 seconds, MESH 2).

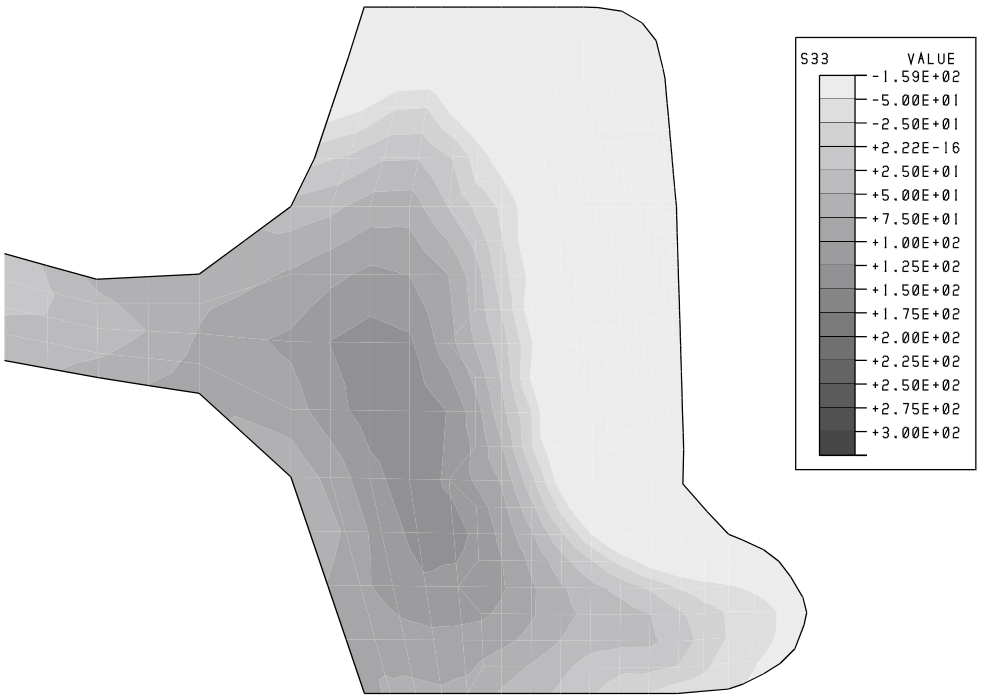

Figure 31. Circumferential (hoop) stress distribution (in MPa) in wheel rim at end of annealing (time=5 hours, MESH 2).

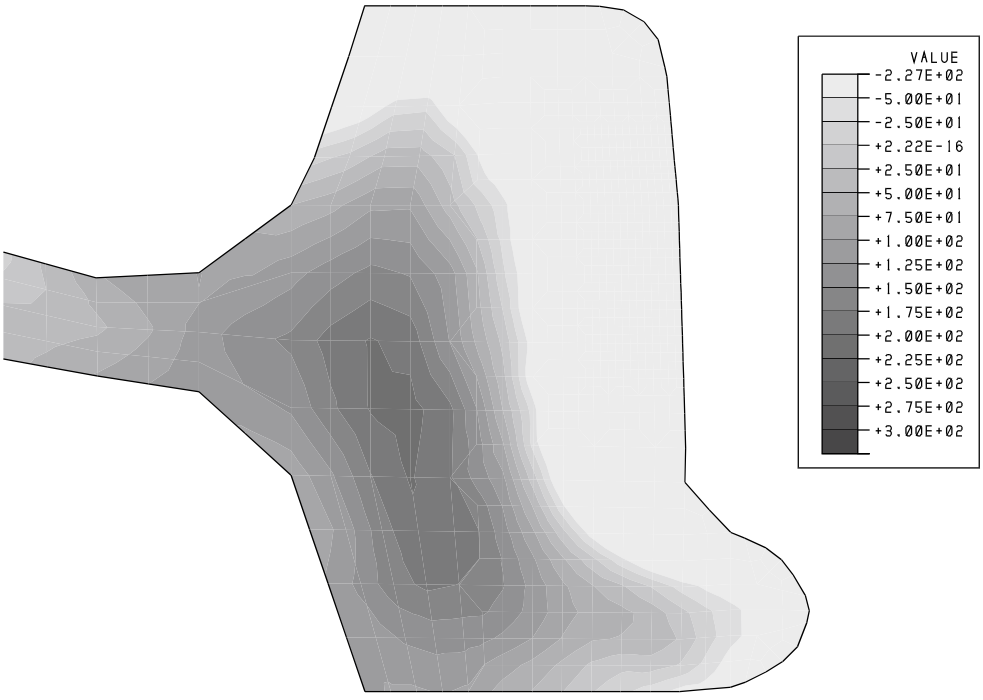

Figure 32. Circumferential (hoop) stress distribution (in MPa) in wheel rim at end of process (time=10 hours, MESH 2).

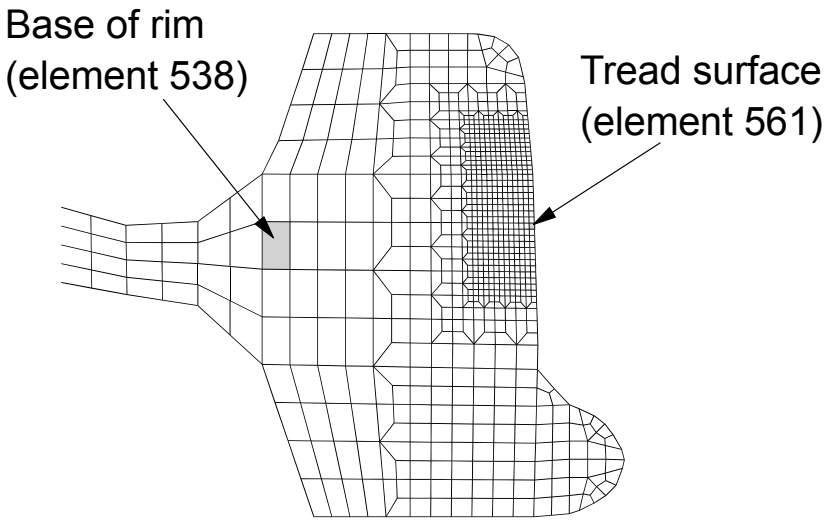

Figure 33. Elements selected for hoop stress time histories.

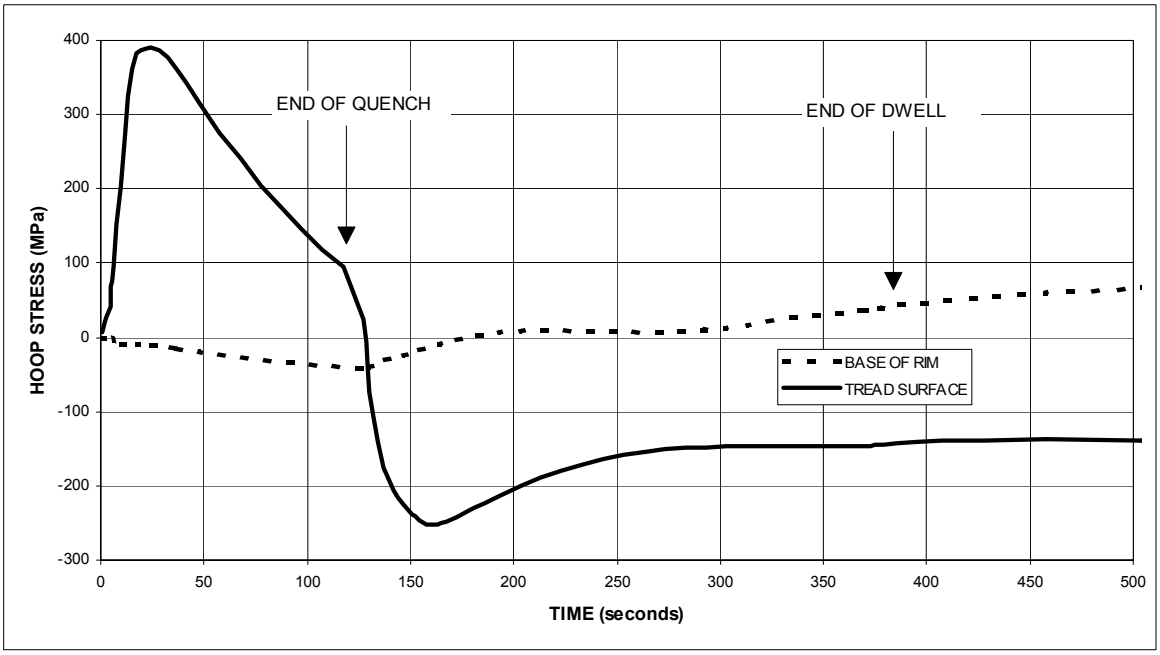

Figure 34. Time history of hoop stress evolution (in MPa) in two elements in wheel rim during first 500 seconds of quenching process.

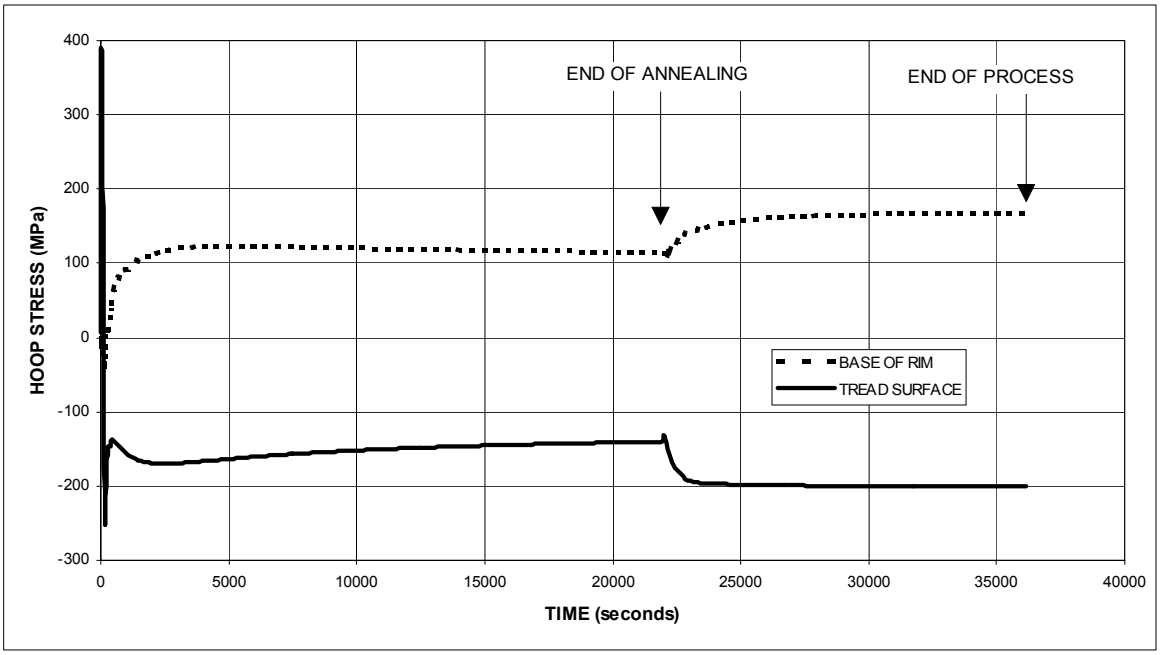

Figure 35. Time history of hoop stress evolution (in MPa) in two elements in wheel rim during entire quenching process.

Figures 34 and 35 illustrate the effects of the quench on the portion of the wheel in the vicinity of the tread. During the first 2 minutes (Figure 34), the tread surface experiences significant tension as this area cools rapidly and shrinks. The shrinkage is resisted by the remainder of the wheel. The base of the rim is essentially unaffected and the stresses here are practically zero. As the cold front progresses into the rim, the surface goes into compression with only slight tension being developed deeper into the rim. During the dwell (from 125 to 375 seconds, or 4 minutes), conduction in the rim reduces the thermal gradients and the stress history assumes a flat character.

The most important detail in Figure 35 is the effect of the annealing. The stresses (both at the surface and at the base of the rim) decrease (more or less monotonically) during this period from 375 to 21,975 seconds (6 hours) due to the inclusion of the creep behavior described in Section 3. The relaxation of the stresses due to the exposure to elevated temperature for an extended period of time is an important effect on the final residual stress distribution.

4.2 MODIFICATIONS TO BASELINE CONDITIONS

The results presented in the previous section illustrate the development of the residual hoop compression in the rim of the commuter wheel for the baseline conditions identified in Table 5. Given several uncertainties in the development of the baseline scenario, it is prudent to identify and assess the impact of the model parameters which have the greatest effect on the results.

4.2.1 Effect of Inclusion of Creep Effects

The effect of creep, discussed above is one of the most important features of the baseline simulation. As described in Section 3, the creep behavior is included in the analysis as a user subroutine. The baseline analysis is repeated, with the creep feature disabled, to obtain a residual stress prediction for the kinematic hardening material. All other baseline parameters (Table 5) remain the same.

Figures 36 and 37 illustrate the time history of the hoop stress for this case in the two elements identified in Figure 33 which are represented by the dashed curves. The data from Figures 34 and 35 (creep included) are included for comparison and appear as solid curves. The behavior of each set of curves is similar, that is, the effects of the external conditions (quench, dwell and anneal) are apparent whether the creep feature is enabled or not. The most important difference occurs during the annealing (from 375 to 21,975 seconds). The dashed curves (creep excluded) are perfectly flat during this portion of the simulation. The solid curves (creep included) illustrate the reduction (relaxation) of the stresses due to the viscoelastic effect. The details of the result appear in Table 6.

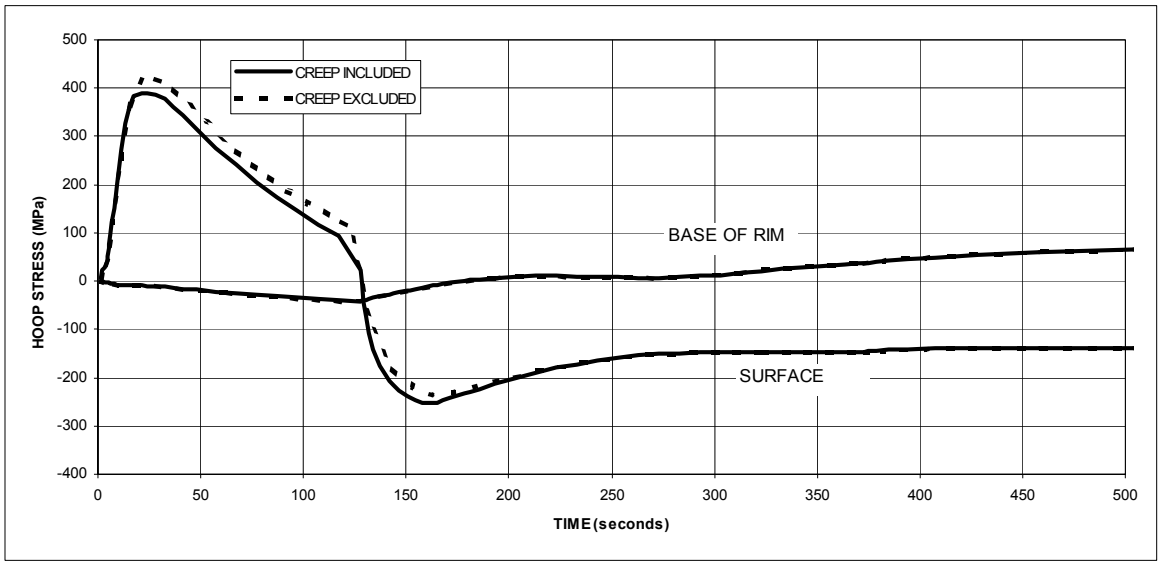

Figure 36. Time history of hoop stress (in MPa) in two elements in wheel rim during first 500 seconds of quenching process with and without creep effects.

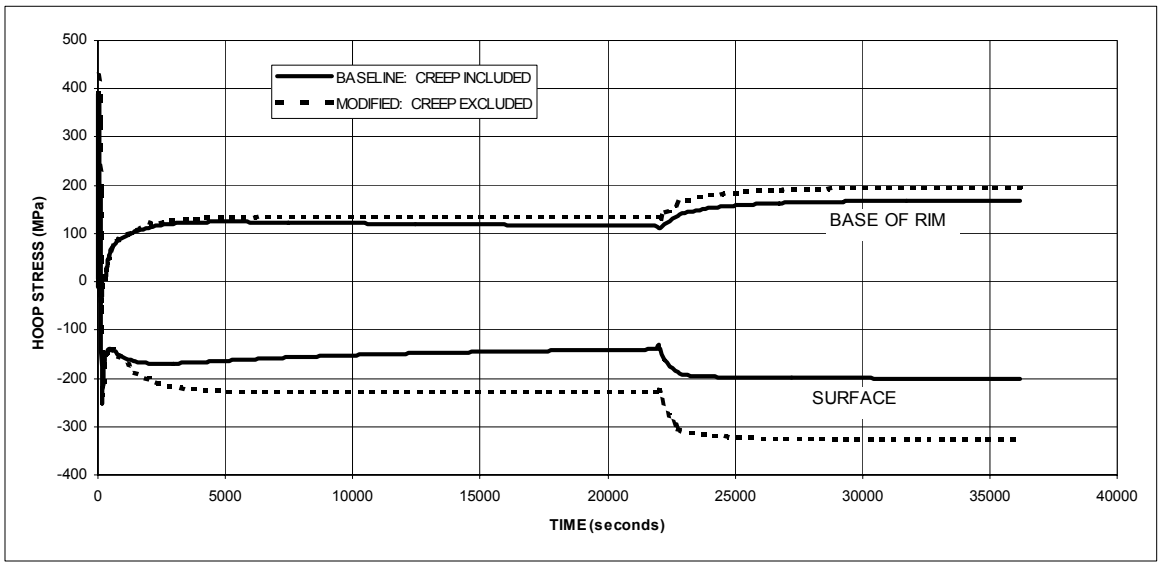

Figure 37. Time history of hoop stress (in MPa) in two elements in wheel rim during entire process with and without creep effects.

Table 6. Effect of creep behavior on hoop stress prediction (MPa).

LOCATION (ELEMENT)	CREEP INCLUDED	CREEP EXCLUDED	PERCENT DIFFERENCE
BASE OF RIM (538)	+168	+197	17
TREAD SURFACE (561)	-200	-326	63

The reduction in hoop residual stress due to viscoelastic creep occurs throughout the rim. Figure 38 shows the distribution through the rim for the two simulations. The general character of the two results is similar and both analyses predict the same depth of residual compression. The reduction of surface compression is a significant outcome of this exercise. Accurate prediction of the as-manufactured residual stress distribution in wheels requires accounting for creep.

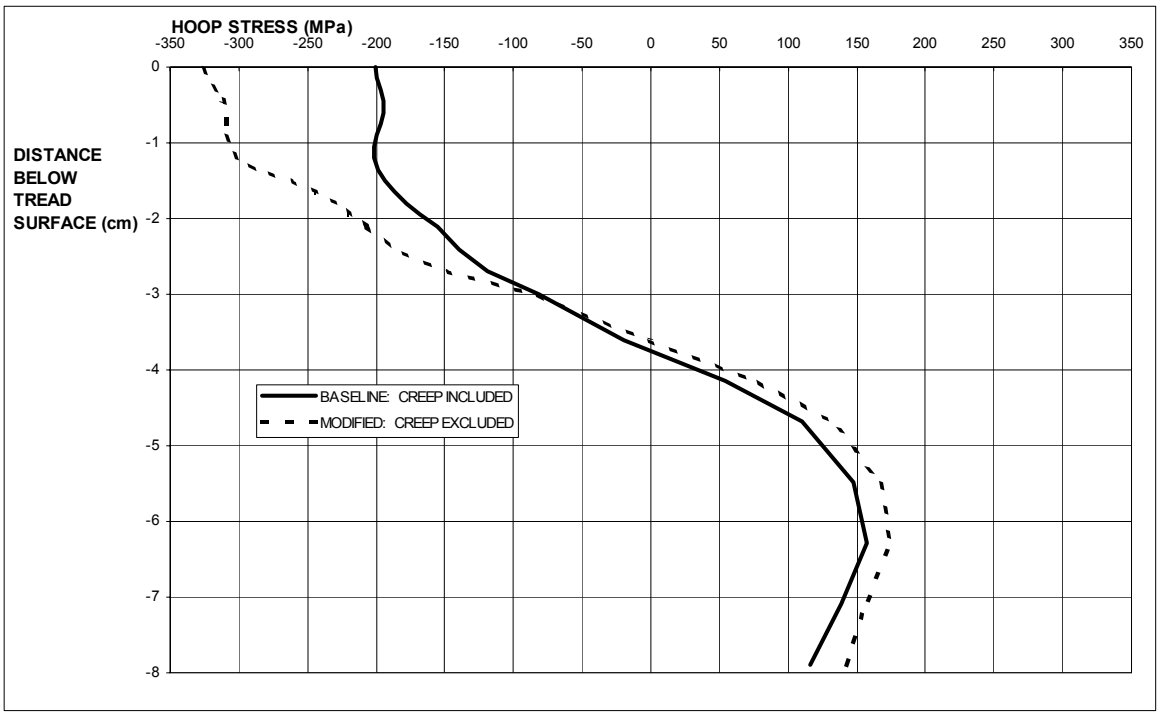

Figure 38. Circumferential (hoop) stress distribution (in MPa) in wheel rim at end of process (time = 10 hours) with and without inclusion of creep effects.

4.2.2 Effect of Variation of Quench Duration

The next set of variations to the baseline conditions involves the specification of the manufacturing variables. The simulated process relies on knowledge of the parameters which define the quenching sequence. The baseline conditions have been selected based on discussions with experts in the field. However, some of these conditions have been specified rather loosely. For example, for the 81 cm (32 inch) passenger wheel, the duration of the quench has been identified as, say, "two to three minutes." In other studies conducted on 91 cm (36 inch) freight wheels by Perfect [6] and Kuhlman et al. [7], the duration of the quench is about 6 minutes. In this section, the importance of the quench duration will be investigated.

In the baseline analysis, the quenchant was applied to the wheel tread surface for 2 minutes. The duration is varied by ±50 percent to assess the effect of shorter and longer quenching intervals. All other baseline conditions remain constant and the analysis is repeated with quench times of 1 and 3 minutes.

The results of this investigation are summarized in Table 7, for the two locations which have been the focus of this work. The data in Table 7 indicate that the duration of the quench has very little effect on the final estimate of residual hoop stress. The residual rim compression varies by only 5 MPa for the two cases and the tension at the base of the rim differs by at most 18 MPa.

Table 7. Effect of quench duration on hoop stress prediction (MPa).

LOCATION (ELEMENT)	SHORT QUENCH (1 MINUTE)	BASELINE QUENCH (2 MINUTES)	LONG QUENCH (3 MINUTES)
BASE OF RIM (538)	150	168	184
TREAD SURFACE (561)	-195	-200	-205

Figures 39, 40, and 41 illustrate the time histories of the residual hoop stress in the wheel tread and at the base of the rim. The differences in quench duration are apparent in Figure 39 which depicts the behavior in the tread surface during the first 500 seconds of the process. Figure 40 shows the same data for the element located at the base of the rim. Figure 41 contains the results for the entire process and indicates that the differences which develop in the three trials during the initial portion of the analysis disappear during the annealing segment. Again, it appears that the inclusion of creep effects is a dominant contributor to the final residual stress estimate.

Figure 42 shows the residual hoop stress distribution through the rim for the three durations of quenching, and highlights the small differences in the three curves near the tread surface. There are some slight differences in the residual tension predicted away from the surface. The predominant effect of varying the duration of the quench is to control the depth of penetration of the residual compression.

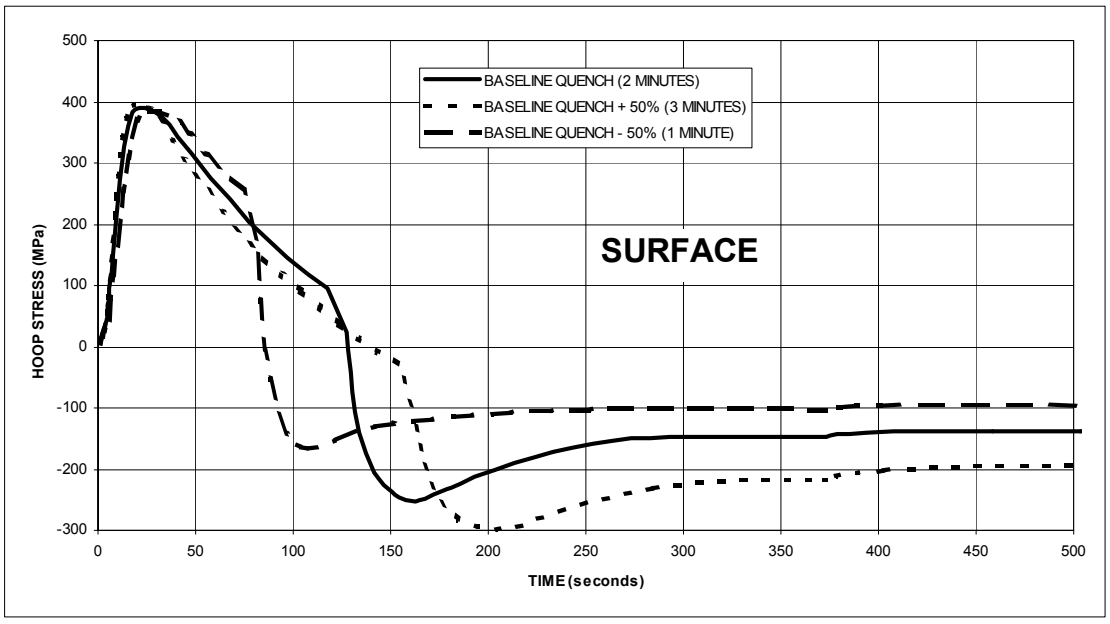

Figure 39. Time history of hoop stress (in MPa) in wheel tread surface during first 500 seconds of process for different quench durations.

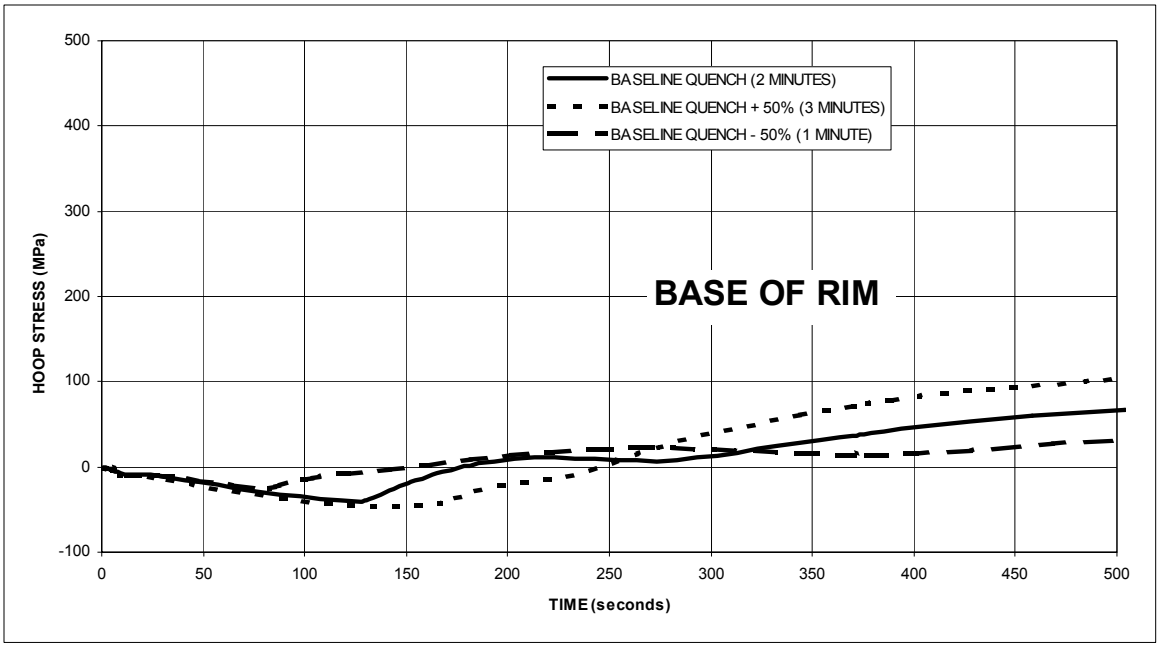

Figure 40. Time history of hoop stress (in MPa) in base of rim during first 500 seconds of process for different quench durations.

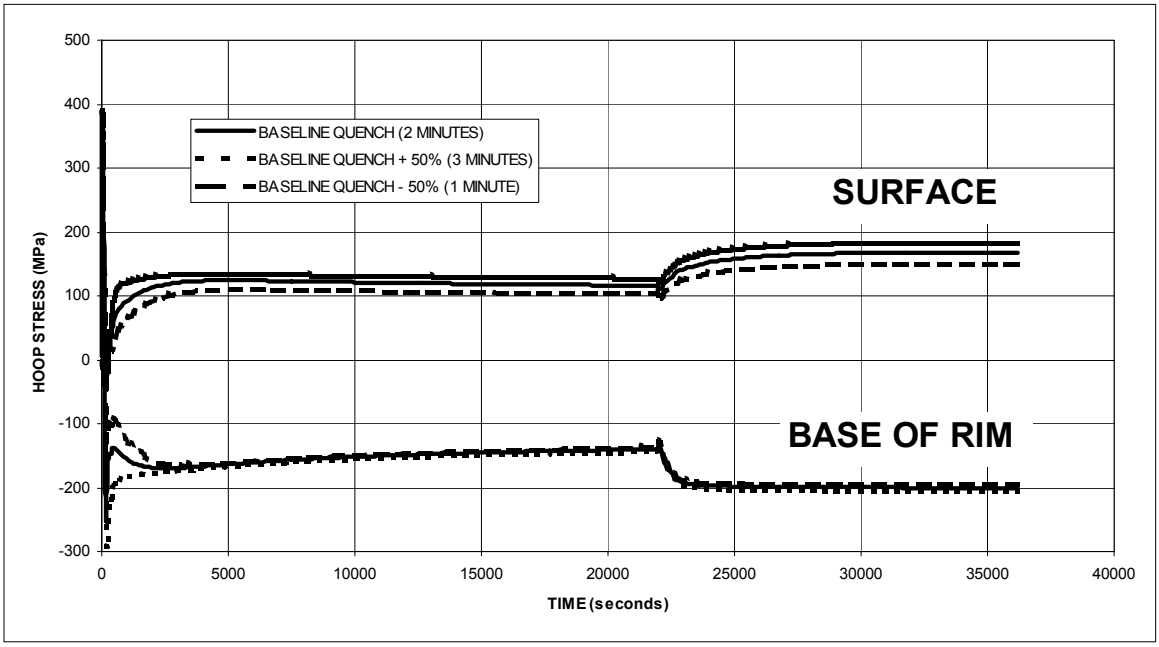

Figure 41. Time history of hoop stress (in MPa) in two elements in wheel rim during entire process for different quench durations.

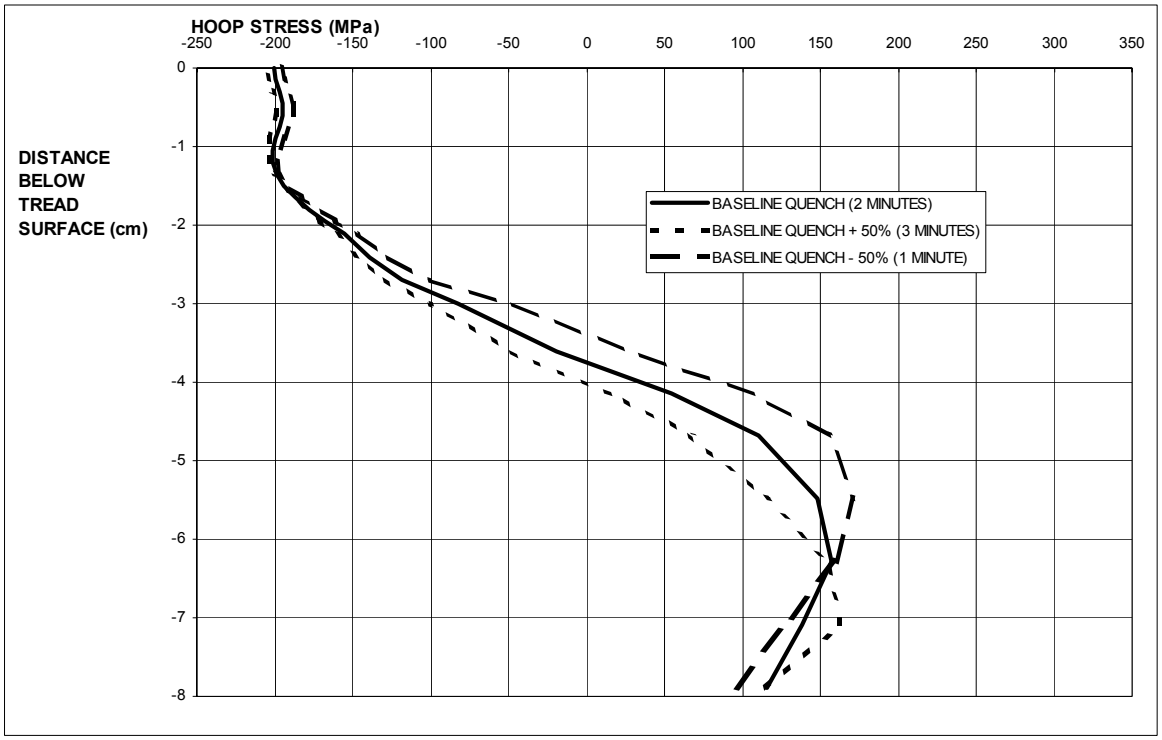

Figure 42. Circumferential (hoop) stress distribution (in MPa) in wheel rim at end of process (time = 10 hours) for different quench durations.

4.2.3 Effect of Variation of Annealing Temperature

It was shown in the preceding sections that the creep behavior exhibited by the material is a significant contributor to the final residual stress state in new wheels. This phenomenon occurs during the annealing and (as shown in Section 3) the creep strain rates are a function of the current state of stress (the local value of the Mises effective stress) and the current temperature.

Examination of Figure 37 for the annealing segment of the process shows the reduction in hoop stress in the wheel. The rate of reduction is rather slow, and suggests that the influence of the annealing duration could be inferred almost by inspection. Rather than examining the effect of duration, the consequences of changing the annealing temperature may be more significant.

The baseline annealing temperature of 496 °C (925 °F) was adjusted by ±150 °C (300 °F) to establish bounds on the predicted residual stresses. The range was selected based on the data developed and plotted in Figure 26. The 650 °C (1200 °F) level represents the maximum allowable temperature which will still result in an austenite phase transformation to pearlite during the process. The 350 °C (660 °F) value denotes the minimum temperature at which this transformation could occur without resulting in the production of martensite. In the following analysis, all other quenching parameters remain the same as for the baseline study.

The results of the simulations conducted at different annealing temperatures are summarized in Table 8. The major finding is that annealing temperature has little effect on the final result. Maximum differences of 61 MPa and 18 MPa in compression and tension, respectively, represent small variances and would do little to either improve or worsen the performance of wheels in service.

Figures 43 and 44 are the time histories of the hoop stress evolution in the tread surface and the base of the rim for the first 500 seconds of the process. As this analysis involves changes to the manufacturing process during the annealing portion only, there are no differences in the curves until the annealing begins (at 370 seconds).

Table 8. Effect of annealing temperature on hoop stress prediction (MPa).

LOCATION (ELEMENT)	LOW TEMPERATURE ANNEAL (350 °C)	BASELINE ANNEAL TEMPERATURE (496 °C)	HIGH TEMPERATURE ANNEAL (650 °C)
BASE OF RIM (538)	186	168	184
TREAD SURFACE (561)	-261	-200	-243

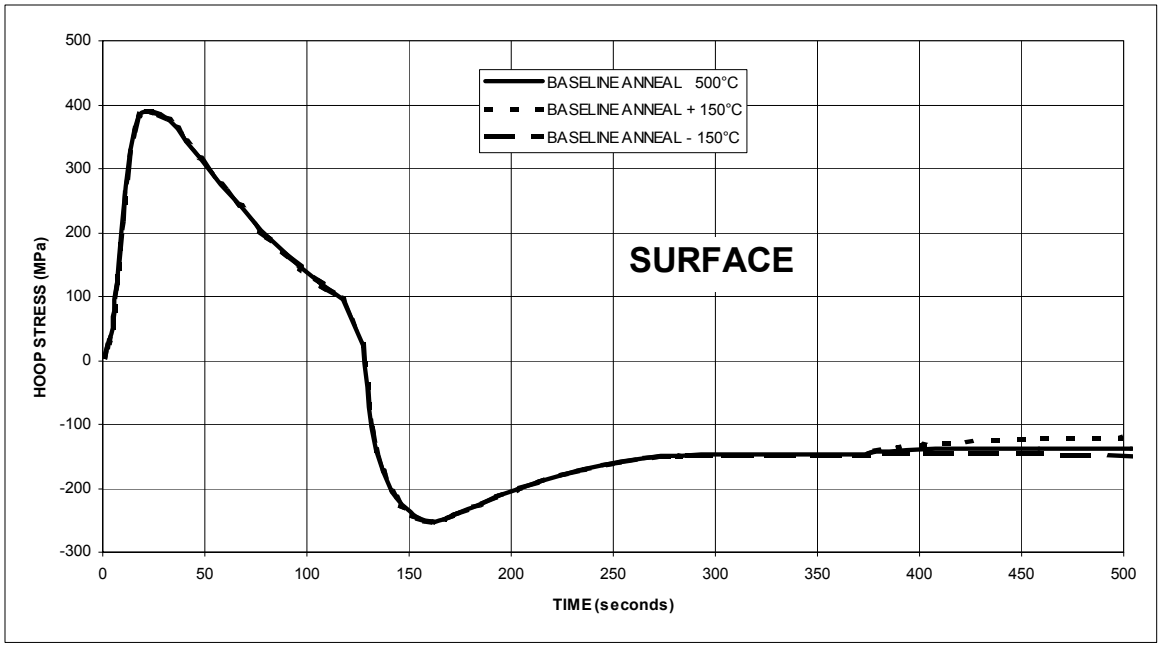

Figure 43. Time history of hoop stress (in MPa) in wheel tread surface during first 500 seconds of process for different annealing temperatures.

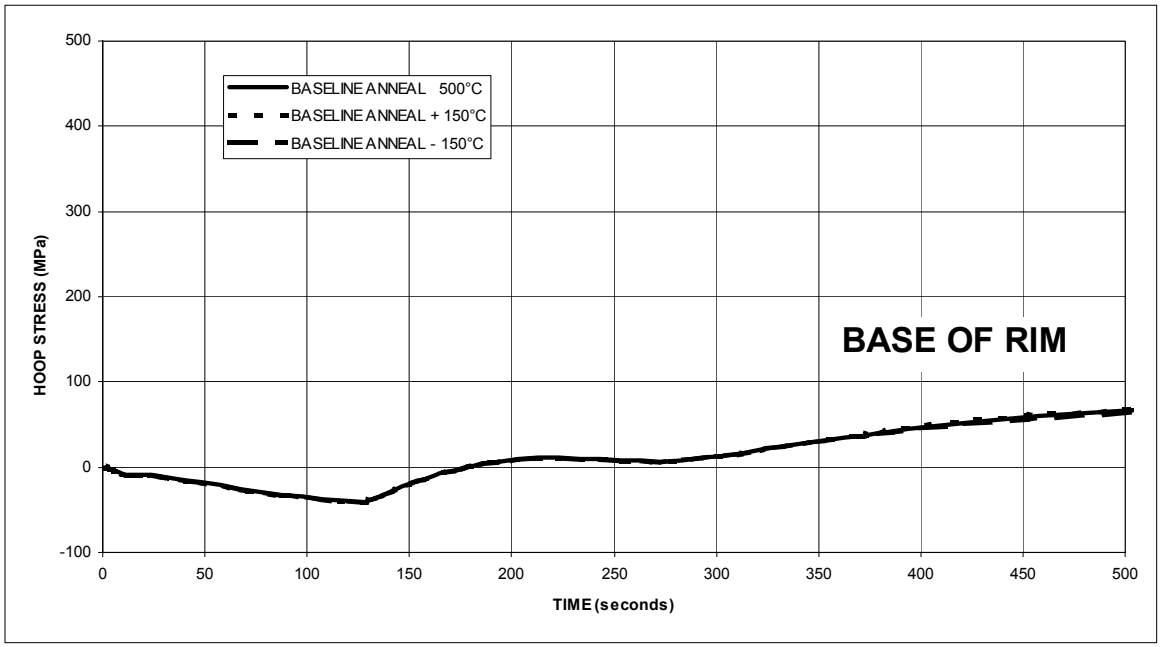

Figure 44. Time history of hoop stress (in MPa) in base of rim during first 500 seconds of process for different annealing temperatures.

Figure 45 is a plot of the hoop stress at the two locations for the entire process. The adjustments to the annealing temperature are evident during the period from 370 to 21,975 seconds. At the point when the wheel has cooled to room temperature, however, the variation from case to case diminishes. The hoop distribution through the rim is shown in Figure 46. The differences in the three analyses are confined to a shallow area below the tread surface.

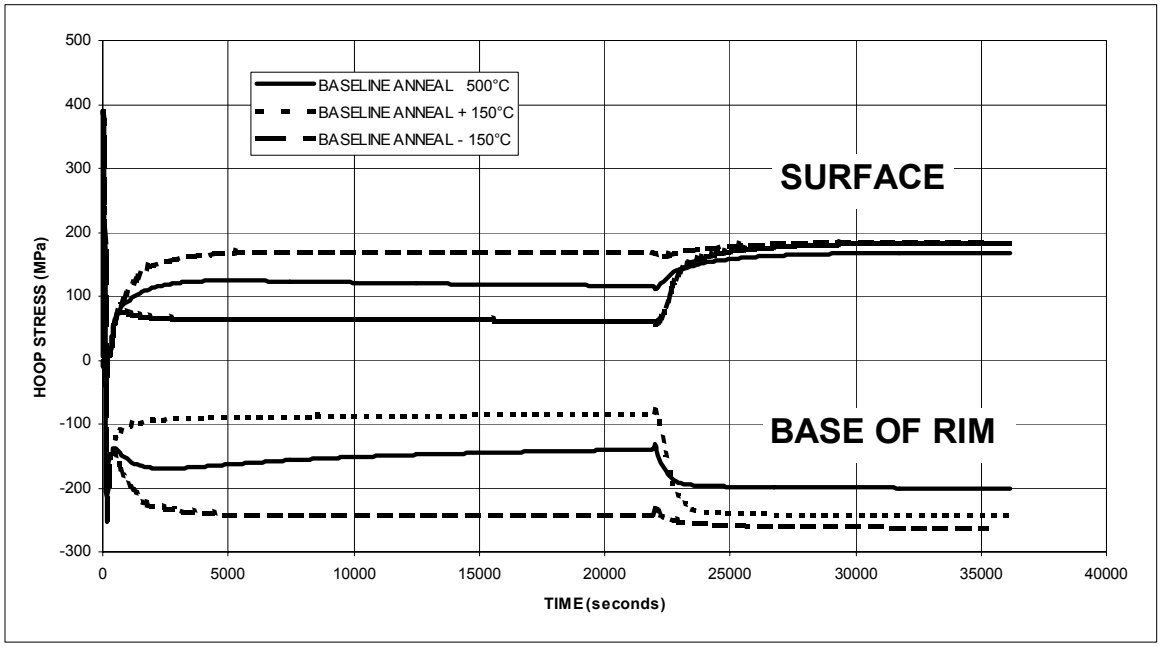

Figure 45. Time history of hoop stress (in MPa) in two elements in wheel rim during entire process for different annealing temperatures.

It is concluded, therefore, that the specification of the annealing temperature does not result in a significant alteration of the estimate of as-manufactured residual stresses in wheels. The two values of annealing temperature examined predict somewhat higher compression at the tread surface than was seen in the baseline case, even though these temperatures lie above and below the baseline temperature.

4.2.4 Effect of Variation of Thermal Expansion Coefficient

As noted previously, the material properties used in the quenching simulation must be specified as functions of temperature. The material data used in the current analysis are given in Appendix A. A review of the literature yielded a wide discrepancy in the reported values for the coefficient of thermal expansion (CTE). As discussed in Section 2, the CTE plays a major role in characterizing thermally induced residual stresses, and proper specification of this material property will directly influence the residual stress prediction.

Figure 47 is a plot of several sets of CTE data. The heavy dashed curve denotes the values used in this study and reported in Appendix A. The other curves in the figure have been collected from other sources. The heavy solid curve denotes the average value of the data collected from the literature.

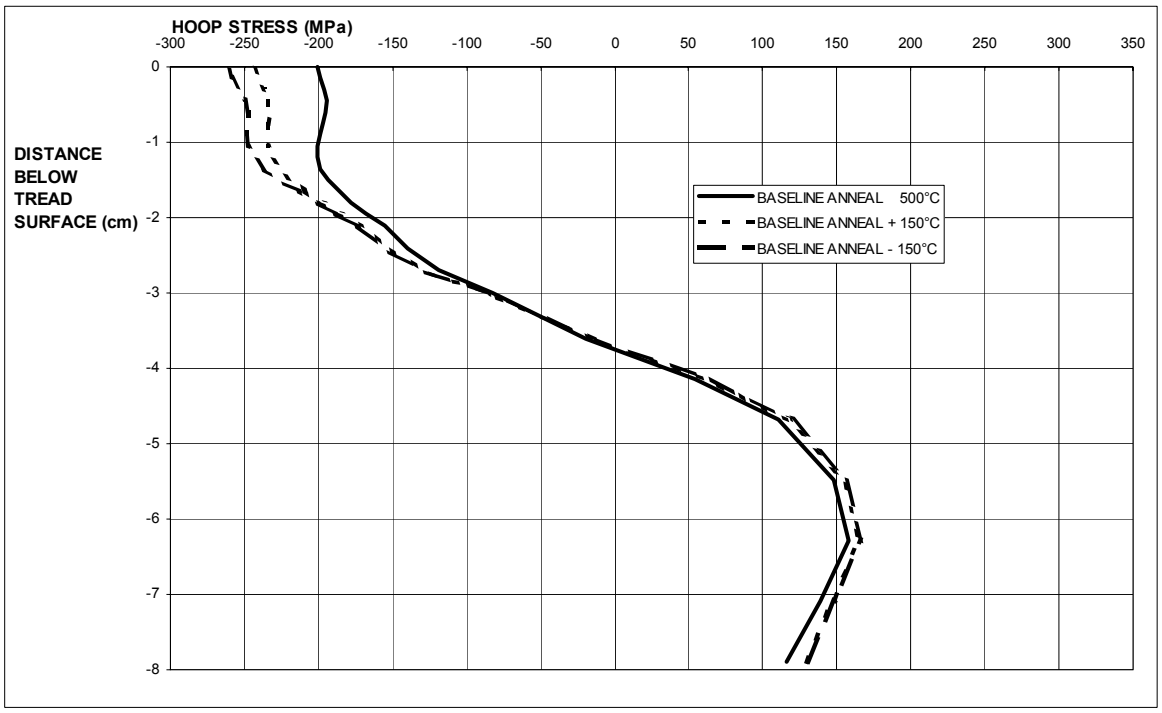

Figure 46. Circumferential (hoop) stress distribution (in MPa) in wheel rim at end of process (time = 10 hours) for different annealing temperatures.

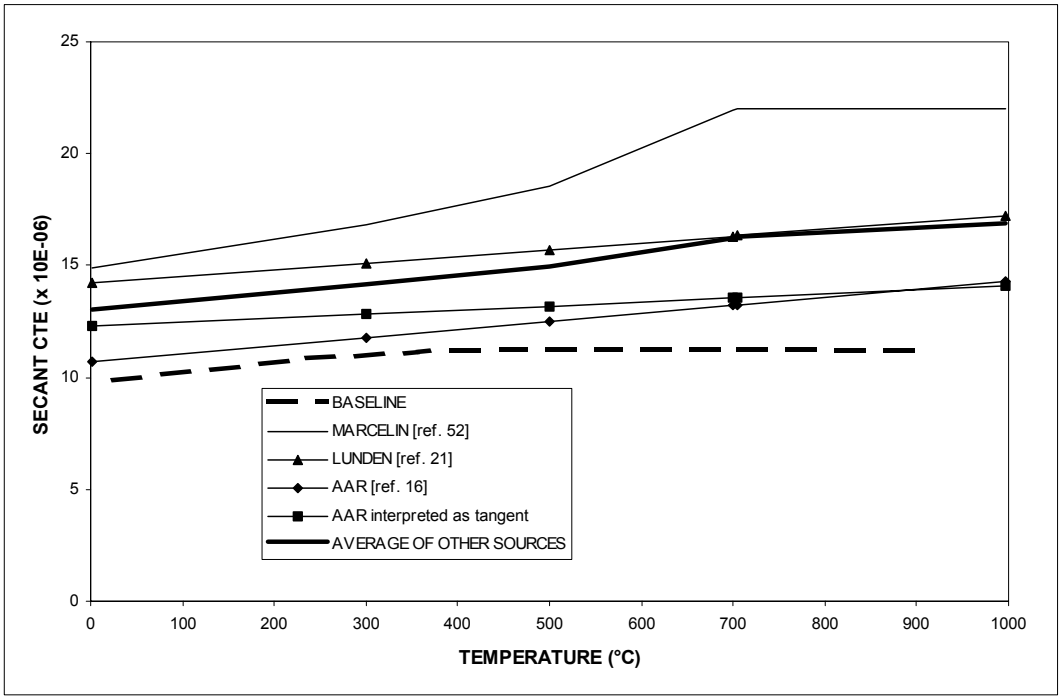

Figure 47. Variation in coefficient of thermal expansion data for steel.

The baseline analysis is repeated, substituting the average CTE data for that originally used and reported in Appendix A. A comparison of the magnitude of the CTE and the relative increase is given in Table 9 for the two sets of material properties.

Table 9. Modifications to thermal expansion coefficient.

TEMPERATURE (°C)	BASELINE (10^{-06})	ADJUSTED (10^{-06})	PERCENT INCREASE
24	9.89	13.11	33
230	10.82	13.88	28
357	11.15	14.38	29
452	11.27	14.78	31
567	11.31	15.41	36
704	11.28	16.28	44
900	11.25	16.69	48
AVERAGE	**10.97**	**14.93**	**36**

Table 10 summarizes the results of the analysis. The residual stresses predicted when the higher CTE data are used differ very little from the baseline result. The primary differences occur early in the process, when the thermal gradients in the rim reach their maximum, as shown in Figure 48 which illustrates the hoop stress evolution during the first 500 seconds of the process for the two locations in the rim which are monitored.

Later in the simulation, these differences disappear as shown in Figure 49, so that at the end of the process the residual compression at the surface is nearly the same value which was obtained for the baseline investigation while the residual tension at the base of the rim exhibits a 30 MPa increase. These variations are not significant from the point of view of wheel performance.

Table 10. Effect of thermal expansion coefficient on hoop stress prediction (MPa).

LOCATION (ELEMENT)	BASELINE EXPANSION COEFFICIENT	ADJUSTED EXPANSION COEFFICIENT
BASE OF RIM (538)	168	196
TREAD SURFACE (561)	-200	-208

Figure 50 is a plot of the hoop stress distribution through the rim obtained using the two sets of CTE data. The primary differences in the two results occur deep in the rim, an area which is not of particular interest in the current study.

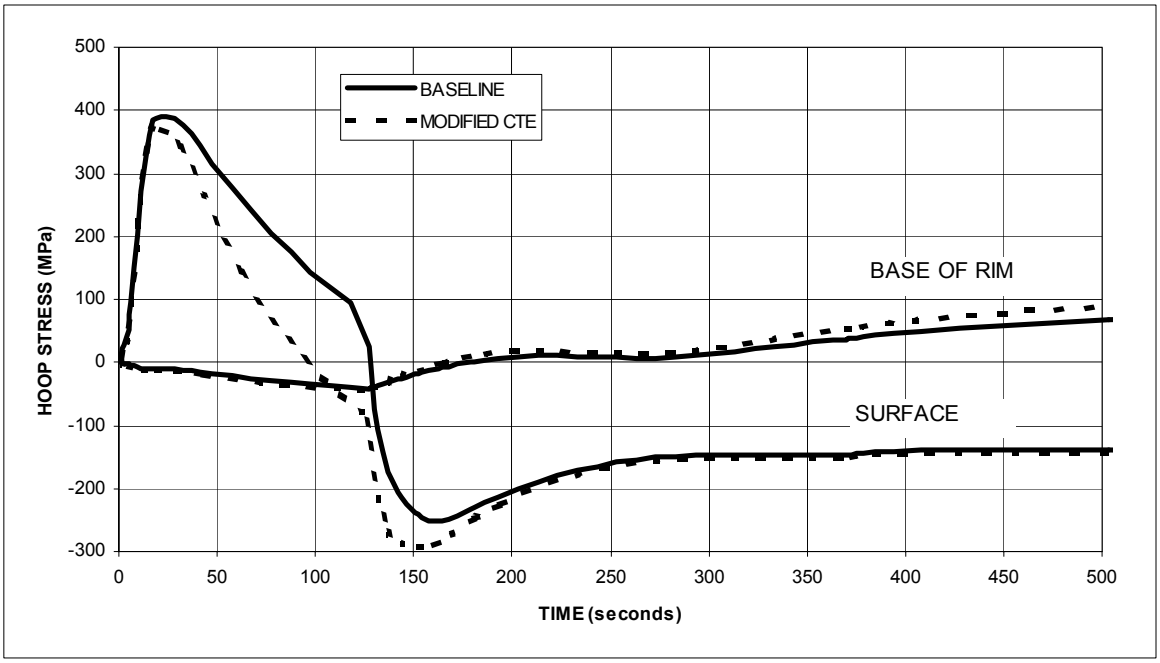

Figure 48. Time history of hoop stress (in MPa) in two elements in wheel rim during first 500 seconds of process for different assumed expansion coefficients.

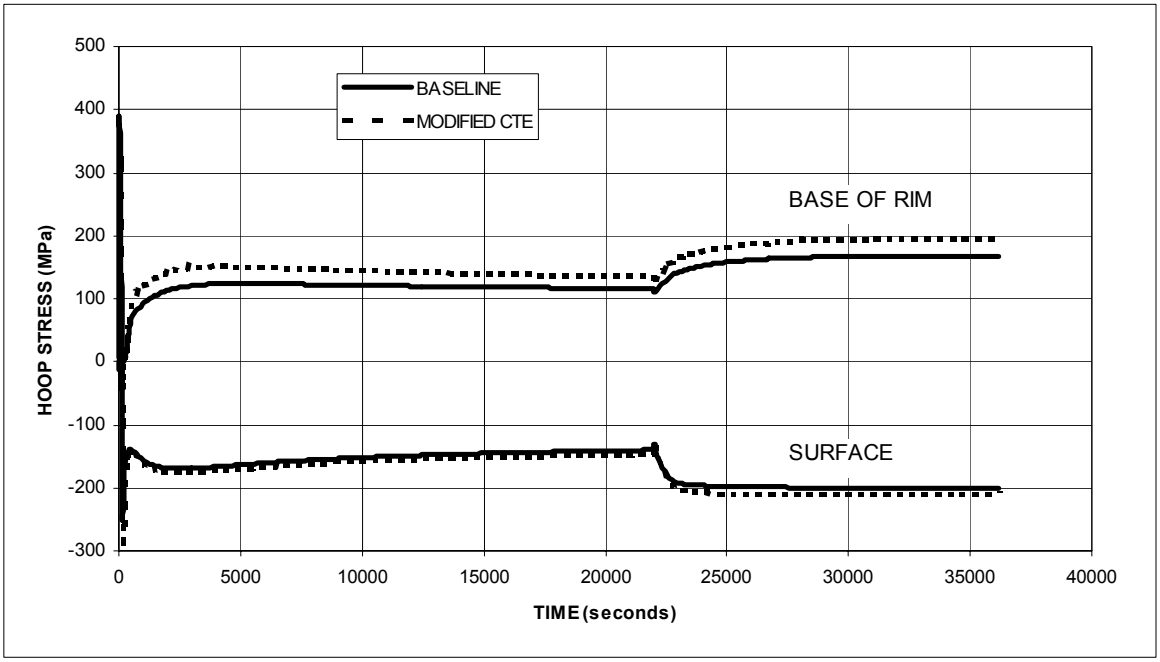

Figure 49. Time history of hoop stress (in MPa) in two elements in wheel rim during entire process for different assumed expansion coefficients.

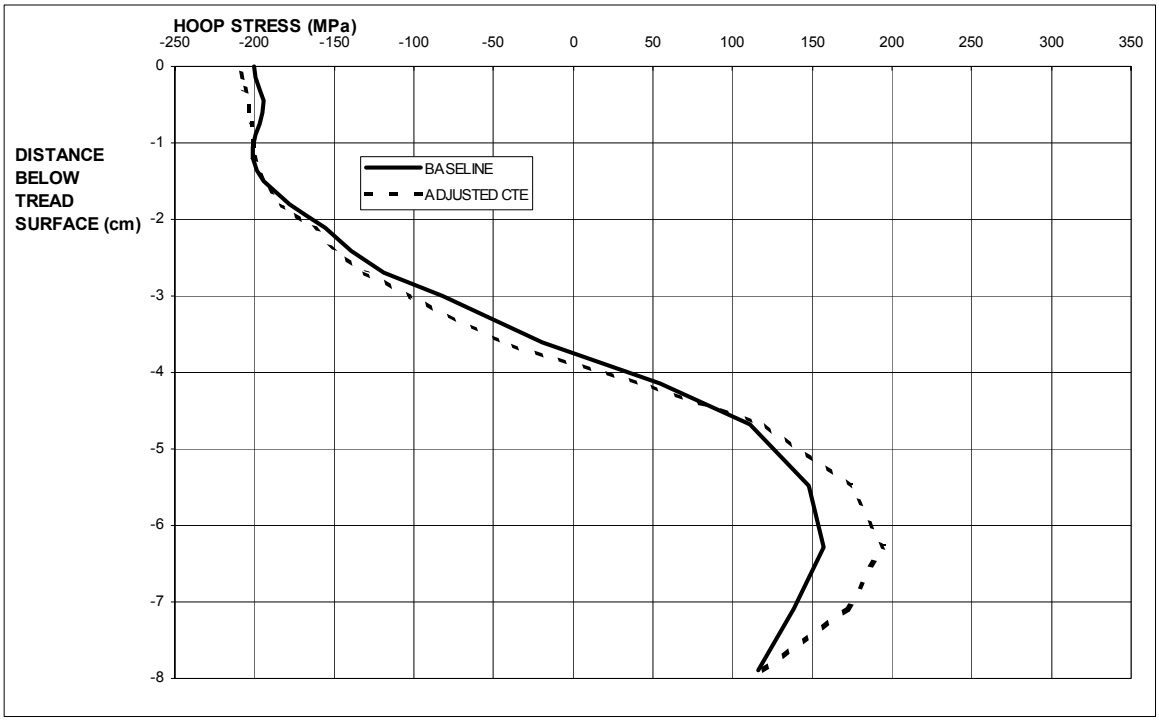

Figure 50. Circumferential (hoop) stress distribution (in MPa) in wheel rim at end of process (time = 10 hours) for different assumed expansion coefficients.

4.3 ASSESSMENT OF BASELINE VARIATIONS

This series of investigations indicates that the baseline set of material properties, in combination with the baseline manufacturing process parameters result in a reasonable estimate of residual stresses in new wheels. In an effort to determine the significance of these characteristics, the manufacturing conditions in the simulation were varied widely. In all cases, including the investigation of what is thought to be the most sensitive material property definition, the coefficient of thermal expansion, the predicted residual hoop compression varied little from the baseline condition. This is an encouraging result, since the exact nature of the manufacturing process is not always available, and the details are often proprietary.

5. CONCLUSIONS

The preceding sections illustrate the development of an analytical strategy for estimating the state of residual stress in as-manufactured commuter railroad vehicle wheels and the effects of service conditions after these wheels are put to use. The initial phase of the study developed an estimate of the residual stresses following manufacture which would serve as a baseline state. The analysis will be extended into a second phase whose broader goal is to create a means for determining the effect that service loads have on this baseline state. Wheel cracking has been attributed to the action of these service loads, due to thermal abuse of these wheels during extreme braking events in combination with the mechanical loads due to wheel-on-rail contact.

The study focused on the magnitude and depth of penetration of the circumferential (hoop) residual stress in the wheel rim since this has been identified as a reasonable means of assessing the likelihood of fatigue cracks to initiate and grow. Residual hoop compression in the wheel rim will aid in preventing the formation of radial cracks, and will impede growth of these cracks if they do manage to form.

The simulation scheme developed here represents the best estimate of the initial manufacturing stresses in the subject 81 cm (32 inch) S-plate commuter car wheels. The analysis described herein is based on a two-step approach comprised of a heat transfer (thermal) and mechanical (stress) analysis which are conducted separately for convenience. The heat transfer portion of the study is designed to yield the transient temperature distribution in the wheel during the simulated manufacturing process. The temperature data is used to estimate the elastic-plastic response of the wheel to the thermal stresses induced by the transient temperature field.

A finite element model has been developed using the ABAQUS finite element code (version 5.5). Several results are presented in the preceding sections which represent variations on several of the manufacturing process parameters. Table 11 presents a summary of the simulated manufacturing conditions and a brief description of the general character of the result in terms of the maximum predicted residual hoop compression at the tread surface (MAX σ_θ) and the depth of penetration of the residual compressive layer (DEPTH).

The data in Table 11 are plotted in Figure 51 to highlight the lack of significant variation in the results. The modifications to the manufacturing process were selected in order to establish bounds on how well these parameters need to be specified (known) since details of processes like this one tend to be manufacturer-specific and proprietary.

Table 11. Summary of results of estimates of manufacturing stresses.

IDENTIFICATION	DESCRIPTION	MAX σ_θ, MPa (ksi)	DEPTH, cm (inches)
BASELINE	Represents the best estimate possible of the manufacturing conditions as well as temperature-dependent material properties with information available.	-200 (-29)	3.75 (1.48)
NO CREEP	Baseline conditions with the effects of viscoelastic creep excluded.	-326 (-47)	3.60 (1.42)
LONG QUENCH	Baseline conditions with the duration of the quench extended by 1 minute.	-205 (-30)	4.00 (1.57)
SHORT QUENCH	Baseline conditions with the duration of the quench reduced by 1 minute.	-195 (-28)	3.40 (1.34)
HIGH TEMP	Baseline conditions with the annealing temperature increased by 150 °C.	-243 (-35)	3.75 (1.48)
LOW TEMP	Baseline conditions with the annealing temperature reduced by 150 °C.	-261 (-38)	3.75 (1.48)
CTE VARIED	Baseline conditions with coefficient of thermal expansion modified to represent the average value of data obtained from other sources.	-208 (-30)	3.90 (1.55)

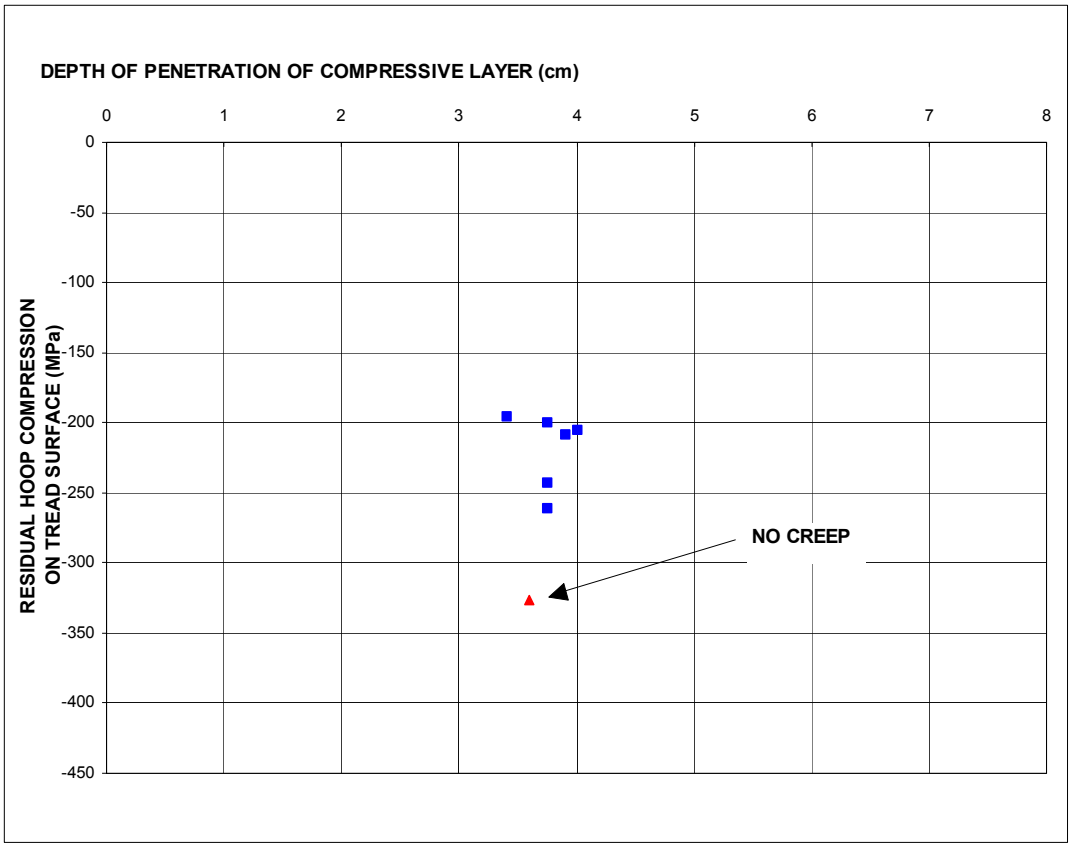

Figure 51. Results of simulations of manufacturing process modifications.

The data in Figure 51 show rather modest variation in the depth of the residual compression at the tread surface which is on the order of 3.4 to 4.0 cm (1.34 to 1.57 inches). With the exception of the result for which creep behavior was suppressed, the predicted compressive stress on the tread surface varies little as well, from -200 to -261 MPa (-29 to -38 ksi). Regardless of the aspect of the manufacturing process which may be poorly specified, the simulation predicts essentially the same distribution in the vicinity of the tread surface where the result in sought (for the purposes of this study).

This is a fortunate outcome, since it makes the predicted residual stress distribution generic and useful for the purposes which have been outline for the second phase of the investigation, namely, the estimation of the effects of service conditions on the as-manufactured stress distribution.

As mentioned in Chapter 1, very few examples of this analysis have been found in the literature. The most complete work has been focused on freight wheels, whose geometry and size differ from the subject wheel and make comparisons of results difficult. The conclusions of Perfect [6] and Kuhlman et al. [7] represent corresponding results for freight wheels and present the data in a form similar to that chosen here (time histories of residual stresses in elements located at the tread surface and at the base of the rim).

For the 102 cm (40 inch) freight (locomotive) wheel in that study, residual stresses at the tread and the base of the rim are on the order of -207 and 40 MPa (-30 and 6 ksi) respectively. The value at the surface agrees well with the prediction obtained here, while away from the surface, the difference is greater. The differences in wheel geometry and simulated manufacturing process may have very little relation to the hoop stress induced near the quenched surface. The data in Figure 51 would tend to support this conclusion.

In the absence of additional analytical data, the estimates of residual stress in the wheel rim developed here represent a reasonable baseline for characterizing the as-manufactured condition of these wheels.

This effort will be extended to provide estimates of the residual stresses in passenger wheels subjected to variations in service conditions. The results of this work will assist in development of a means for predicting wheel performance based on the type of service conditions envisioned.

APPENDIX A

Material Properties Used in Analyses

A.1 Thermal Properties

Table A1. Specific heat [4]

Temperature (°C)	c_p (J/kg K or °C)
0	419.5
350	629.5
703	744.5
704	652.9
710	653.2
800	657.7
950	665.2
1200	677.3

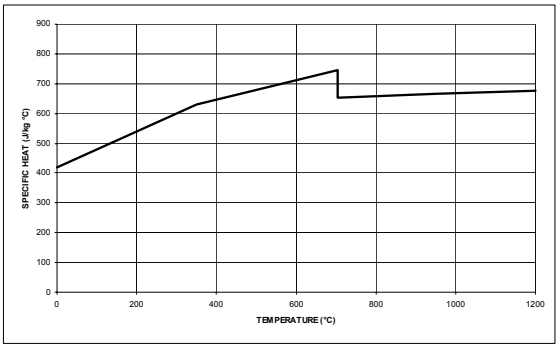

Figure A1. Specific heat versus temperature (°C).

Table A2. Thermal conductivity [4]

Temperature (°C)	k (W/m K or °C)
0	59.71
350	40.88
703	30.21
704	30.18
710	30.00
800	25.00
950	27.05
1200	30.46

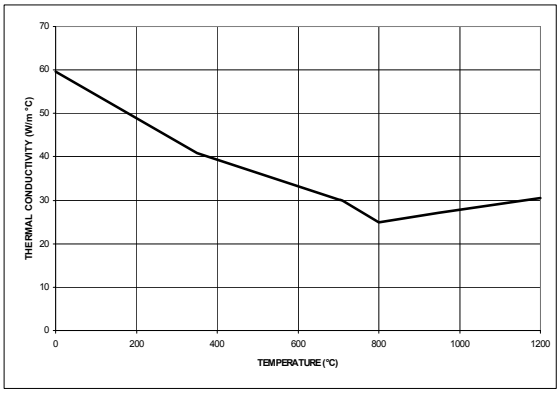

Figure A2. Thermal conductivity versus temperature (°C).

A.2 Mechanical Properties

Table A3. Young's modulus [29]

Temperature (°C)	*E* (GPa)
24	213
230	201
358	193
452	172
567	102
704	50
900	43

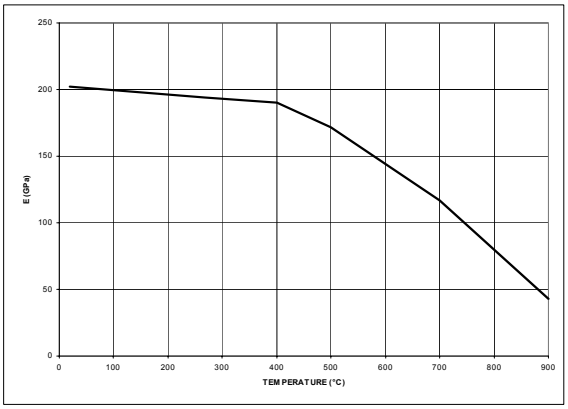

Figure A3. Young's modulus versus temperature (°C).

Table A4. Poisson's ratio [4]

Temperature (°C)	ν
24	0.295
230	0.307
358	0.314
452	0.320
567	0.326
704	0.334
900	0.345

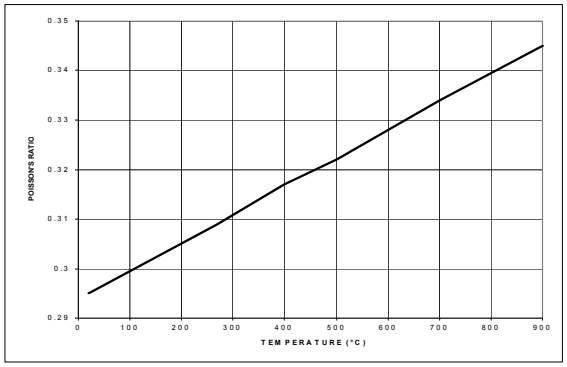

Figure A4. Poisson's ratio versus temperature (°C).

Table A5. Yield strength [29]

Temperature (°C)	σ_y (MPa)
24	422.9
230	424.7
358	366.7
452	291.0
567	132.3
704	39.4
900	11.7

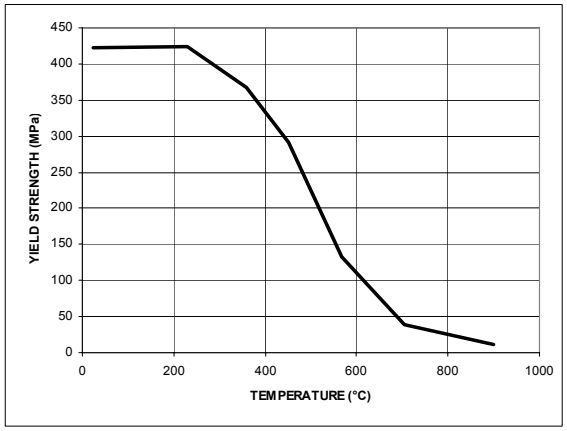

Figure A5. Yield strength versus temperature (°C).

Table A6. Secant coefficient of thermal expansion for quench simulation [29]

Temperature (°C)	$\bar{\alpha}$ (10^{-06}) T_R = 871 °C
0	9.89
230	10.82
358	11.15
452	11.27
567	11.31
704	11.28
900	11.25

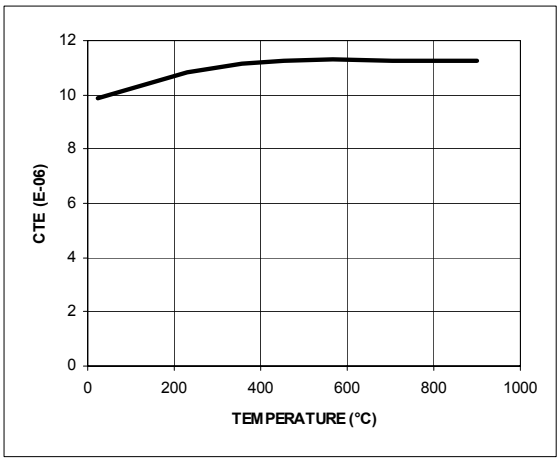

Figure A6. Secant coefficient of thermal expansion for quench simulation versus temperature (°C).

Table A7. Hardening modulus [29]

Temperature (°C)	E_k (GPa)
24	21.66
230	25.73
358	20.29
452	14.89
567	5.93
704	0.92
900	0.085

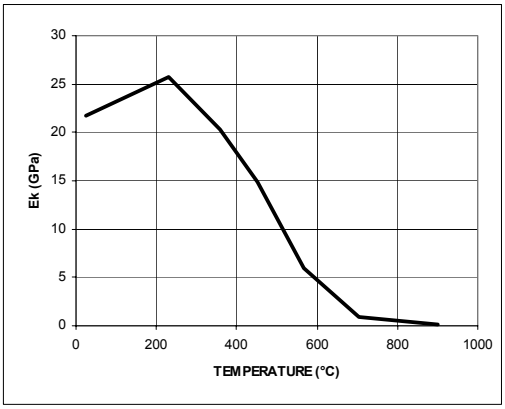

Figure A7. Hardening modulus versus temperature (°C).

A.3 Conversion of Tangent CTE to Secant CTE

Determination of coefficient of thermal expansion for FEM calculations
All temperatures in Centigrade, $\alpha * 10^{-06}$

$i := 1..7$

Low temperature reference
$T0 := 27$

High temperature reference
$T1 := 871$

Tangent coefficient of thermal expansion

$$\alpha\_tang := \begin{bmatrix} 5.30 \\ 8.81 \\ 10.25 \\ 10.95 \\ 11.38 \\ 11.30 \\ 11.25 \end{bmatrix} \quad Temp := \begin{bmatrix} 20 \\ 230 \\ 358 \\ 452 \\ 567 \\ 704 \\ 900 \end{bmatrix}$$

$T := 0, 10..900$
$\alpha(T) := linterp(Temp, \alpha\_tang, T)$

Secant values for low temperature reference

$TLOW_{ref} := T0$

$$\alpha LOW_i := \frac{1}{(Temp_i - TLOW_{ref})} \cdot \left(\int_{TLOW_{ref}}^{Temp_i} \alpha(T)\, dT \right)$$

Secant values for high temperature reference

$THIGH_{ref} := T1$

$$\alpha HIGH_i := \frac{1}{(Temp_i - THIGH_{ref})} \cdot \left(\int_{THIGH_{ref}}^{Temp_i} \alpha(T)\, dT \right)$$

Data now ready for input to ABAQUS/TOPAZ2D:

$Temp_i$	$\alpha(Temp_i)$	αLOW_i	$\alpha HIGH_i$
20	5.3	5.36	9.89
230	8.81	7.11	10.82
358	10.25	8.05	11.15
452	10.95	8.61	11.27
567	11.38	9.16	11.31
704	11.3	9.6	11.28
900	11.25	9.97	11.25

A.4 Determination of Plastic Material Constants

Plastic material constants for meshes 1, 2 and 3

Source data scaled to AAR values for room temperature yield and ultimate strengths

ORIGIN := 1

n := 1.. 7

Baseline yield strength $YSG := \begin{bmatrix} 422.9 \\ 424.7 \\ 366.7 \\ 291.0 \\ 132.3 \\ 39.4 \\ 11.7 \end{bmatrix}$

Convert to ksi $rt\_base := \frac{422.9}{6.895}$

Source RT yield (ksi) $rt\_base = 61.3343$

AAR RT yield (ksi) $actual := 65$

$scale := \frac{actual}{rt\_base}$ $scale = 1.059766$ YS = YSG * scale

Yield strength $YS = \begin{bmatrix} 448.175 \\ 450.082579 \\ 388.616156 \\ 308.391878 \\ 140.207029 \\ 41.754777 \\ 12.399261 \end{bmatrix}$

Young's modulus $EMOD := \begin{bmatrix} 213331.3 \\ 200713.5 \\ 192853.2 \\ 172306.1 \\ 101701.3 \\ 49781.9 \\ 43014.706 \end{bmatrix}$

Plastic modulus $EKMOD := \begin{bmatrix} 21657.2 \\ 25725.25 \\ 20285.09 \\ 14893.2 \\ 5929.7 \\ 917.035 \\ 84.602369 \end{bmatrix}$

Ultimate strength $UTS := \begin{bmatrix} 723.975 \\ 722.0444 \\ 623.34937 \\ 494.6473 \\ 224.93567 \\ 66.929765 \\ 19.36 \end{bmatrix}$

Elastic strain $EE_n := \frac{YS_n}{EMOD_n}$

Incremental strain $EI_n := \frac{UTS_n - YS_n}{EKMOD_n}$

Total strain $ET_n := EE_n + EI_n$

Plastic strain $EP_n := ET_n - \frac{UTS_n}{EMOD_n}$

$$EE = \begin{bmatrix} 2.10084.10^{-3} \\ 2.242413.10^{-3} \\ 2.015088.10^{-3} \\ 1.789791.10^{-3} \\ 1.378616.10^{-3} \\ 8.387542.10^{-4} \\ 2.882563.10^{-4} \end{bmatrix} \quad EI = \begin{bmatrix} 0.012735 \\ 0.010572 \\ 0.011572 \\ 0.012506 \\ 0.014289 \\ 0.027453 \\ 0.082276 \end{bmatrix} \quad ET = \begin{bmatrix} 0.014836 \\ 0.012814 \\ 0.013587 \\ 0.014296 \\ 0.015667 \\ 0.028291 \\ 0.082564 \end{bmatrix} \quad EP = \begin{bmatrix} 0.011442 \\ 9.21681 \cdot 10^{-3} \\ 0.010355 \\ 0.011425 \\ 0.013456 \\ 0.026947 \\ 0.082114 \end{bmatrix}$$

Appendix B

Sample ABAQUS Data Files

B.1 Input File for Thermal Analysis

```
**---------------------------------------------------------------------
** adjustments have been made so this calculation is done in SI
** units with temperatures in Centigrade
**---------------------------------------------------------------------
**---------------------------------------------------------------------
** insert introductory material for this analysis
**
*HEADING
WHEEL QUENCH ANALYSIS WITH IMPROVED USER CONTROLS (MESH 2)
**
** end of introductory material for this analysis
**---------------------------------------------------------------------
**---------------------------------------------------------------------
** inserted after data check run to improve cpu performance
**
*WAVEFRONT MINIMIZATION,SUPPRESS
**
** end of bw minimization
**---------------------------------------------------------------------
**---------------------------------------------------------------------
** define nodal coordinates [node number, r, z] in meters
**
*NODE,NSET=ALL_N,SYSTEM=R
    10.069110000.20574400
    20.069110000.18957800
    30.069110000.17341200
    40.069110000.15724701
    50.069110000.14108101
    .
    .
    nodes 6 through 627
    .
    .
  6280.406078010.07076490
  6290.406183990.06723550
  6300.406289990.06370610
  6310.406396000.06017670
  6320.406502010.05664730
**
** end of nodal coordinate definitions
**---------------------------------------------------------------------
**---------------------------------------------------------------------
** define node sets
**
** define nodes through rim
*NSET,NSET=TREAD
  624  582  540
**
** define line of nodes through rim
*NSET,NSET=T1
  624  603  582  561  540  519  498  477  456  407  390  376  238  223
  210  197  184  171
**
```

```
*NSET,NSET=F1,GENERATE
  957  989    1
*NSET,NSET=FLUX
   F1  536  560  550
**
** end of node set definitions
**-----------------------------------------------------------------------
**-----------------------------------------------------------------------
** define element connectivity, and element type
**
*ELEMENT,TYPE=DCAX4,ELSET=ALL_E
    1    1    2   14   13
    2   13   14   26   25
    3   25   26   38   37
    4   37   38   50   49
    5    2    3   15   14
    .
    .
    elements 6 through 554
    .
    .
  555  355  356  365  364
  556  356  357  366  365
  557  357  358  367  366
  558  358  359  368  367
  559  359  360  361  368
**
** end of element connectivity definitions
**-----------------------------------------------------------------------
**-----------------------------------------------------------------------
** define element set through rim
**
*ELSET,ELSET=ELRIM
  323  321  319
**
** end of element set definition
**-----------------------------------------------------------------------
**-----------------------------------------------------------------------
** define convective and radiative surfaces
**
*ELSET,ELSET=BACKF,GENERATE
  504  507    1
  516  522    1
*ELSET,ELSET=FLAN2
  530  537  543  551
*ELSET,ELSET=FLAN3
  559  558  557  556  555  554
*ELSET,ELSET=FLAN4
  553  552  544  538  531  523
*ELSET,ELSET=TREAD
  446  439  434  417  408  396  387  370  361  349  340  323  314  302
  293  276  267  255  246  229  220  208  199  182  173
*ELSET,ELSET=FRNT3
  165  153
*ELSET,ELSET=FRNT4
  145  144  143  142  141  140  139  138  136  135  134  133
*ELSET,ELSET=WTOP1
  133  154  183  230
*ELSET,ELSET=WTOP4
  129  125  121  117  113  109  105  101   97   93   89   85   81   77
```

```
   73   69   65   61   57   53   49   45
*ELSET,ELSET=WTOP3
    8    4
*ELSET,ELSET=BRTOP
    4    3    2    1
*ELSET,ELSET=IBORE,GENERATE
    1   41    4
*ELSET,ELSET=BRBOT
   41   42   43   44
*ELSET,ELSET=WBOT3
   44   40   36   32   28
*ELSET,ELSET=WBOT2
   48   52   56   60   64   68   72   76   80   84   88   92   96  100
  104  108  112  116  120  124  128  132
*ELSET,ELSET=WBOT1
  447  466  485  504
**
** end of surface definitions
**------------------------------------------------------------------------
**------------------------------------------------------------------------
** define time-dependent variables (not all are used)
**
*AMPLITUDE,NAME=T_AMB,DEFINITION=TABULAR,TIME=TOTAL TIME,VALUE=ABSOLUTE
      0.00    871.00      5.00     21.00    125.00     21.00    130.00
     21.00    370.00     21.00    375.00    496.00  21975.00    496.00
  21980.00     21.00  36175.00     21.00
**
** end of definition of time-dependent variables
**------------------------------------------------------------------------
**------------------------------------------------------------------------
**define material properties
**
*SOLID SECTION,ELSET=ALL_E,MATERIAL=WHLSTEEL
*MATERIAL,NAME=WHLSTEEL
*DENSITY
     7861.
*LATENT HEAT
    40310.      703.      720.
*SPECIFIC HEAT
     419.5        0.
     629.5      350.
     744.5      703.
     652.9      704.
     653.2      710.
     657.7      800.
     665.2      950.
     677.3     1200.
*CONDUCTIVITY,TYPE=ISO
     59.71        0.
     40.88      350.
     30.21      703.
     30.18      704.
     30.00      710.
     25.00      800.
     27.05      950.
     30.46     1200.
**
** end of material property definition
**------------------------------------------------------------------------
**------------------------------------------------------------------------
```

```
** assign initial temperature to all nodes [827 degrees C]
**
*INITIAL CONDITIONS,TYPE=TEMPERATURE
ALL_N 871.
**
** end of nodal initial temperature assignment
**------------------------------------------------------------------------
*USER SUBROUTINE
C
C User subroutine to calculate heat transfer coefficient
C for quenched surface and rim back face (in contact with suppport)
C
C
      SUBROUTINE FILM(H,SINK,TEMP,KSTEP,KINC,TIME,NOEL,NPT,COORDS,
     +                 JLTYP)
      INCLUDE 'ABA_PARAM.INC'
      DIMENSION H(2),COORDS(3),TIME(2)
      DIMENSION IBOTM(11)
      DIMENSION IQNCH(25)
      DIMENSION TEMPS(8)
      DIMENSION SUPPK(8)
      DATA IBOTM/504,505,506,507,516,517,518,519,520,521,522/
      DATA IQNCH/446,439,434,417,408,396,387,370,361,349,
     +            340,323,314,302,293,276,267,255,246,229,
     +            220,208,199,182,173/
      DATA TEMPS/0.,350.,703.,704.,710.,800.,950.,1200./
      DATA SUPPK/59.71,40.88,30.21,30.18,30.00,25.00,27.05,30.46/
C
C Initialize variables
C
C     define time variable so know where you are during quench
C
      TTIME=TIME(2)
C
C     initialize switches which tell whether you are on the
C     quenched surface or on the back rim face (on support)
C
      IBOTTOM=0
      IQUENCH=0
C
C     establish dummy variable to hold value for H(1)
C
      VAL=    0.
C
C     set scale factor to adjust pseudo-h for back rim face
C     this number scales the conductivity into an effective "h"
C     for the part of the wheel in contact with the support
C
      SCALE=  1./2.2094
C
C     define heat transfer coefficients for wheel to water (HMAX)
C     and wheel to air (HMIN)
C
      HMAX=3066.
      HMIN=  28.
C
C     initialize sink (ambient) temperature
C
      SINK=   0.
C
```

```
C     establish exponent on delta-T part of convection calculation
C
      XPON=   0.00
C
C     set quench temperature and duration (in minutes)
C
      QT=   871.
      QD=     2.00
      QDS=QD*60.
C
C     set dwell duration between quench and draw (in minutes)
C
      DWL=4.
      DWS=DWL*60.
C
C     set draw temperature and duration (in minutes)
C
      DT=   496.
      DD=   360.
      DDS=DD*60.
C
C     set ambient (room) temperature
C
      RT=    21.
C
C     set ramp time (seconds)
C
      TR=5.
C
C Determine where the element is (which group: quench surface or support)
C
      DO 10 I=1,11
      IF(NOEL.EQ.IBOTM(I))IBOTTOM=1
10    CONTINUE
C
C
      DO 20 I=1,25
      IF(NOEL.EQ.IQNCH(I))IQUENCH=1
20    CONTINUE
C
C Have different values for H(1) and H(2) depending on whether
C quenched or in contact with support or just a free surface
C
      IF(IBOTTOM.EQ.1)THEN
         DO 30 I=1,7
            IF(TEMP.GE.TEMPS(I).AND.TEMP.LT.TEMPS(I+1))THEN
            RAT=(TEMP-TEMPS(I))/(TEMPS(I+1)-TEMPS(I))
            DIF=SUPPK(I+1)-SUPPK(I)
            CONST=RAT*DIF
            VAL=(SUPPK(I)+CONST)*SCALE
C
C     Patch by jg (03/31/95) to fix conductivity curve dip
C
         IF(TTIME.GT.1500..AND.TEMP.GT.340..AND.TEMP.LT.360.)THEN
                  CONST=-1.*(TEMP*0.042)
                  VAL=((SUPPK(1)-4.143)+CONST)*SCALE
         END IF
                  IF(TTIME.GE.0..AND.TTIME.LT.TR)THEN
                    SINK=QT-((QT-RT)*(TTIME/TR))
                  END IF
```

```
                IF(TTIME.GE.TR.AND.TTIME.LT.(TR+QDS))THEN
                  SINK=RT
                END IF
                IF(TTIME.GE.(TR+QDS).AND.TTIME.LT.(TR+QDS+TR))THEN
                  SINK=RT
                END IF
                IF(TTIME.GE.(TR+QDS+TR))THEN
                  IF(TTIME.LT.(TR+QDS+TR+DWS))SINK=RT
                  IF(TTIME.GE.(TR+QDS+TR+DWS).AND
     +                    .TTIME.LT.(TR+QDS+TR+DWS+TR))THEN
                     T=TTIME-(TR+QDS+TR+DWS)
                     SINK=RT+((DT-RT)*(T/TR))
                  END IF
                  IF(TTIME.GE.(TR+QDS+TR+DWS+TR).AND
     +                    .TTIME.LT.(TR+QDS+TR+DWS+TR+DDS))SINK=DT
                  IF(TTIME.GE.(TR+QDS+TR+DWS+TR+DDS).AND
     +                    .TTIME.LT.(TR+QDS+TR+DWS+TR+DDS+TR))THEN
                     T=TTIME-(TR+QDS+TR+DWS+TR+DDS+TR)
                     SINK=DT-((DT-RT)*(T/TR))
                  END IF
                  IF(TTIME.GE.(TR+QDS+TR+DWS+TR+DDS+TR))SINK=RT
                END IF
                H(1)=VAL
                H(2)=DIF/(TEMPS(I+1)-TEMPS(I))
             END IF
30        CONTINUE
       END IF
C
C
       IF(IQUENCH.EQ.1)THEN
          IF(TTIME.GE.0..AND.TTIME.LT.TR)THEN
             VAL=HMIN+((TTIME/TR)*(HMAX-HMIN))
             SINK=QT-((QT-RT)*(TTIME/TR))
             H(1)=VAL*((ABS((0.5*(TEMP+SINK))-SINK))**XPON)
             H(2)=0.0
          END IF
          IF(TTIME.GE.TR.AND.TTIME.LT.(TR+QDS))THEN
             VAL=HMAX
             SINK=RT
             H(1)=VAL
             H(2)=0.00
          END IF
          IF(TTIME.GE.(TR+QDS).AND.TTIME.LT.(TR+QDS+TR))THEN
             T=TTIME-(TR+QDS)
             VAL=HMAX-((T/TR)*(HMAX-HMIN))
             SINK=RT
             H(1)=VAL*((ABS((0.5*(TEMP+SINK))-SINK))**XPON)
             H(2)=0.0
          END IF
          IF(TTIME.GE.(TR+QDS+TR))THEN
             IF(TTIME.LT.(TR+QDS+TR+DWS))SINK=RT
             IF(TTIME.GE.(TR+QDS+TR+DWS).AND
     +             .TTIME.LT.(TR+QDS+TR+DWS+TR))THEN
                T=TTIME-(TR+QDS+TR+DWS)
                SINK=RT+((DT-RT)*(T/TR))
             END IF
             IF(TTIME.GE.(TR+QDS+TR+DWS+TR).AND
     +             .TTIME.LT.(TR+QDS+TR+DWS+TR+DDS))SINK=DT
             IF(TTIME.GE.(TR+QDS+TR+DWS+TR+DDS).AND
     +             .TTIME.LT.(TR+QDS+TR+DWS+TR+DDS+TR))THEN
```

```
                T=TTIME-(TR+QDS+TR+DWS+TR+DDS)
                SINK=DT-((DT-RT)*(T/TR))
             END IF
             IF(TTIME.GE.(TR+QDS+TR+DWS+TR+DDS+TR))SINK=RT
             VAL=HMIN
             H(1)=VAL*((ABS((0.5*(TEMP+SINK))-SINK))**XPON)
             H(2)=0.00
          END IF
       END IF
C
       IF(IQUENCH.EQ.0.AND.IBOTTOM.EQ.0)THEN
          IF(TTIME.GE.0..AND.TTIME.LT.TR)THEN
             SINK=QT-((QT-RT)*(TTIME/TR))
          END IF
          IF(TTIME.GE.TR.AND.TTIME.LT.(TR+QDS))THEN
             SINK=RT
          END IF
          IF(TTIME.GE.(TR+QDS).AND.TTIME.LT.(TR+QDS+TR))THEN
             SINK=RT
          END IF
          IF(TTIME.GE.(TR+QDS+TR))THEN
             IF(TTIME.LT.(TR+QDS+TR+DWS))SINK=RT
             IF(TTIME.GE.(TR+QDS+TR+DWS).AND
     +             .TTIME.LT.(TR+QDS+TR+DWS+TR))THEN
                T=TTIME-(TR+QDS+TR+DWS)
                SINK=RT+((DT-RT)*(T/TR))
             END IF
             IF(TTIME.GE.(TR+QDS+TR+DWS+TR).AND
     +             .TTIME.LT.(TR+QDS+TR+DWS+TR+DDS))SINK=DT
             IF(TTIME.GE.(TR+QDS+TR+DWS+TR+DDS).AND
     +             .TTIME.LT.(TR+QDS+TR+DWS+TR+DDS+TR))THEN
                T=TTIME-(TR+QDS+TR+DWS+TR+DDS)
                SINK=DT-((DT-RT)*(T/TR))
             END IF
             IF(TTIME.GE.(TR+QDS+TR+DWS+TR+DDS+TR))SINK=RT
          END IF
             VAL=HMIN
             H(1)=ABS(VAL*((ABS((0.5*(TEMP+SINK))-SINK))**XPON))
             H(2)=0.00
       END IF
C
       IF(NOEL.EQ.622)THEN
             WRITE(6,*)TTIME,H(1)
       END IF
       RETURN
       END
**----------------------------------------------------------------------
** begin step definition of analysis
**
*STEP,INC=10000
**----------------------------------------------------------------------
** assign heat transfer solution parameters
**
*HEAT TRANSFER,DELTMX=50.,END=PERIOD
** assign time step, duration, min. step, max. step
1.0,370.00,0.0001,1.
**
** end of heat transfer solution parameter assignment
**----------------------------------------------------------------------
**----------------------------------------------------------------------
```

```
** define DOF monitor
**
*MONITOR,NODE=621,DOF=11,FREQUENCY=0
**
** end of DOF monitor assignment
**------------------------------------------------------------------
**------------------------------------------------------------------
** controls section (used to control convergence criteria)
**
*CONTROLS,ANALYSIS=DISCONTINUOUS
**
** end of controls section
**------------------------------------------------------------------
**------------------------------------------------------------------
** define radiation boundary conditions
**
*PHYSICAL CONSTANTS,ABSOLUTE ZERO=-273.15
*RADIATE,AMPLITUDE=T_AMB
BACKF   R2      5.3865E-08
FLAN2   R2      5.3865E-08
FLAN3   R3      5.3865E-08
FLAN4   R4      5.3865E-08
TREAD   R3      5.3865E-08
FRNT3   R3      5.3865E-08
FRNT4   R4      5.3865E-08
WTOP1   R1      5.3865E-08
WTOP4   R4      5.3865E-08
WTOP3   R3      5.3865E-08
BRTOP   R4      5.3865E-08
IBORE   R1      5.3865E-08
BRBOT   R2      5.3865E-08
WBOT3   R3      5.3865E-08
WBOT2   R2      5.3865E-08
WBOT1   R1      5.3865E-08
**
** end of radiation boundary condition definition
**------------------------------------------------------------------
**------------------------------------------------------------------
** define film [convection] coefficients and sink temperatures
**
*FILM
**
** this is for ALL surfaces except the contact surface and
** the quenched area
**
FLAN2 F2NU
FLAN3 F3NU
FLAN4 F4NU
FRNT3 F3NU
FRNT4 F4NU
WTOP1 F1NU
WTOP4 F4NU
WTOP3 F3NU
BRTOP F4NU
IBORE F1NU
BRBOT F2NU
WBOT3 F3NU
WBOT2 F2NU
WBOT1 F1NU
**
```

```
** this is for the quenched region
**
TREAD F3NU
**
** this is for the rim back face [on support]
**
BACKF F2NU
**
** end of convection coefficient definition
**-----------------------------------------------------------------------
**-----------------------------------------------------------------------
** define results file (*.RES) requirements
**
*RESTART,WRITE,FREQUENCY=1
**
** this line controls output to ".MSG" file
**
*PRINT,FREQUENCY=0
**
** this line controls output to ".DAT" file
**
*NODE PRINT,FREQUENCY=0
**
** the next three lines control output to ".FIL" file
** (for stress analysis)
** (writes NT variable to ".FIL" file)
**
*NODE FILE,FREQUENCY=1,NSET=ALL_N
NT
**
** end of results file requirements definition
**-----------------------------------------------------------------------
*END STEP
**
** end of step definition
**-----------------------------------------------------------------------
*STEP,INC=10000
*HEAT TRANSFER,DELTMX=50.,END=PERIOD
1.,21610.,0.00000001,10.
*CONTROLS,ANALYSIS=DISCONTINUOUS
*RESTART,WRITE,FREQUENCY=5
*NODE FILE,FREQUENCY=1,NSET=ALL_N
NT
*END STEP
**-----------------------------------------------------------------------
*STEP,INC=10000
*HEAT TRANSFER,DELTMX=50.,END=PERIOD
10.,14195.,0.1,100.
*CONTROLS,ANALYSIS=DISCONTINUOUS
*RESTART,WRITE,FREQUENCY=5
*NODE FILE,FREQUENCY=1,NSET=ALL_N
NT
*END STEP
**-----------------------------------------------------------------------
```

B.2 Input File for Stress Analysis

```
**-----------------------------------------------------------------------
** insert introductory material for this analysis
**
*HEADING
WHEEL STRESS ANALYSIS USING AAR/TTC MATERIAL PROPERTIES (MESH 2)
**
** end of introductory material for this analysis
**-----------------------------------------------------------------------
**-----------------------------------------------------------------------
** inserted after data check run to improve cpu performance
**
*WAVEFRONT MINIMIZATION,SUPPRESS
**
** end of bw minimization
**-----------------------------------------------------------------------
**-----------------------------------------------------------------------
** define nodal coordinates [node number, r, z] in meters
**
*NODE,NSET=ALL_N,SYSTEM=R
    10.069110000.20574400
    20.069110000.18957800
    30.069110000.17341200
    40.069110000.15724701
    50.069110000.14108101
    .
    .
    nodes 6 through 627
    .
    .
  6280.406078010.07076490
  6290.406183990.06723550
  6300.406289990.06370610
  6310.406396000.06017670
  6320.406502010.05664730
**
** end of nodal coordinate definitions
**-----------------------------------------------------------------------
**-----------------------------------------------------------------------
** define element connectivity, and element type
**
*ELEMENT,TYPE=CAX4,ELSET=ALL_E
    1    1    2   14   13
    2   13   14   26   25
    3   25   26   38   37
    4   37   38   50   49
    5    2    3   15   14
    .
    .
    elements 6 through 554
    .
    .
  555  355  356  365  364
  556  356  357  366  365
  557  357  358  367  366
  558  358  359  368  367
  559  359  360  361  368
**
** end of element connectivity definitions
**-----------------------------------------------------------------------
```

```
**------------------------------------------------------------------
** define node sets
**
** define nodes resting on support
*NSET,NSET=BOTTM
  178  191  204  217  230  279  287  295  303  311  319  327
**
** define nodes in rim
*NSET,NSET=TREAD
  624  582  540
**
** define nodes on line through rim
*NSET,NSET=T1
  624  603  582  561  540  519  498  477  456  407  390  376  238  223
  210  197  184  171
**
** end of node set definitions
**------------------------------------------------------------------
**------------------------------------------------------------------
** define element set through rim
**
*ELSET,ELSET=ELRIM
  323  321  319
**
** end of element set definition
**------------------------------------------------------------------
** assign boundary condition to support nodes
**
*BOUNDARY
BOTTM2
**
** end of boundary constraint definition
**------------------------------------------------------------------
**------------------------------------------------------------------
** define material properties
** stress-related quantities have been scaled so that results are in MPa
**
*SOLID SECTION,ELSET=ALL_E,MATERIAL=WHLSTEEL
*MATERIAL,NAME=WHLSTEEL
*ELASTIC,TYPE=ISO
  2.13E+05     0.295       24.
  2.01E+05     0.307      230.
  1.93E+05     0.314      358.
  1.72E+05     0.320      452.
  1.02E+05     0.326      567.
  0.50E+05     0.334      704.
  0.43E+05     0.345      900.
*EXPANSION,TYPE=ISO,ZERO=871.
  9.89E-06       20.
 10.82E-06      230.
 11.15E-06      358.
 11.27E-06      452.
 11.31E-06      567.
 11.28E-06      704.
 11.25E-06      900.
*PLASTIC,HARDENING=KINEMATIC
 4.483E+02  0.000000      24.
 7.240E+02  0.011439      24.
 4.502E+02  0.000000     230.
 7.220E+02  0.009212     230.
```

```
 3.887E+02  0.000000     358.
 6.2335+02  0.010352     358.
 3.085E+02  0.000000     452.
 4.946E+02  0.011423     452.
 1.402E+02  0.000000     567.
 2.249E+02  0.013448     567.
 0.418E+02  0.000000     704.
 0.669E+02  0.026971     704.
 0.124E+02  0.000000     900.
 0.194E+02  0.082082     900.
*CREEP,LAW=USER
*USER SUBROUTINE
C
C
C
      SUBROUTINE CREEP(DECRA,DESWA,STATEV,SERD,EC0,ESW0,P,QTILD,
     +                 TEMP,DTEMP,PREDEF,DPRED,TIME,DTIME,CMNAME,
     +                 LEXINP,LEND,COORDS,NSTATV,NOEL,NPT,LAYER,
     +                 KSPT,KSTEP,KINC)
C
      INCLUDE 'ABA_PARAM.INC'
C
      CHARACTER*8 CMNAME
C
      DIMENSION DECRA(5),DESWA(5),STATEV(*),PREDEF(*),DPRED(*),TIME(2),
     +          COORDS(*)
C
C     exponent on stress term
C
      PWR=12.5
C
C     convert equivalent stress into ksi
C
      QKSI=QTILD/6.895
C
C     convert temperature into Fahrenheit
C
      FTEMP=(TEMP*(9./5.))+32.
C
C     apply Kuhlman creep equation
C
      A=-53712./(FTEMP+460.)
C
      EDOT=4.64E-08*(QKSI**PWR)*(EXP(A))
C
C     multiply by time increment to get incremental strain
C
      DECRA(1)=EDOT*DTIME
C
C
C
      RETURN
      END
**
** end of material property definition
**-----------------------------------------------------------------------
**-----------------------------------------------------------------------
** assign initial temperature to all nodes [827 degrees C]
**
*INITIAL CONDITIONS,TYPE=TEMPERATURE
```

```
ALL_N 871.
**
** end of nodal initial temperature assignment
**-------------------------------------------------------------------
**-------------------------------------------------------------------
** begin step definition of analysis (STEP 1)
**
*STEP,INC=10000
**-------------------------------------------------------------------
**
*VISCO,CETOL=2.5E-04
1.0,370.00,0.0001,10.
**
**-------------------------------------------------------------------
** define nodal temperature input file
**
*TEMPERATURE,FILE=qt2,BSTEP=1,BINC=1,ESTEP=1,EINC=373
**
** end of nodal temperatures definition
**-------------------------------------------------------------------
**-------------------------------------------------------------------
** define DOF monitor
**
*MONITOR,NODE=621,DOF=2,FREQUENCY=0
**
** end of DOF monitor assignment
**-------------------------------------------------------------------
**-------------------------------------------------------------------
** controls section (used to control convergence criteria)
**
*CONTROLS,ANALYSIS=DISCONTINUOUS
**
** end of controls section
**-------------------------------------------------------------------
**-------------------------------------------------------------------
** define output requirements
**
*PRINT,FREQUENCY=0
*NODE PRINT,FREQUENCY=0,NSET=ALL_N
*EL PRINT,FREQUENCY=0,ELSET=ALL_E,POSITION=CENTROIDAL
*EL FILE,FREQUENCY=0,ELSET=ALL_E,POSITION=CENTROIDAL
S
*RESTART,WRITE,FREQUENCY=1
**
** end of output plotting requirements definition
**-------------------------------------------------------------------
*END STEP
**
** end of step 1 definition
**-------------------------------------------------------------------
**-------------------------------------------------------------------
** begin step definition of analysis (STEP 2)
**
*STEP,INC=10000
**-------------------------------------------------------------------
**
*VISCO,CETOL=2.5E-04
5.0,21610.,0.0001,100.
**
**-------------------------------------------------------------------
```

```
** define nodal temperature input file
**
*TEMPERATURE,FILE=qt2,BSTEP=2,BINC=1,ESTEP=2,EINC=2167
**
** end of nodal temperatures definition
**------------------------------------------------------------------
**------------------------------------------------------------------
** define DOF monitor
**
*MONITOR,NODE=621,DOF=2,FREQUENCY=0
**
** end of DOF monitor assignment
**------------------------------------------------------------------
**------------------------------------------------------------------
** controls section (used to control convergence criteria)
**
**CONTROLS,ANALYSIS=DISCONTINUOUS
**
** end of controls section
**------------------------------------------------------------------
**------------------------------------------------------------------
** define output requirements
**
*PRINT,FREQUENCY=0
*NODE PRINT,FREQUENCY=0,NSET=ALL_N
*EL PRINT,FREQUENCY=0,ELSET=ALL_E,POSITION=CENTROIDAL
*EL FILE,FREQUENCY=0,ELSET=ALL_E,POSITION=CENTROIDAL
S
*RESTART,WRITE,FREQUENCY=1
**
** end of output plotting requirements definition
**------------------------------------------------------------------
*END STEP
**
** end of step 2 definition
**------------------------------------------------------------------
**------------------------------------------------------------------
** begin step definition of analysis (STEP 3)
**
*STEP,INC=10000
**------------------------------------------------------------------
**
*VISCO,CETOL=2.5E-04
5.0,14195.,0.0001,100.
**
**------------------------------------------------------------------
** define nodal temperature input file
**
*TEMPERATURE,FILE=qt2,BSTEP=3,BINC=1,ESTEP=3,EINC=148
**
** end of nodal temperatures definition
**------------------------------------------------------------------
**------------------------------------------------------------------
** define DOF monitor
**
*MONITOR,NODE=621,DOF=2,FREQUENCY=0
**
** end of DOF monitor assignment
**------------------------------------------------------------------
**------------------------------------------------------------------
```

```
** controls section (used to control convergence criteria)
**
**CONTROLS,ANALYSIS=DISCONTINUOUS
**
** end of controls section
**-------------------------------------------------------------------
**-------------------------------------------------------------------
** define output requirements
**
*PRINT,FREQUENCY=0
*NODE PRINT,FREQUENCY=0,NSET=ALL_N
*EL PRINT,FREQUENCY=999,ELSET=ALL_E,POSITION=CENTROIDAL
*EL FILE,FREQUENCY=0,ELSET=ALL_E,POSITION=CENTROIDAL
S
*RESTART,WRITE,FREQUENCY=1
**
** end of output plotting requirements definition
**-------------------------------------------------------------------
*END STEP
**
** end of step 3 definition
**-------------------------------------------------------------------
```

REFERENCES

[1] O. Orringer, D.E. Gray, and R.J. McCown. *Evaluation of Immediate Actions Taken to Deal with Cracking Problems on Wheels of Rail Commuter Cars.* Volpe National Transportation Systems Center. Report No. DOT/FRA/ORD-93/15. 1993.

[2] Y.H. Tang, J.E. Gordon, A.B. Perlman, and O. Orringer. *Finite Element Models, Validation, and Results for Wheel Temperature and Elastic Thermal Stress Distributions.* Volpe National Transportation Systems Center. Report No. DOT/FRA/ORD-93/17. 1993.

[3] Y.H. Tang, J.E. Gordon, O. Orringer, and A.B. Perlman. *Stress Reconstruction Analysis of Wheel Saw Cut Tests and Evaluation of Reconstruction Procedure.* Volpe National Transportation Systems Center. Report No. DOT/FRA/ORD-93/18. 1993.

[4] J.E. Gordon and O. Orringer. *Investigation of the Effects of Braking System Configurations on Thermal Input to Commuter Car Wheels.* Volpe National Transportation Systems Center. Report No. DOT/FRA/ORD-96/01. 1996.

[5] D.L. Mikrut. *Elevated Temperature Time-Dependent Behavior of 0.7% Carbon Steels.* Masters Thesis. University of Illinois at Urbana-Champaign, Illinois. 1990.

[6] S.A. Perfect. *Stress Changes in Railroad Car Wheels Due to Axially Symmetric Thermal Loads.* Ph.D. Thesis. University of Illinois at Urbana-Champaign, Illinois. 1986.

[7] C. Kulhman, H. Sehitoglu, and M. Gallagher. "The Significance of Material Properties on Stresses Developed During Quenching of Railroad Wheels." Proceedings of the 1988 Joint ASME IEEE Railroad Conference, April 1988, pp. 55-63.

[8] H. Sehitoglu and J. Morrow. "Characterization of Thermo-Mechanical Fatigue." ASME PVP., Vol. 71, pp. 93-100, 1983.

[9] T.M. Rusin, J.M. Coughlin and G. Damergis. "Curved Plate Wheel Design for a Commuter Railroad's Reverse Dish 32" Car Wheel." ASME Rail Transportation Division, Vol. 12, 1996.

[10] J.M. Coughlin, private communication.

[11] S. Kalpakjian. Manufacturing Engineering and Technology. Addison-Wesley Publishing Company, Inc. 1989. Page 401.

[12] The Making, Shaping and Treating of Steel. 10th Edition. Chapter 28. Production of Steel Wheels. 1985. pp. 911-919.

[13] A.K. Leighton. *Residual Stresses in Quenched Solid and Hollow Cylinders with Application to Railroad Axles.* Masters Thesis, Tufts University, Medford, Massachusetts. November 1993.

[14] D. Lorenzon. *Residual Stresses in Railroad Car Axles Resulting from Manufacturing and Service Loads.* Masters Thesis, Tufts University, Medford, Massachusetts. February 1996.

[15] R.G. Fata. *Residual Stresses Resulting from Quench Hardening the Head of a Railroad Rail.* Masters Thesis, Tufts University, Medford, Massachusetts. May 1996.

[16] J.A. Jones. *Optimization of Alloy Content and Heat Treatment for Head-Hardened Railroad Rails.* Masters Thesis, Tufts University, Medford, Massachusetts. February 1997.

[17] Association of American Railroads, Manual of Standards and Recommended Practices, Section G, Mechanical Division Standard M-107-84, "Wheels, Wrought Carbon Steel," Washington, DC, March 1985, pp. G-5 to G-8A.

[18] G.F. van der Voort (ed.). Atlas of Time-Temperature Diagrams for Irons and Steels. ASM International, 1991. pp. 3-12, pp. 15.

[19] G. Krauss. Steels: Heat Treatment and Processing Principles. ASM International, Materials Park, OH. 1990.

[20] F.M. White. Heat Transfer. Addison-Wesley Publishing Company, 1984.

[21] A.P. Boresi, O.M. Sidebottom, F.B. Seely and J.O. Smith. Advanced Mechanics of Materials. Third Edition. John Wiley & Sons, 1978.

[22] ABAQUS/Standard User's Manual (I and II), Version 5.5. Hibbitt, Karlsson & Sorenson, Inc. 1995.

[23] A.B. Shapiro. "TOPAZ2D - A Two-Dimensional Finite Element Code for Heat Transfer Analysis, Electrostatic, and Magnetostatic Problems." Lawrence Livermore National Laboratory, Livermore, California. UCID-20824. July 1986.

[24] B. Engelmann, and J.O. Hallquist. "NIKE2D - A Nonlinear, Implicit, Two-Dimensional Finite Element Code for Solid Mechanics." Lawrence Livermore National Laboratory, Livermore, California. UCRL-MA-105413. April 1991.

[25] J.O. Hallquist. "MAZE - An Input Generator for DYNA2D and NIKE2D." Lawrence Livermore National Laboratory, Livermore, California. UCID-19029, Rev. 2. June 1983.

[26] Edgewater Steel Company. Manufacturing Drawing No. C-22743-1. Oakmont, Pennsylvania. January 13, 1986.

[27] B. Liščič, H.M. Tensi and W. Luty. Theory and Technology of Quenching, Springer-Verlag, New York, New York. 1992, p. 126.

[28] J.E. Gordon and O. Orringer. "Prospects for Making Carbide-Free Bainitic Thick Steel Plate By Means of Controlled Quenching: A First Estimate." ASME International Mechanical Engineering Congress and Exposition. 1995. RTD Vol. 10, pp. 119-126.

Reports in this series:

1. Orringer, D.E. Gray, and R.J. McCown, "Evaluation of Immediate Actions Taken to Deal with Cracking Problems Observed in Wheels of Rail Commuter Cars," Volpe National Transportation Systems Center, Cambridge, Massachusetts, and Federal Railroad Administration, Washington, D.C., Report No. DOT/FRA/ORD-93/15, July 1993.

2. C. Stuart and S. Yu, "Thermal Measurements of Commuter Rail Wheels under Revenue Service Conditions," ENSCO, Inc., Springfield, Virginia, Report No. DOT/FRA/ORD-93/19, September 1993.

3. Y.H. Tang, J.E. Gordon, A.B. Perlman and O. Orringer, "Finite Element Models, Validation and Results for Wheel Temperature and Elastic Thermal Stress Distributions," Volpe National Transportation Systems Center, Cambridge, Massachusetts, Report No. DOT/FRA/ORD-93/17, September 1993.

4. Y.H. Tang, J.E. Gordon, O. Orringer and A.B. Perlman, "Stress Reconstruction Analysis of Wheel Saw Cut Tests and Evaluation of Reconstruction Procedure," Volpe National Transportation Systems Center, Cambridge, Massachusetts, Report No. DOT/FRA/ORD-93/18, September 1993.

5. R.M. Pelloux and D.C. Grundy, "Thermomechanical Testing and Microstructural Development of Class L Steel Wheel Alloy," Department of Materials Science and Engineering, MIT, Cambridge, Massachusetts, Report No. DOT/FRA/ORD-94/01, March 1994.

6. J.E. Gordon and O. Orringer, "Investigation of the Effects of Braking System Configurations on Thermal Input to Commuter Car Wheels," Volpe National Transportation Systems Center, Cambridge, Massachusetts, Report No. DOT/FRA/ORD-96/01, March 1996.

7. M. Holowinski and E.S. Bobrov, "Estimation of Actual Residual Stresses Due to Braking and Contact Loading of Rail Vehicle Wheels," Francis Bitter National Magnet Laboratory, MIT, Cambridge, Massachusetts, Report No. DOT/FRA/ORD-96/02, March 1996.

8. K.E. Crowe and P.K. Raj, "Analyses of Rail Chill Effect," Technology and Management Systems, Inc., Burlington, Massachusetts, Report No. DOT/FRA/ORD-97/07, June 1998.

9. R. Czarnek, "Experimental Determination of Release Fields in Cut Railroad Car Wheels," Concurrent Technologies Corporation, Johnstown, Pennsylvania, Report No. DOT/FRA/ORD-97/06, February 1999.